COO-2195-12

Department of Meteorology

MASSACHUSETTS INSTITUTE OF TECHNOLOGY

Cambridge, Massachusetts 02139

DENSITY VARIATIONS IN THE LOWER THERMOSPHERE

William F. Johnson
Lt. Colonel, U.S.A.F.

Scientific Report No. 2

February 19, 1974

Support for this work was provided partly by the U.S. Atomic Energy Commission under Contract AT(11-1)-2195, Principal Investigator Reginald E. Newell.

DISCLAIMER

COO-2195-12

Department of Meteorology

MASSACHUSETTS INSTITUTE OF TECHNOLOGY

Cambridge, Massachusetts 02139

DENSITY VARIATIONS IN THE LOWER THERMOSPHERE

William F. Johnson
Lt. Colonel, U.S.A.F.

Scientific Report No. 2

February 19, 1974

Support for this work was provided partly by the U.S. Atomic Energy Commission under Contract AT(11-1)-2195, Principal Investigator Reginald E. Newell.

DENSITY VARIATIONS IN THE LOWER THERMOSPHERE

by

William F. Johnson

Submitted to the Department of Meteorology on 11 February 1974 in partial fulfillment of the requirements for the degree of Doctor of Philosophy.

ABSTRACT

Accelerometer derived thermospheric density data from the LOGACS and SPADES satellites are processed to yield the equivalent density variation at 150 and 160 km respectively. Definite latitudinal and longitudinal variations are found which conflict with Jacchia's 1971 model. Time-latitude analyses are presented of density at a single altitude. The density response to a great geomagnetic storm is nearly the same from 25°S to 85°N except that a density trough forms just equatorward of the auroral oval. Gravity waves are observed during the storm. The structure and dynamics of the lower thermosphere are far more complex than previous studies indicate.

ACKNOWLEDGEMENTS

The author wishes to acknowledge the unflagging enthusiasm, strong encouragement, and helpful counsel and guidance provided by the thesis supervisor Professor R. E. Newell. A deep debt of gratitude is due to Dr. Leonard L. DeVries who not only graciously provided the LOGACS data, related information, and copies of his own work, but also a strong example to follow and some much needed encouragement. The author is especially grateful to Mr. Frank A. Marcos of the Air Force Cambridge Research Laboratories who made a special effort to obtain the SPADES data in the format required for study. Mrs. Susan Ary is heartily thanked for the many long hours she spent doing the tedious data extraction and calculations required in this study. The efforts of Ms. Isabelle Kole and Mr. Sam Ricci in producing the many drawings and figures of this study in a most timely manner are highly appreciated. The opportunity to attend M.I.T. and make this investigation was provided and funded by the U.S.A.F. under the Air Force Institute of Technology. The many, generous recommendations of Dr. Donald E. Martin were instrumental in the author's selection for this opportunity. The author is grateful most of all to his wife and family without whose patience, time, understanding, and support this work could not have been completed.

TABLE OF CONTENTS

LIST OF FIGURES

LIST OF TABLES

I. INTRODUCTION

Artificial earth satellites have opened up an entirely new area of the atmosphere to direct observation. Satellites have proven to be a valuable platform from which the weather and structure of the troposphere and stratosphere can be observed. A number of scientific satellites have been designed and flown to gather information on the charged particle population and the structure of the geomagnetic field as well as their interaction with the solar wind. Satellite systems have been launched to provide communication and navigation links, to investigate the shape of the geoid and its gravitational field, to find and monitor earth resources, and to put man himself as an observer in a new environment. More recently scientific satellites have been orbited to investigate the composition, ionization levels, and atmospheric density of the satellite environment.

The fact that a portion of the atmosphere, however tenuous, is present at the altitudes where satellites are flown causes perturbations and decay of satellite orbits which can be measured and used to infer the atmospheric density near the perigee altitudes of the satellites. By this means a considerable amount of information has been gathered from a large number of satellites on the density structure and variation of the upper atmosphere.

Inferring density from orbital decay measurements

has several very important limitations. The first is that the atmosphere perturbation drag force is not limited to a single point in the atmosphere but extends over a 20° arc or more of the satellite orbit, depending on the orbital eccentricity. Further, the perturbation force is quite small compared to the total orbit energy and due to tracking accuracy limitations several revolutions around the orbit may be required before the atmospheric density signal can be adequately isolated. The number of revolutions required is mainly dependent on the minimum altitude of the orbit and the satellite area to mass ratio. A minimum of two revolutions are required to determine the density. The number actually used is almost always greater, ranging up to several days duration. The resulting density value is thus derived from the integrated atmospheric drag force on the satellite over a range of altitudes down to the minimum altitude, along a 20° arc or more of the orbit for usually six or more revolutions around the orbit. Thus the structure and time variations of the density are considerably smeared by the orbital decay observation technique.

The orbital decay density observations are not uniformly distributed. Relatively few are available from low altitudes due to the more rapid orbit decay rate which quickly reduces orbital lifetime. Most satellites with long design lifetimes are placed in orbits with minimum altitudes above 200-250 km. A further deficiency in the distribution of observations is the lack of high latitude observations.

The reason for this is that lack of sufficient rocket booster capability made it necessary to use a large portion of the earth's angular momentum to put a payload into orbit, thus resulting in relatively low orbital inclinations. More recently more satellites have been launched into near polar orbits but sampling of the high latitude region is still relatively sparse, particularly at certain local times of day at lower altitudes.

Orbital decay observations accumulated for over 10 years have revealed much about the structure and variation of the density in the region of the atmosphere known as the thermosphere. The density in this region is largely controlled by solar extreme ultraviolet (EUV) and corpuscular radiations. The density varies over the eleven year solar cycle in concert with the variation of the mean background solar EUV flux. Shorter term density variations are observed with the appearance and fluctuations of active areas on the solar disk. These result in short-term variations in the solar EUV output which in turn cause density changes with a lag of about one day. The most prominent density variation is that caused by direct solar heating. This causes a density bulge to form which is thought to be at the latitude of the solar subpoint with a maximum lagging local noon by two hours. Minimum density lags the antisolar point by about 3-4 hours. This subsolar density bulge is believed to migrate with the sun. A rather unexpected semi-annual density varitaion is observed with maxima in early

April and late Oct. and minima in mid-Jan. and late July. The extrema in Oct. and July are larger than those in Jan. and April. There is still considerable disagreement as to the cause of this semi-annual variation. The last recognized density variation is that due to corpuscular radiation. This is usually associated with geomagnetic activity and in general lags the variation in geomagnetic activity by several hours. Due to the short-term nature of geomagnetic storms the exact character of the atmospheric density response is poorly known from orbital decay measurements. Density increases of two orders of magnitude have been observed at some altitudes in response to a strong geomagnetic storm.

Because of the wide range in the altitude, latitude, local time of day, solar EUV flux level, etc., a model concept is used to incorporate the density observations. The model is based on the static diffusion equilibrium equations with a temperature profile specified by the angle from the center of the modelled sub-solar bulge and the levels of EUV flux and geomagentic activity. Lower boundary conditions of temperature and composition are assumed at a level near 100 km where static diffusion begins to become effective. These lower boundary conditions are based on the results of various rocket flights. The shape of the temperature profile is adjusted to match static diffusion densities to those observed over the altitude range up to 1200 km (Echo balloon).

Considerable uncertainty still exists as to the density structure at low altitudes. The nature of the very dynamic response of the density level and distribution are poorly known from orbital decay measurements. Recently density observations have become available from very sensitive satellite-borne accelerometers flown aboard two satellites. These density observations have high resolution in time and space. Their accuracy exceeds that from orbital decay measurements. A few of these measurements have been presented and discussed in the open literature (DeVries, 1972, 1972b; Forbes and Marcos, 1973; Marcos and Champion, 1972; Marcos et al, 1971). However, to date no thorough, integrated investigation has been made using all or even a large portion of this density data. Density observations by accelerometers have been obtained on 36 different days. The major portion of the data is for altitudes below 200 km. During the days when accelerometer density measurements were obtained, an extremely large geomagnetic storm occurred. These data afford a unique opportunity to not only obtain information on the low altitude density structure of the thermosphere, but to also determine the nature of the density response to a large corpuscular heating event.

II. SOURCES OF DATA

The density data used in this study were obtained from the direct measure of the atmospheric drag force by satellite-borne accelerometers. The accelerometers were capable of measuring atmospheric drag forces of less than 10^{-6}g. This level of sensitivity was more than sufficient to measure the drag force accurately on the satellites below 250 km.

The drag force is related to the density by

$$ma_D = -1/2\rho V^2 C_D A \qquad (1)$$

where

- m = satellite mass
- a_D = atmospheric drag acceleration
- ρ = atmospheric density
- V = satellite velocity along the orbit
- C_D = drag coefficient
- A = effective satellite cross-sectional area, normal to the velocity vector.

The advantages of this method of density determination over that of observing satellite orbit decay are very significant. The accelerometer is capable of determining drag on a nearly instantaneous basis, thus yielding density information with a high degree of resolution in time and space. This is far superior to the resolution obtained by orbit decay measurements.

THE LOW-G ACCELEROMETER CALIBRATION SYSTEM

Data from two separate satellites are used in this study. The first is the Low-G Accelerometer Calibration System (LOGACS). LOGACS was flown on a United States Air Force Agena satellite placed in near-polar orbit on 22 May 1967. The orbit inclination was 91.5°. The initial perigee, apogee, and latitude of perigee were 148 km, 357 km, and 43.3°N. On revolution 18 an orbit adjustment was performed which raised apogee to 407 km and reduced the latitude of perigee to 40.7°N. During the portion of the flight in which useful data was obtained these orbital elements decayed to 141 km, 296 km, and 59°N respectively. Minimum satellite altitude decayed from 145.1 km on rev 5 to 137.4 on rev 66. The Agena vehicle was attitude-stabilized in the plane of the local horizon by intermittent firing of gas jets in the attitude control system. A single-axis, electrostatically pulse-rebalanced Bell Miniature Electrostatic Accelerometer (MESA) was used. The MESA was placed on a turntable which could rotate in the plane of the local horizon at two precisely fixed rates or be held fixed in either a fore or aft direction relative to the vertical motion. This permitted in-orbit calibration and scaling of the instrument. Density data were obtained by LOGACS up to 330 km but only that portion of the entire data set below 210 km was used in this study. Details on the orbits, times, and locations of the data are

given in Table 1. A full description of the instrumentation, data processing methods, and other pertinent details concerning LOGACS are given by Fotou (1968).

A major problem in processing the LOGACS data was the elimination of "noise" from the thrusters of the vehicle attitude control system. This prevented continuous measurement of the drag force. Other data losses occurred due to tape recorder saturation and to instrument shut-down during the orbit adjustment period. The data sampling rate was about one observation per second. Final data resolution time of 20 seconds was obtained from LOGACS. The actual errors in the measured accelerations are estimated to be less than one percent (Bruce, 1968). The absolute density values deduced from the acceleration measurements have a total uncertainty of ±10% due principally to a lack of knowledge on the precise value of the drag coefficient (Cook, 1965).

A possibly greater source of error is that caused by winds. During the latter portion of the LOGACS flight a major geomagnetic storm occurred. Side-force accelerations, normal to the plane of the orbit, were fortuitously obtained during the rotating modes of the MESA. Feess (1968) made a thorough study of these side forces and the attitude control jet firings necessary to correct for them. The Agena center of mass was different from the sidewards center of aerodynamic pressure. Feess was able to

TABLE 1

LOGACS EPHEMERIS DATA

Inclination, 91.5°

Rev No.	Date	GMT	Minimum Alt. (km)	Latitude of Min. Alt.	Longitude of the Descending Node (°E)	Local Time	Solar Declination
5	23 May	0203	145.1	31.0°N	126	1037	20.3
6	"	0332	145.1	31.9	104	1037	"
7	"	0501	145.1	32.4	81	1037	"
9	"	0759	145.0	32.7	37	1037	"
10	"	0928	144.8	33.1	352	1037	"
11	"	1057	144.7	33.5	330	1037	"
12	"	1226	144.5	33.8	307	1037	20.4
13	"	1355	144.2	34.1	285	1037	"
14	"	1524	144.2	34.4	262	1037	"
18	"	2122	144.7	31.1	195	1037	"
20	24 May	0020	144.9	31.4	150	1035	20.5
21	"	0150	144.8	31.8	128	1034	"
24	"	0620	144.7	33.2	60	1034	"
25	"	0750	144.7	33.6	38	1034	"
26	"	0920	144.6	33.8	16	1034	"
27	"	1050	144.5	34.0	354	1033	"
28	"	1219	144.3	34.2	331	1033	"
29	"	1349	144.2	34.4	309	1033	20.6
30	"	1519	144.0	34.6	286	1033	"
31	"	1648	144.1	34.9	264	1033	"
32	"	1818	144.0	35.1	241	1032	"
33	"	1947	144.3	35.3	219	1032	"
34	"	2117	144.2	35.6	197	1032	"
35	"	2246	143.9	35.9	174	1032	"
36	25 May	0015	143.7	36.2	151	1031	20.7
37	"	0145	143.5	36.5	129	1031	"
38	"	0314	143.5	36.7	106	1031	"
39	"	0444	143.5	37.0	84	1031	"
40	"	0613	143.3	37.2	61	1031	"

TABLE 1 Continued

Rev No.	Date	GMT	Minimum Alt. (km)	Latitude of Min. Alt.	Longitude of the Descending Node (°E)	Local Time	Solar Declination
41	25 May	0742	143.3	37.5°N	39	1031	20.7
43	"	1040	142.9	38.0	354	1030	"
44	"	1210	142.9	38.3	332	1030	"
45	"	1339	143.0	38.6	310	1030	"
46	"	1508	143.0	38.9	287	1030	"
47	"	1637	143.0	39.1	265	1030	"
48	"	1806	142.9	39.4	243	1030	"
49	"	1935	142.7	39.6	220	1029	"
50	"	2105	142.3	39.9	198	1029	"
51	"	2234	142.0	40.1	176	1029	"
52	26 May	0003	141.6	40.3	153	1029	"
53	"	0132	141.0	40.5	130	1029	"
54	"	0301	140.8	40.8	108	1029	"
55	"	0430	140.6	41.1	86	1029	"
56	"	0559	140.2	41.3	64	1029	"
57	"	0728	139.9	41.6	41	1029	20.8
58	"	0857	140.0	41.9	19	1028	"
59	"	1026	140.3	42.2	357	1028	"
61	"	1321	139.7	42.4	335	1028	"
62	"	1552	138.8	42.5	313	1028	"
63	"	1620	138.4	42.3	291	1028	"
64	"	1849	138.1	42.2	268	1028	"
65	"	1918	137.7	42.4	246	1028	"
66	"	2146	137.4	42.4	224	1028	"

calculate winds normal to the plane of the orbit. He found wind speeds in excess of 1 km/sec in the polar regions during the magnetic storm. Fedder and Banks (1972) made theoretical calculations of polar thermospheric wind generation by convection electric fields. They found that neutral wind speeds approaching 800 m/sec in the antisolar direction and 400 m/sec eastward could be generated within 4 to 5 hours by a steady electric field of 40 mV/m. Using a somewhat different theoretical approach Cole (1971) estimated that west to east wind speeds on the order of 2 km/sec could be generated by an auroral electric field which had been observed to reach 100 mV/m. Wind observations have been made from rocket releases of trimethyl aluminum trails and grenade clouds between 90 and 200 km at high latitudes at twilight. Westward winds of 500 to 600 m/sec were observed following a strong positive magnetic bay. Between 120 and 150 km there was a strong correlation between the E to W neutral wind and the perturbation of the H component of the geomagnetic field during the previous two hours (Rees, 1972).

Hayes and Roble (1971) have calculated north to south winds in mid-latitudes of 400 m/sec at 400 km from observations of the Doppler shift of the 6300Å emission. This observation was made at night during an auroral event. Smith (1968) deduced eastward winds at Kauai, Hawaii of 227 m/sec at 147 km from a vapor trail experiment made

18 hours after the peak of geomagnetic storm. Theoretical calculations of winds generated by the subsolar bulge as specified in thermospheric density models, have been made by several investigators using a variety of assumptions regarding boundary conditions, subsolar density bulge amplitude and shape, and including ion drag but omitting or including various other terms in the equations of motion (Lindzen, 1966, 1967; Geisler, 1966, 1967; Kohl and King, 1967; Challinor, 1968, 1969 and 1970; Dickinson and Geisler, 1968; Rishbeth, 1972). All of these theoretical models yield maximum winds on the order of 250 m/sec in the lower thermosphere. Satellite velocity for a nearly circular orbit at 200 km is almost 8 km/sec. From equation (1) a wind component of 1 km/sec along or opposite the satellite direction of motion could cause a deduced density error of about ±27%. This error would be restricted to high latitudes at times during geomagnetic storms. The observed density variations from LOGACS during the storm period of 25-26 May 1967 were nearly an order of magnitude greater than 27%. Winds of 250 m/sec in the direction of satellite motion would result in a 6% error in the deduced density. The density variations observed with LOGACS during geomagnetically quiescent periods were considerably in excess of 6%. All LOGACS data were obtained at nearly the same local time in the sunlit hemisphere. The theoretical estimates of winds resulting from the subsolar pressure bulge show

them to depend mostly on local time and to a lesser extent on latitude and season. Thus on each revolution LOGACS would experience nearly the same variation of wind due to a subsolar density bulge if the models of its size and shape are accurate. The absolute density values would therefore be in error by an amount no more than 6% but the relative density variation from one revolution to the next would be much less subject to this source of error. The same argument can be made regarding the error due to the uncertainty of C_D. In conclusion, the relative density variations observed with LOGACS are the result of true thermospheric density variations.

SPADES

The second source of data used in this study is from the USAF/Aerospace Corp./AFCRL satellite OV1-15 (1968-59A) also known as the Solar Perturbation of Atmospheric Density Experiments Satellite (SPADES). SPADES was launched on 11 July 1968 into a 89.8° inclination orbit with an initial perigee and apogee of 158 km and 1850 km. A more complete description of SPADES payload and orbital data is given by Champion and Marcos (1969) and by Morse (1970). Times and locations of the SPADES accelerometer data used in this study are given in Table 2. SPADES was spin stabilized with three Bell MESA's mounted as near as possible to the vehicle center of mass, aligned normal to each

TABLE 2

SPADES EPHEMERIS DATA

Inclination, 89.8°

Rev No.	Date	GMT	Minimum Alt. (km)	Latitude of Perigee	Longitude of Perigee (°E)	Local Time	Solar Declination
21	13 July	0828	159.0	12.3°S	42.3	1117	21.7°
25	"	1527	158.7	11.4	297.3	1116	21.7
29	"	2226	158.6	10.5	192.4	1115	21.7
33	14 July	0525	157.9	9.7	87.4	1113	21.6
37	"	1224	157.8	8.9	342.5	1112	21.6
41	"	1922	157.7	7.9	237.6	1111	21.5
45	15 July	0220	157.6	7.1	132.7	1110	21.5
49	"	0918	157.3	6.3	27.9	1109	21.5
53	"	1617	157.6	5.3	283.0	1108	21.4
57	"	2315	157.3	4.5°S	178.2	1106	21.4
157	23 July	0450	150.4	17.2°N	86.9	1037	20.0
160	"	1002	151.4	17.7	8.8	1036	19.9
163	"	1513	151.4	18.4	290.8	1036	19.9
166	"	2024	152.3	19.0	212.8	1035	19.8
172	24 July	0646	152.6	20.3	56.8	1033	19.8
175	"	1157	152.7	20.9	338.8	1032	19.7
178	"	1708	152.7	21.6	260.9	1031	19.7
181	"	2219	152.8	22.2	182.9	1030	19.6
187	25 July	0841	152.7	23.5	27.1	1029	19.5
190	"	1352	152.7	24.2	309.2	1028	19.5
199	26 July	0523	152.8	26.1	75.7	1025	19.3
202	"	1033	152.9	26.8	357.9	1024	19.2
205	"	1543	153.0	27.5	280.0	1023	19.2
208	"	2053	153.3	28.2	202.3	1022	19.1
253	30 July	0219	155.6	38.1	117.6	1010	18.3
256	"	0728	156.2	38.8	40.0	1009	18.3
259	"	1238	156.3	39.5	332.5	1008	18.2
262	"	1747	156.4	40.3	245.1	1007	18.2

TABLE 2 Continued

Rev No.	Date	GMT	Minimum Alt.(km)	Latitude of Perigee	Longitude of Perigee (°E)	Local Time	Solar Declination
265	30 July	2256	155.9	40.8	167.6	1006	18.1
268	31 July	0405	155.2	41.4	90.1	1005	18.1
271	"	0914	155.8	42.1	12.7	1004	18.0
274	"	1422	155.4	42.8	295.2	1003	18.0
277	"	1931	155.3	43.4	217.8	1002	18.0
280	1 Aug.	0040	155.8	44.2	140.5	1001	17.9
283	"	0549	155.9	44.8	63.1	1000	17.9
286	"	1057	155.9	45.5	345.7	0958	17.8
289	"	1606	156.2	46.1	268.3	0958	17.8
292	"	2115	156.6	46.9	191.0	0958	17.7
344	5 Aug.	1553	157.7	59.1	267.5	0938-0943	16.9
352	6 Aug.	0349	157.8	60.7	87.8	0935-0941	16.8
355	"	0857	157.9	61.4	10.8	0932-0940	16.7
358	"	1404	158.0	62.1	293.8	0927-0939	16.6
361	"	1911	158.3	62.8	216.8	0923-0939	16.6
364	7 Aug.	0018	158.0	63.4	139.9	0918-0938	16.5
367	"	0525	158.4	64.1	63.0	0824-0937	16.4
370	"	1032	158.8	64.9	346.1	0627-0936	16.4
373	"	1538	158.9	65.6	269.2	0222-0935	16.3
376	"	2044	159.4	66.4	192.3	2219-0934	16.2
379	8 Aug.	0151	159.3	67.1	115.5	0341-0933	16.2
382	"	0558	160.3	67.8	38.6	2128-0932	16.1
385	"	1204	159.8	68.5	321.8	2128-0932	16.0
388	"	1711	159.5	69.2	245.0	2035-0931	16.0
391	"	2217	159.6	69.9	168.2	2116-0930	15.9

other, and along and normal to the nominal vehicle spin axis. The SPADES spin axis was fixed normal to the orbital plane. The spin rate was initially 10 rpm. Superimposed upon this was a precession of the spin axis with a period of 23 secs. One of the two MESAs aligned normal to the spin axis failed on launch. In spite of the spin axis precession, the MESA aligned along the spin axis yielded density data of doubtful value. The remaining MESA performed excellently. Above 250 km the accelerometer signal had a constant component due to the centrifugal acceleration resulting from the vehicle spin. This signal was modulated by the precession of the spin axis. As the satellite altitude decreased to below 250 km a second modulation due to atmospheric drag began. This modulation occurred at the satellite spin period and increased in amplitude with increasing density. Density values were derived by coupling the accelerometer output to separate information on the vehicle attitude. Numerical filtering techniques were employed to eliminate the accelerometer signal due to vehicle dynamics (spin rate and spin axis precession rate) and yield density values for those times when the MESA was aligned most nearly into and away from the satellite direction of motion. Marcos et al (1972) gives a more complete description of the experiment and data processing. The resulting density values have a time resolution of less than one second and are available approximately every three

seconds. The location of the density measurement is within 0.1° latitude and 0.1 km altitude. These limits are within the range of the satellite ephemeris errors. Due to power limitations the accelerometer experiment on SPADES was operated only every three or four revolutions around the orbit. Additionally, power supply problems frequently resulted in the loss of data for periods of several days at a time. Data were available for various periods in the interval between 13 July and 28 Sept. 1968. A complete gap occurred in the data between 8 and 28 Aug. During this time the perigee latitude moved over the pole from the sunlit to the dark hemisphere. Only the data collected through 8 Aug. was included in this study in order to limit the amount of processing to tractable proportions and also since the geographical area and local times covered were similar to that of LOGACS.

The statistical errors in the density values derived from the accelerometer output are estimated to be: numerical filtering technique, varies from negligible at perigee to ±2% at 250 km, attitude, ±2%, satellite area, ±2%, and overall, ±4% at perigee to ±6% at 250 km (Marcos et al, 1972). Only data below 210 km was used in this study. Even with this limitation, some errors in the density data due to filtering with slightly inaccurate values for the spin and spin axis precession rates are evident in the final data. These will be pointed out later. An

additional source of absolute density error of up to ±10% may exist due to uncertainty about the assumed value of 2.2 for C_D (Cook, 1965). As with LOGACS, the accelerometer derived densities from SPADES are subject to errors due to thermospheric winds. During the period covered by data from SPADES there were no large geomagnetic storms. Thus wind speeds of the order of 1 km/sec would not be expected. The comments made regarding the LOGACS data about wind and drag coefficient errors not affecting the measured relative density variations apply equally to the SPADES data.

III. DATA PROCESSING

The density data from the two sources covered the entire altitude range from 210 km to below 138 km. The variation of density with altitude almost completely dominates the density relationships with other parameters. There are several ways of overcoming this difficulty. One is to compare the density values with those specified by some standard model of thermospheric density for the same time, location, altitude, and solar/geomagnetic conditions. Ratios of measured to model (Jacchia, 1971) densities have been calculated for the SPADES data at 5 km altitude intervals (Marcos et al, 1972). Such a procedure normalizes out any of the density variations specified (perhaps incorrectly) by the model used. The density ratios obtained are not representative of a single altitude but the entire range of altitudes covered by the data. This method requires considerable computational effort to obtain the model densities corresponding to the measured values. In his analysis of the LOGACS data obtained during the geomagnetic storm period on 25-26 May 1967, DeVries (1972) chose the data from rev 41 which occurred at the end of a geomagnetically quiet interval as the basis for the normalization of the subsequent data obtained during the geomagnetic storm. The normalization was accomplished by computing the ratios of density values at discrete altitudes to those observed during rev 41. This method was undoubtedly chosen

by DeVries for reasons of expediency in order to obtain a quick, rough picture of the density variation associated with the great geomagnetic storm immediately following rev 41. The primary drawback of this technique is the "representativeness" of the rev 41 data. The density variation on a particular revolution may be a significant function of the geographic or geomagnetic coordinates sampled. The altitude profile may also contain variations of this sort. Subsequent revolutions do not sample the density at the same location with respect to the earth and even should the ground track of the satellite be the same 24 hours later, the decay of the orbit and the movement of the perigee location would alter the altitude profile of density sampling and change the location of the profile with respect to surface coordinates.

The procedure finally adopted in this study was to use model density profiles to normalize all density values to the nearest of a set of fixed altitudes as was done by DeVries (1966). In this manner the relative density variation could be more easily seen. The density profiles in the most complete, up-to-date model of thermospheric density available (Jacchia, 1971) were chosen for this purpose.

In the altitude range covered by the data, the density scale height varies from about 14 km at 138 km to 40 km at 210 km. In order to avoid errors from normalization over too large a range of altitude, the "standard"

altitudes were more closely spaced at the lower heights where the density scale height was smaller. All data below 150 km were normalized to the standard altitude of 145 km. The only data in this height range were from LOGACS. The major fraction of the densities below 150 km were normalized over an altitude range of 5 km or less. It was not until revs 62 through 66 that the minimum vehicle altitude for LOGACS decayed below 140 km to the lowest sampled altitude of 137.7 km on rev 66. Densities for altitudes between 145 and 155 km were normalized to 150 km. A 160 km standard altitude was chosen for data in the 155 to 170 km height range. Densities obtained between 170 and 190 km and between 190 and 210 km were normalized to 180 and 200 km respectively. Between revs 157 and 208 some density values were obtained from the SPADES accelerometer data at altitudes ranging down to 150.4 km. Since the proportion of such data below 155 km was very small and since the scale height at those altitudes was almost 20 km, all such data were normalized up to the 160 km standard altitude. In all only 14 density values were normalized to a standard altitude over an interval of more than one half the local density scale height. This minimized the effect of any errors in the model density scale heights on the normalized density values.

The thermospheric density model (Jacchia, 1971), hereafter referred to as J71, was derived by using the

static diffusion equations to match the composition at 150 km as observed from various rocket flights and the observed density as derived from satellite orbital decay measurements at greater altitudes. Static diffusion is assumed to begin at 100 km. The temperature profile for the static diffusion equations assumes a constant lower boundary temperature of 183°K at 90 km. The temperature increases from 90 km to an inflection point at 125 km and then approaches an exospheric temperature value, T_∞, asymptotically. A detailed mathematical description of the temperature profile and the derived density profile is given by Jacchia (1971). The principal variable in J71 is T_∞. T_∞ is calculated from a knowledge of the solar declination, local time, latitude, the geomagnetic index K_p, and the solar radio flux at 10.7 cm (2800 MHz). These factors account for the T_∞ changes and thus density scale height changes with season, time of day, solar corpuscular energy flux, and solar EUV energy flux. The 2800 MHz solar radio flux is an indicator of the amount of solar EUV radiation absorbed by the thermosphere (Nicolet, 1963; Neupert et al, 1964). This index is very successful in helping to specify T_∞ and thus thermospheric density (Bourdeau et al, 1964; Knight et al, 1973). Use of J71 as a model for the T_∞ variation does not eliminate the modeled density variations from the normalized density values. The change in the amplitude of the model density variations over the height

interval of normalization is introduced into the normalized density values. This effect is very small and well below the "natural" variation of the observed density values. For example, the total change in the amplitude of the diurnal bulge model of J71 between 200 and 210 km over the range of latitudes and local times sampled by LOGACS is less than 0.5%.

T_∞ was calculated exactly by the method given in J71. The values of the three-hour planetary geomagnetic index, K_p, and the 2800 MHz solar radio flux, $F_{10.7}$, used in the calculations are given in Table 3 for the LOGACS data and in Table 4 for the SPADES data. A one day lag was used in applying the $F_{10.7}$ data. The K_p data were used with a 6.7 hr. lag. These lag times approximate the atmospheric response time to changes in these indices and are the ones recommended in J71. There is no variation of response time with altitude (Roemer, 1971a). The response time of the thermosphere to K_p enhancements has been found to be significantly less than 6.7 hours at high latitudes (DeVries, 1972; DeVries et al, 1967; Taeusch et al, 1971a, 1971b; Waldteufel et al, 1972). In a situation of rapidly changing magnetic activity the difference between real and model thermospheric density response could introduce some error in the normalization procedure. Observations of $F_{10.7}$ are made daily and K_p values are derived every three hours. These values were plotted against time with the

TABLE 3

Planetary Geomagnetic Indices and 2800 MHz Solar Radio Flux
Observed During the Flight of LOGACS, May 1967

DAY[1]	$F_{10.7}$	$\overline{F_{10.7}}^{81}$	K_p								ΣK_p	A_p
			00-03	03-06	06-09	09-12	12-15	15-18	18-21	21-24		
QQ 20	143	139	2+	1+	1+	1°	1-	1°	1+	2+	11+	6
Q 21	156	139	1°	1°	0+	1°	1-	1°	3+	2+	11-	6
QQ 22	178	139	2+	1°	1+	1-	0+	0+	0+	0°	6+	3
23	189	139	1-	2-	1°	1+	1°	2-	4°	3+	15-	9
24	196	139	2-	1+	2-	2-	2+	3+	4+	2+	19-	11
D 25	205	139	2-	2°	1°	5+	8+	7+	8-	9°	42+	130
D 26	213	139	9°	9-	7+	7-	7-	4-	4°	5-	51-	146
27	208	139	4°	3+	3+	2+	3°	2-	4+	4+	26+	20

[1]Monthly five quiet days (QQ), ten quiet days (Q), and five disturbed days (D).

TABLE 4

Planetary Geomagnetic Indices and 2800 MHz Solar Radio Flux Observed During the Flight of SPADES, July-August 1968

Day[1]	$F_{10.7}$	$\overline{F}^{81}_{10.7}$	K_p								ΣK_p	A_p
			00-03	03-06	06-09	09-12	12-15	15-18	18-21	21-24		
Q 12	161	144	3°	2+	1-	1°	1+	2+	1+	1°	13	7
D 13	151	144	2-	3-	2-	1-	0+	5°	6°	4-	22-	22
D 14	151	144	6-	5-	2+	2+	3°	2+	3+	2+	26	22
Q 15	143	145	2+	2°	1+	2°	1°	1+	2+	2-	14	6
16	145	145	2°	2°	2°	1°	2-	4°	3-	1+	17-	9
Q 17	139	145	1-	1°	1°	1+	2°	1+	2+	2°	12-	6
18	131	145	2+	3°	2-	1+	3+	3+	1°	1°	17	10
19	131	146	1+	2°	2+	2+	1+	2+	1+	3°	16	8
QQ20	130	146	3-	1+	0+	0+	1-	1°	1+	1°	9-	5
21	129	145	2-	1-	1°	1+	2+	3°	3°	3-	16-	9
D 22	135	145	4°	3-	4-	4°	4+	3-	3-	2°	26	19
23	142	145	2°	2+	4-	3-	3+	3-	1+	2-	20-	11
QQ24	148	145	1-	1-	1°	1-	1-	1°	1-	1-	6	3
25	153	145	1-	1°	1+	1+	3°	3°	2-	2-	14-	7
26	150	145	1+	2+	2°	4-	3°	3°	3+	4°	23-	15
27	142	145	3+	3+	3°	3-	3-	1+	1+	1+	19	11
28	139	145	2-	2°	1-	1+	2-	3-	3°	2-	15-	8
QQ29	140	145	2-	2-	2-	1°	1+	1+	1°	1°	11-	5
30	134	145	1+	1+	1°	1°	2°	2+	3°	2°	14	7
QQ31	131	145	2°	1+	2°	2°	1°	1+	1°	1°	12-	5
QQ 1	130	145	1-	1-	1+	1+	1°	1-	1-	1-	7	4
QQ 2	130	145	1-	1°	1°	1+	1-	1°	1-	1+	8-	4
3	137	145	2-	4°	3+	2°	2+	3+	2°	1+	20	12
4	132	145	3°	2°	2-	1°	0+	0+	0+	2-	10+	6
5	132	145	1+	3-	1-	3°	3°	3+	3-	3+	20	12
6	144	145	3+	4°	3°	3°	2°	2+	4-	3-	24	16
7	136	144	3+	3°	3°	3+	3°	2°	2-	2+	22-	13
8	138	144	4+	3+	4-	1+	3-	2-	2-	3-	21+	14

[1]Monthly five quiet days (QQ), ten quiet days (Q), and five disturbed days (D).

recommended time lags after first converting K_p values to exospheric temperature increment by use of Table 2b in Jacchia (1971). Linearly interpolated values were read off for the times of the satellite accelerometer readings. To obtain the T_∞ variation due to location with respect to Jacchia's model of the subsolar heating bulge, values of the solar declination and of the latitude and local time of the density observation were used to linearly interpolate the ratio of the local temperature to the global minimum temperature as found in Table 1 of Jacchia (1971). The global minimum temperature is calculated from a knowledge of $F_{10.7}$ and $\overline{F_{10.7}}$ where $\overline{F_{10.7}}$ is a three solar rotation or 81-day average of $F_{10.7}$. The exospheric temperature increment due to K_p is added to the local temperature to obtain the value of T_∞. T_∞ was calculated for all density observations.

The next problem was the calculation of the coefficients for normalization of the observed density values. These coefficients varied with the standard altitude, height difference of the density observation from the standard altitude, and exospheric temperature. The basic relation for the normalization of density is

$$\rho_o = \rho \exp\left(\frac{Z - Z_o}{H}\right) \qquad (2)$$

where

ρ = density
z = altitude of the density value
H = local density scale height

The subscript "o" refers to values for the standard altitude. The principal difficulty in this facet of the normalization procedure is the variation of H with altitude. Over the height range of the observed density data, values for H are given for every 5 km below 160 km and every 10 km above 160 km in Table 6 of J71. A separate set of values is given for each 100°K increment of T_∞. For a given value of T_∞ (1000°K for example) the values of H were plotted against height, a smooth curve was drawn through the plotted points, and values of H were read off at one kilometer intervals. Additional values of H were then linearly interpolated from these at 0.2 km intervals. An example of the resulting interpolated H variation with altitude is given in the first two columns of Table 5. A factor of $\exp(\pm\frac{0.2}{H})$ was calculated for each value of H. Whether the altitude of the value of H was above or below the standard altitude determined the choice of the sign. For the value of H at the standard altitude the factor $\exp(\pm\frac{0.1}{H})$ was computed for both signs. These values are shown in the third column of Table 5. The values in the third column represent the normalization factor for density over a 0.2 km interval (0.1 km either side of the standard altitude)

TABLE 5

Extract from the Normalization Table for the 150 km Standard Altitude

Alt. (km)	$H_{1000°}$ (km)	exp $\frac{\pm 0.2}{H}$	Fact.	$H_{1100°}$ (km)	exp $\frac{\pm 0.2}{H}$	Fact.	Alt. (km)
		0.98862	0.91873		0.98883	0.92017	148.5
148.6	17.47			17.80			
		0.98866	0.92931		0.98887	0.93057	148.7
148.8	17.54			17.87			
		0.98871	0.93997		0.98891	0.94105	148.9
149.0	17.61			17.94			
		0.98875	0.95071		0.98896	0.95160	149.1
.2	17.68			18.01			
		0.98880	0.96152		0.98900	0.96222	.3
.4	17.75			18.08			
		0.98884	0.97242		0.98905	0.97292	.5
.6	17.82			18.16			
		0.98888	0.98339		0.98909	0.98370	.7
.8	17.89			18.23			
		0.99445	0.99445		0.99455	0.99455	.5
150.0	17.96			18.30			
		1.00558	1.00558		1.00548	1.00548	150.1
.2	18.03			18.37			
		1.01115	1.01680		1.01095	1.01649	.3
.4	18.10			18.44			
		1.01111	1.02810		1.01091	1.02757	.5
.6	18.17			18.52			
		1.01107	1.03948		1.01086	1.03873	.7
.8	18.24			18.59			
		1.01103	1.05094		1.01082	1.04996	.9
151.0	18.31			18.66			
		1.01098	1.06248		1.01078	1.06128	151.1
.2	18.38			18.73			
		1.01094	1.07410		1.01074	1.07267	151.3
.4	18.45			18.80			
		1.01090	1.08581		1.01070	1.08414	151.5

centered on height values on the left hand column of Table 5. The successive product of these factors to a given altitude from the standard altitude is given in the fourth column of Table 5. These are the normalization factors for converting density values at heights given in the right-hand column to the standard altitude of 150 km for an exospheric temperature of 1000°K. Similar results for 1100°K are also given in Table 5. A complete set of such tables was constructed for each standard altitude covering the height range of densities to be normalized to that altitude. Normalization factors were calculated for each 100°K increment between 1000°K and 1400°K (the T_∞ range of density data). Normalization factors for the even tenths of a kilometer of altitude were linearly interpolated from those calculated at the odd tenths (see Table 5). Linear interpolation was used to obtain the normalization factor at a T_∞ intermediate to the calculated values. A density value of $2.52 \times 10^{-12} gm/cm^3$ measured at 148.5 km and with T_∞ = 1056°K would be converted as follows:

From Table 5		1000°K	1100°K
148.5 Fact	=	0.91873	0.92017
Difference	=		0.00144
Interpolating for 1056°K	=		x 0.56
Interpolation increment	=		0.00081
Add back 1000°K factor	=		+0.91873
Final normalization factor	=		0.91954
Times the density at 148.5 km	=		x 2.52

Density value normalized to 150 km = $2.32 \times 10^{-12} gm/cm^3$.

A complete set of these tables is included in the appendix.

Use of the normalization tables derived in the same manner as the portion shown in Table 5 does not introduce any error into the normalization data other than that inherent in J71. The T_∞ calculations are accurate to within ±2°K. The error introduced by an inaccurate T_∞ depends upon the size of the normalization interval. For a 100°K error in T_∞ the maximum resulting error in the normalization factor in the entire set of normalization tables is 1.3 percent for a 10 km interval. The normalization factors were checked against the density values in Table 6 of J71. Density values are given in Table 6 of J71 for the same intervals as the scale height. Hence the normalization factor for any 5 or 10 km interval of the table could be multiplied by the density at that level and the resulting "normalized" density could then be checked against the table density value. For example the density value at 210 km for T_∞ = 1000° in Table 6 of J71 could be normalized to 200 km and compared with the 200 km density value for T_∞ = 1000°K given in the same table. Such a check was made for all the tables of normalization factors at each standard altitude for all the T_∞ values used, and over all possible 5 or 10 km intervals where density values for confirmation were available. The density values in Table 6 of J71 were given to four significant figures and in no case was a "normalized" density different from the value at the standard altitude by more than one in the

fourth significant figure. This confirms the complete accuracy of the tables of factors constructed for the normalization of density values.

The largest uncertainty in the normalization process is the model used for calculating exospheric temperature, T_∞ , at high latitudes and particularly during geomagnetically disturbed conditions. Orbital decay derived densities from high inclination satellites have shown that the atmospheric response to changes in K_p is enhanced at high latitudes. Jacchia et al (1967) report a 15-20% greater density response to ΔK_p for latitudes above 55°N as compared to lower latitudes. At 65° the density response has been found to be 20% higher than at the equator (Jacchia, 1970). Marcos et al (1971) also found the density response to geomagnetic activity to increase from the equator to high latitudes. In a very comprehensive analysis of orbital decay measurements in the 250-800 km altitude range for over 210 geomagnetic storms the following relation was obtained by Roemer (1971a):

$$\Delta T_\infty = \bar{K}_p \, (21.4 \sin |\phi| + 17.9) + 0.03 \exp(\bar{K}_p) \pm 83°K \qquad (3)$$

where

ΔT_∞ = exospheric heating increment due to K_p
$\bar{K}_p$ = the 0.4 day average of K_p
ϕ = geographic latitude

This result yields an increase from 119°K to 226°K between 0° and 90° latitude for a $\bar{K}_p$ of 5. Roemer (1971b) later

reported that the maximum response was at 60° to 70° but few data were available at latitudes above 70° to confirm this. Density gauge measurements from Explorer 32 made between 300 and 400 km showed that high latitude density was 20% higher than at low latitudes even on quiet days and that during geomagnetic disturbances the density between 55° and 65° exceeded that at the equator by a factor of three (Newton and Pelz, 1969). Composition measurements from OGO-6 made at 500 km during a magnetic storm showed a 400° difference in T_∞ at the equator and between 60° and 80° geomagnetic latitude (Taeusch et al, 1971b). Doppler temperatures from the 6300Å line of OI observed from OGO-6 before and during a 3 day geomagnetic storm have revealed large irregular temperature increases of 350°K at 275 km in the auroral zone (Blamont and Luton, 1972). Equatorial changes were smooth and much smaller (50°K) and mid-latitude changes were intermediate (110-125°K). After the storm there was little latitudinal temperature gradient. Even during extended quiet periods before the storm the temperatures observed at high latitudes were always greatest. The temperature maximum was found at the geomagnetic poles during a storm and not at the auroral zone (Blamont and Luton, 1972). A 400°K underestimate in T_∞ at a T_∞ value of 1300°K (geomagnetic storm condition during the latter portion of LOGACS) would result in a density normalization error of 2.4% over the interval from 210 to 200 km.

Over the same height interval at lower altitudes the error would be less. Thus the normalization process is relatively unaffected even by a severe underestimate of T_∞ at high latitudes during geomagnetic storm conditions.

The above calculation assumed the static diffusion profile of J71. During an intense geomagnetic storm the assumption of a state of static diffusion equilibrium would not be valid. Further, the altitude profile of auroral heating might not be the same as that which gave the shape of temperature profile used in J71. However, even with these limitations the maximum error in the normalized densities is estimated to be less than 4 percent. Such an error would occur only in those densities normalized over a 10 km interval during the peak of the geomagnetic storm that occurred during the latter day and a half of the LOGACS flight. The maximum anticipated error due to the normalization procedure would be considerably less for the major portion of the density data.

The normalized density values for LOGACS are shown in Figures 1, 2, and 3 plotted against geographic latitude. Densities normalized to 200, 180, 160, and 150 km obtained while the LOGACS vehicle was approaching perigee are displayed in Figure 1. In Figure 1 circles are used for density normalized to 150 km, triangles for 160 km, upside down triangles for 180 km, and squares for 200 km. The densities around perigee, normalized to 145 km, are

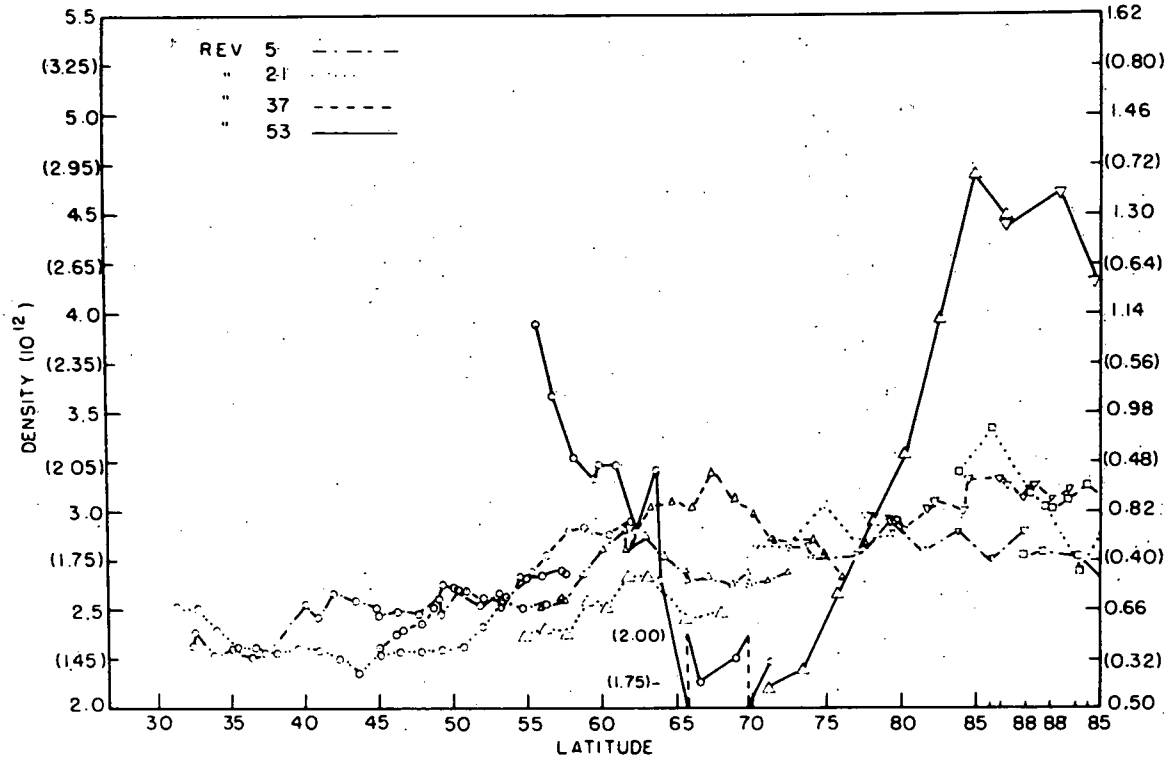

Figure 1a

Figure 1. LOGACS downleg densities, normalized to 200, 180, 160, and 150 km. The circles (o), triangles (Δ), upside-down triangles (∇), and squares (□) refer to density values normalized to 150, 160, and 200 km respectively. The scales for the 150 and 160 km density are interposed on the left side, the 160 km scale is in parentheses. The 180 and 200 km scales are interposed on the right side with the 200 km scale in parentheses. All density values are in units of gm/cm^3 and scaled by 10^{12}.

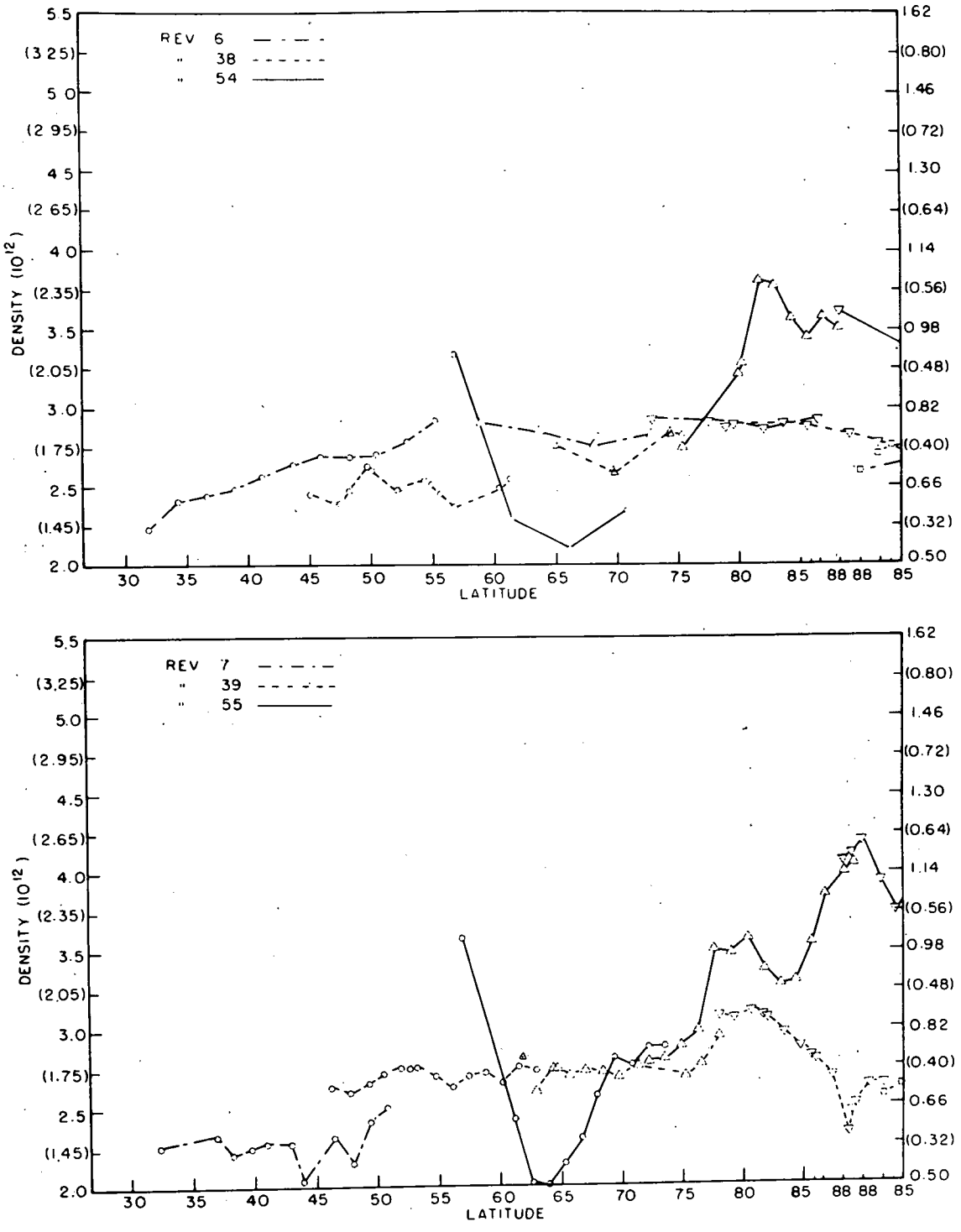

Figure 1b (top) and 1c (bottom)

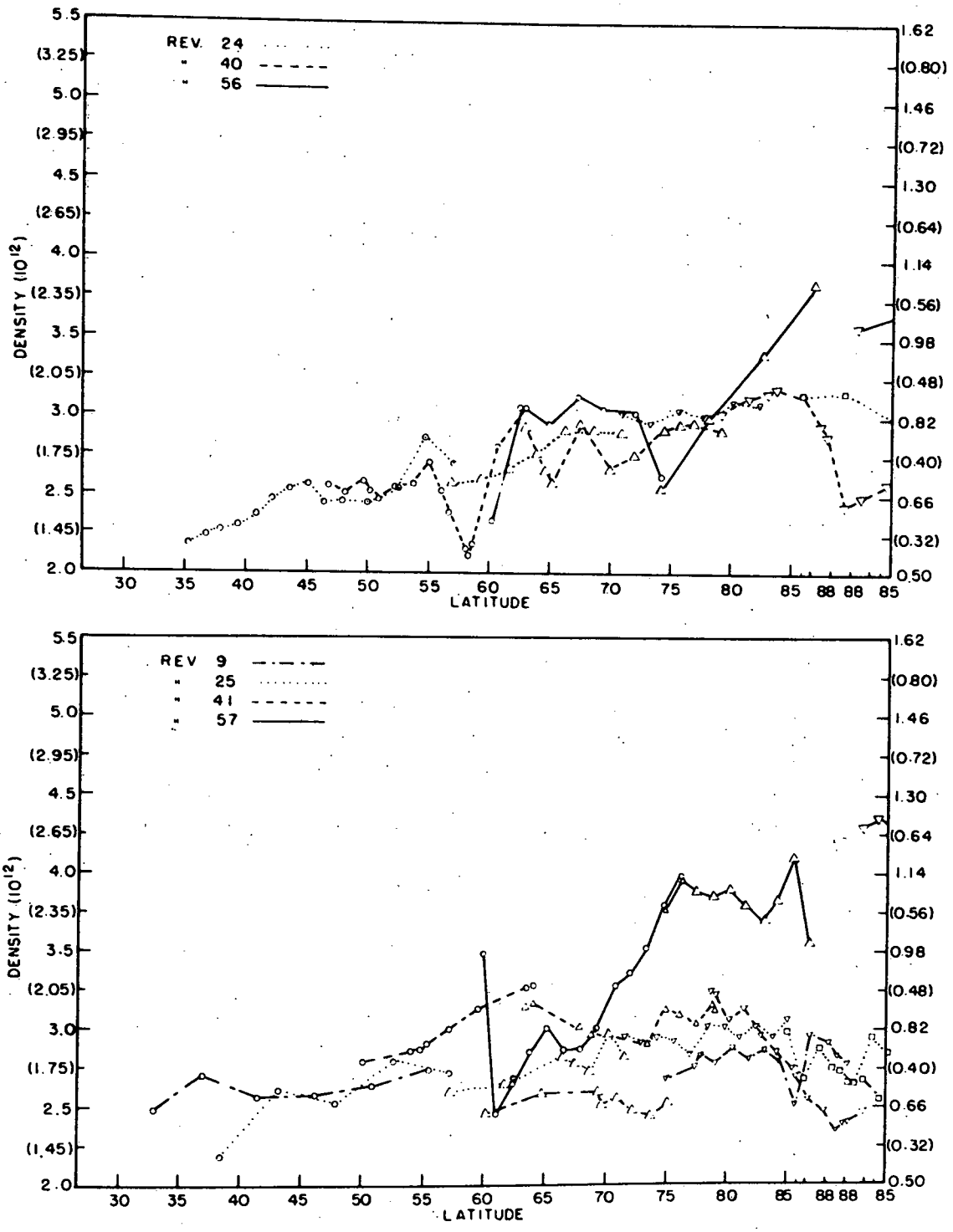

Figure 1d (top) and 1e (bottom)

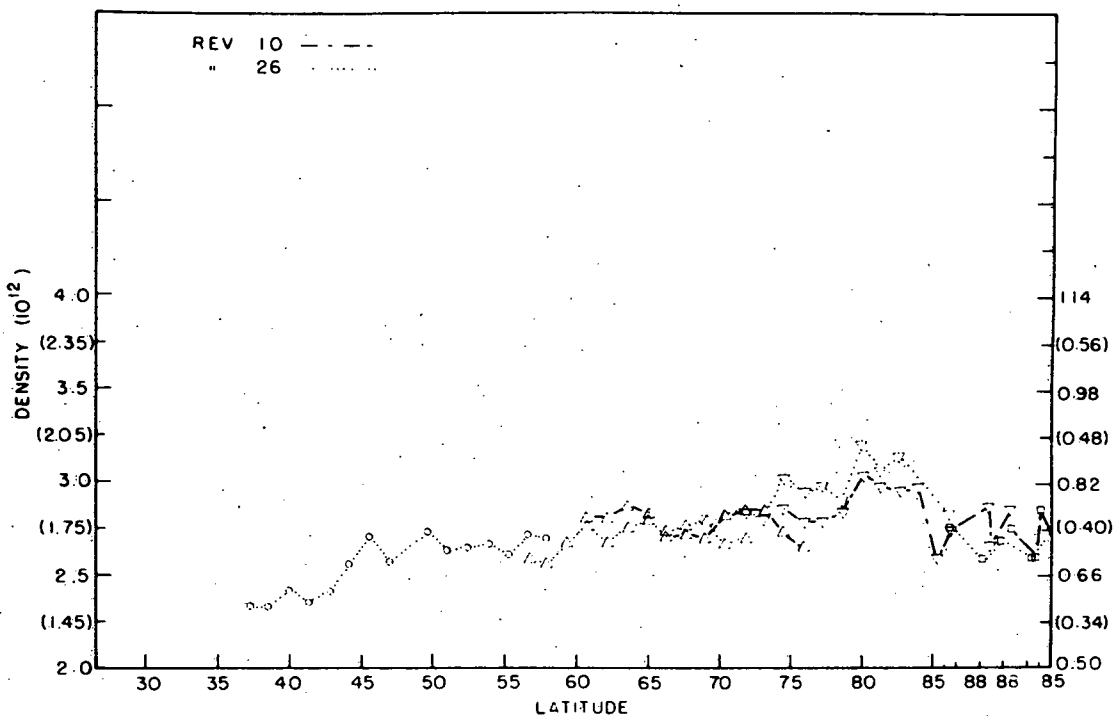

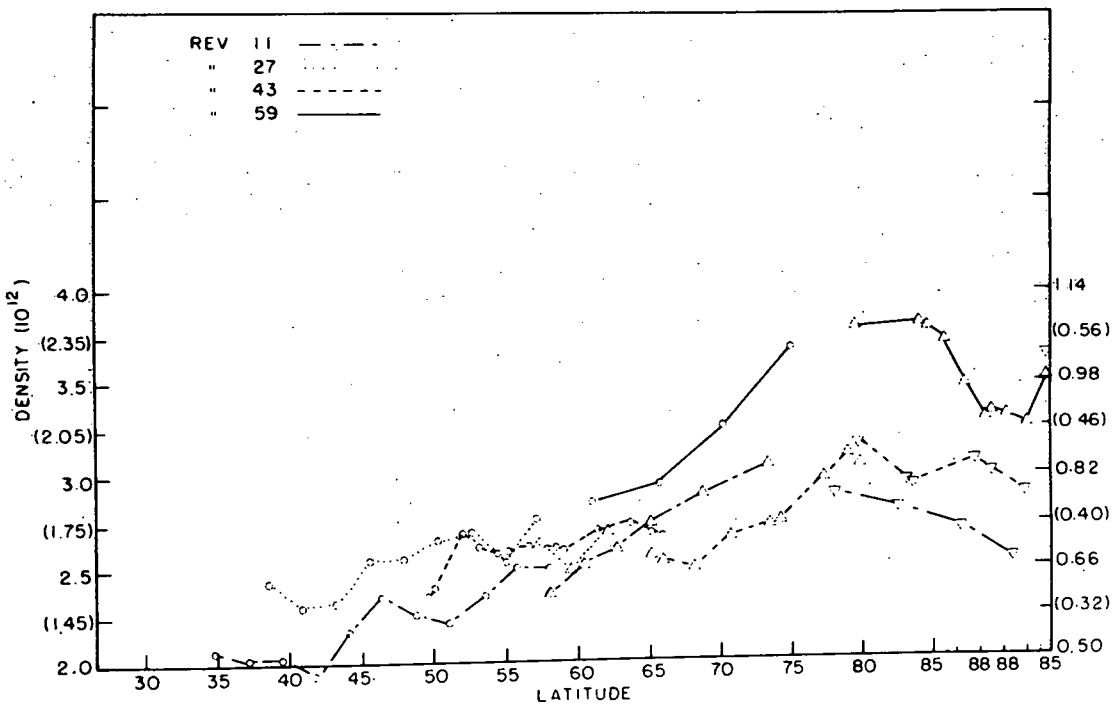

Figure 1f (top) and 1g (bottom)

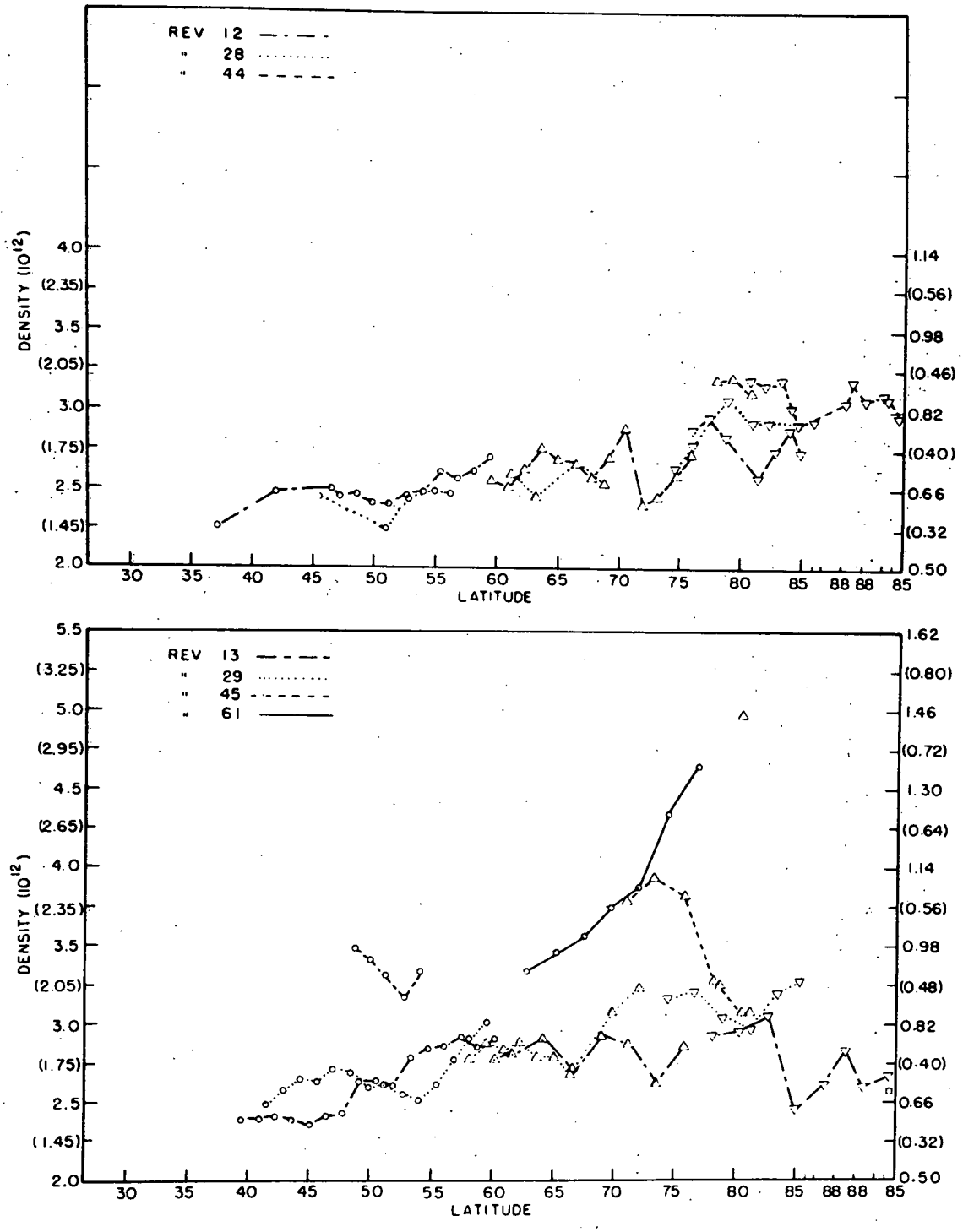

Figure 1h (top) and 1i(bottom)

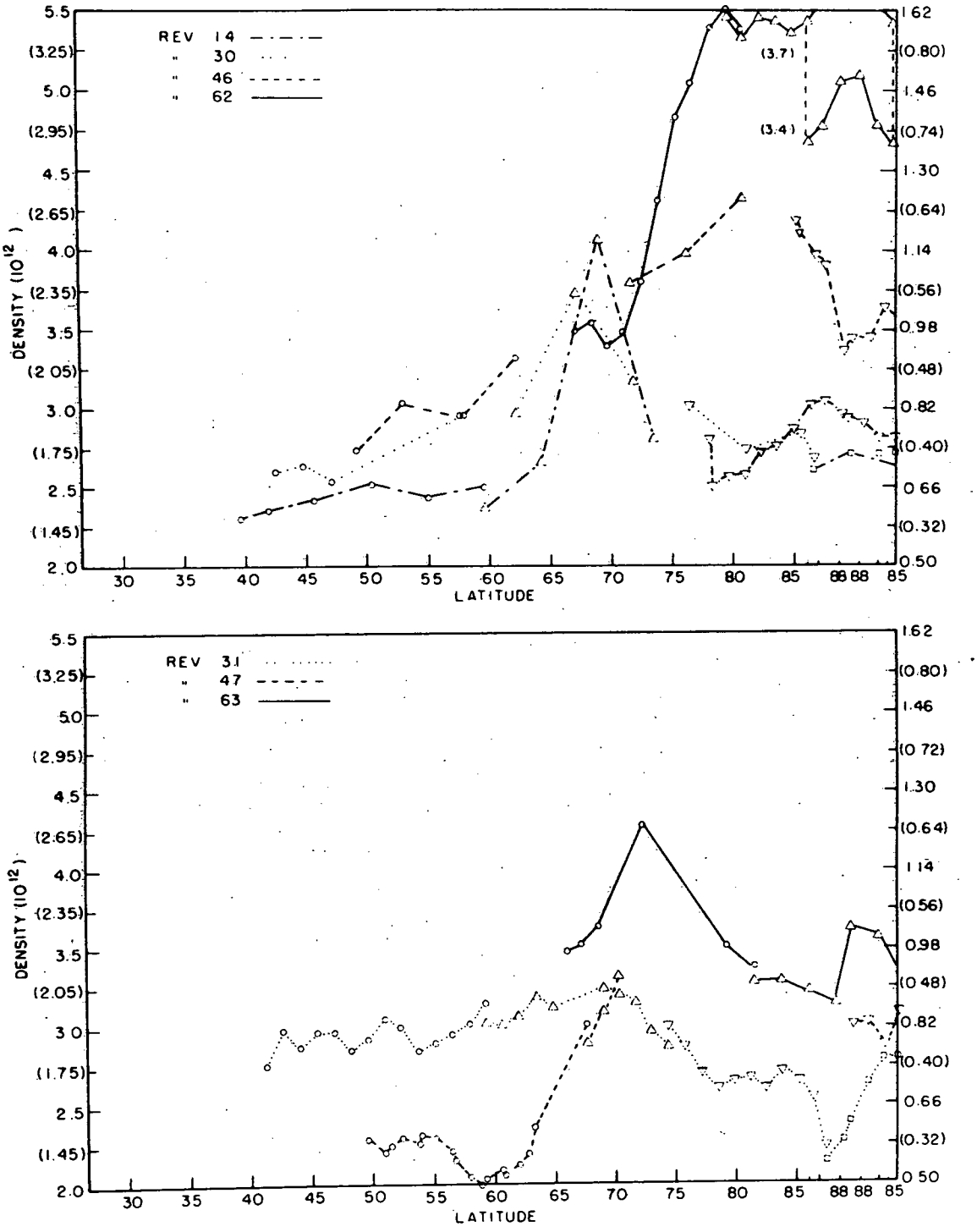

Figure 1j (top) and 1k (bottom)

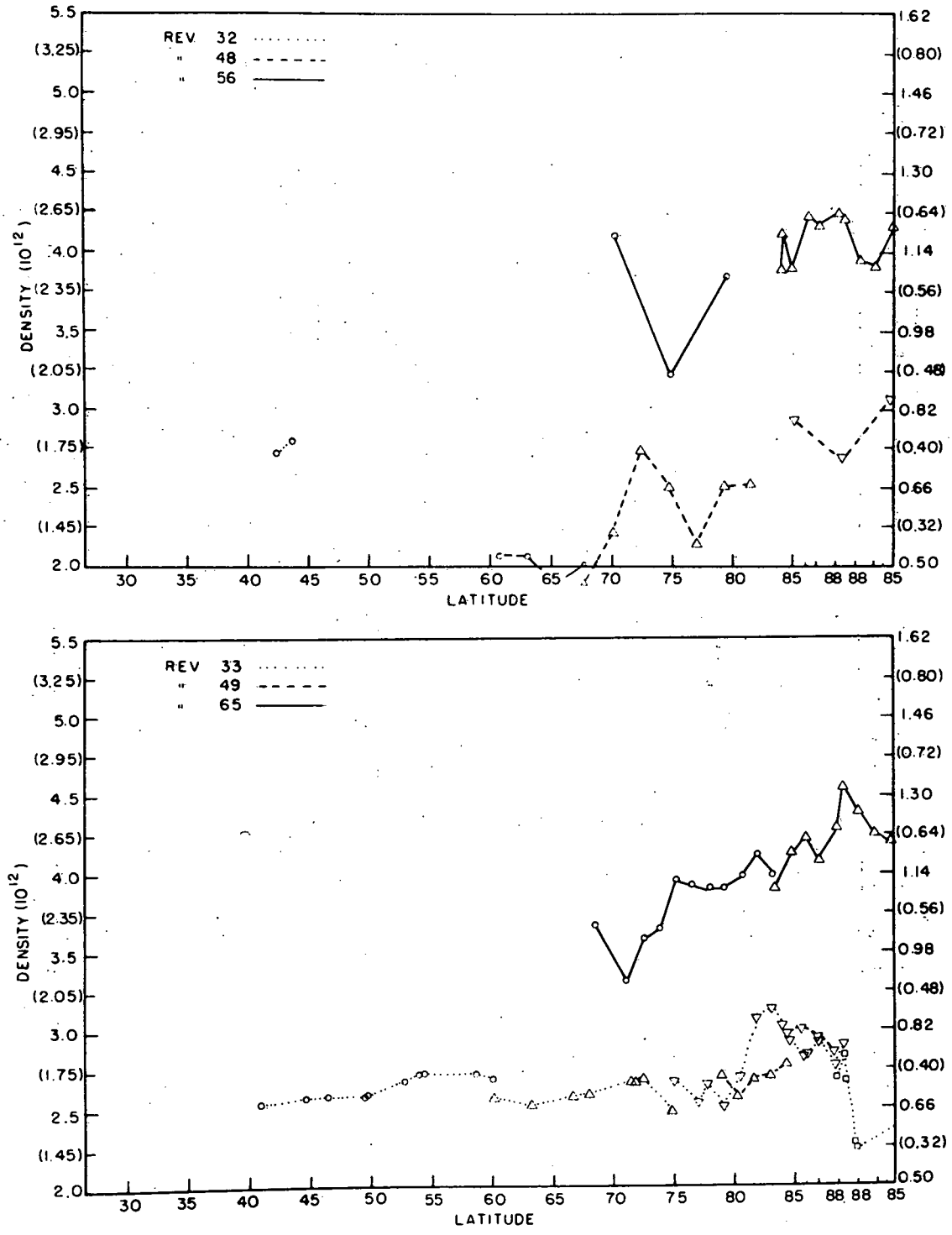

Figure 11 (top) and 1m (bottom)

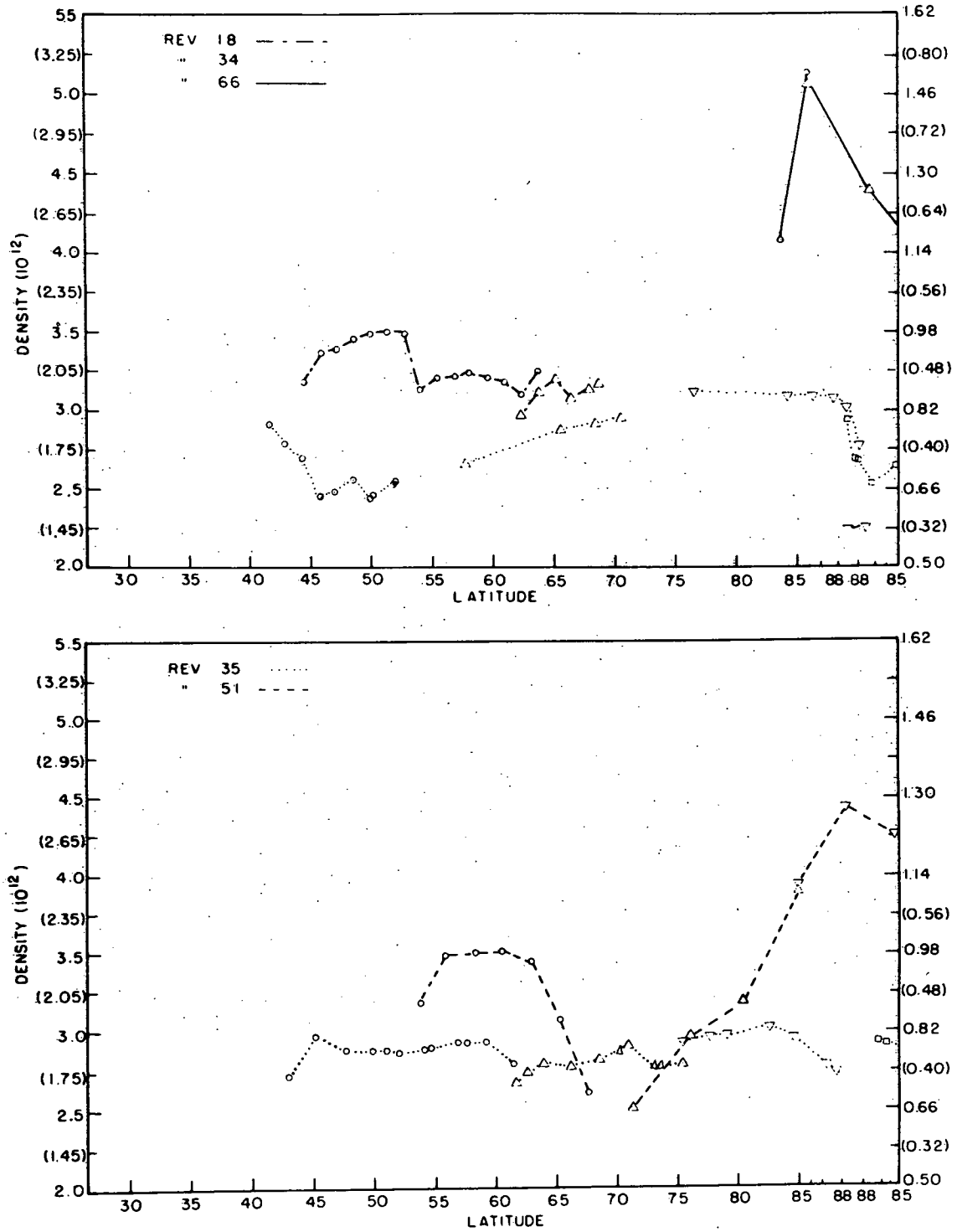

Figure 1n (top) and 1o (bottom)

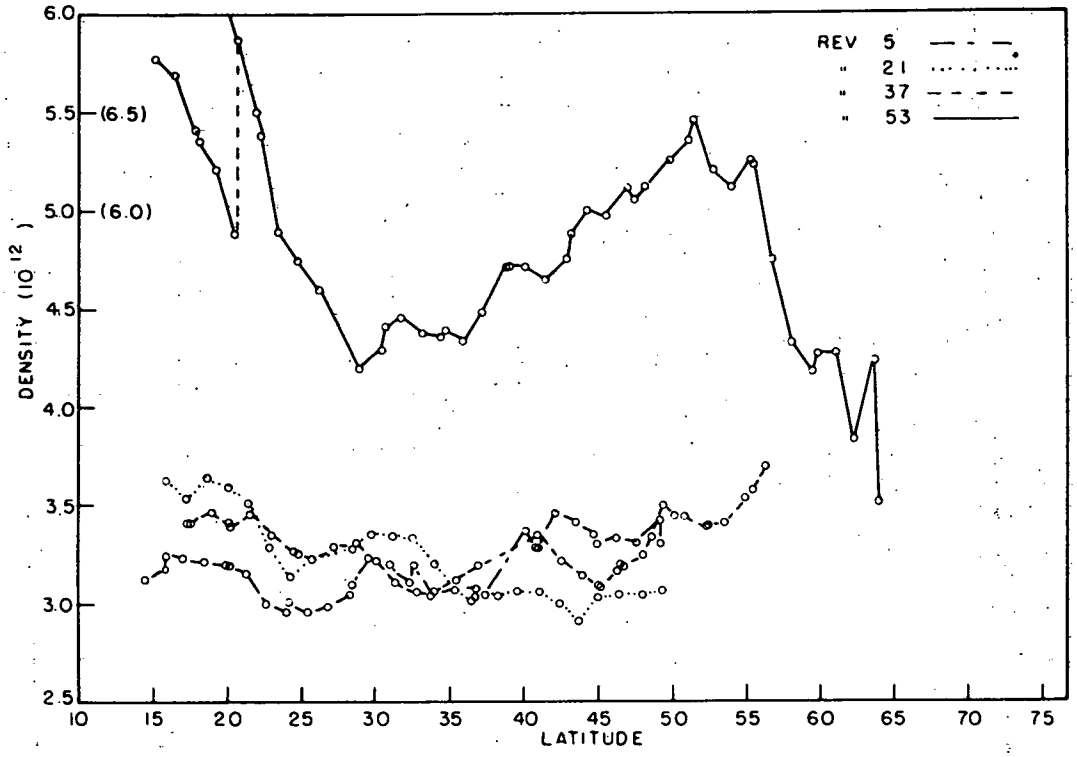

Figure 2a

Figure 2. LOGACS densities around perigee, normalized to 145 km. The density values have the units of gm/cm^3 and are scaled by 10^{12}.

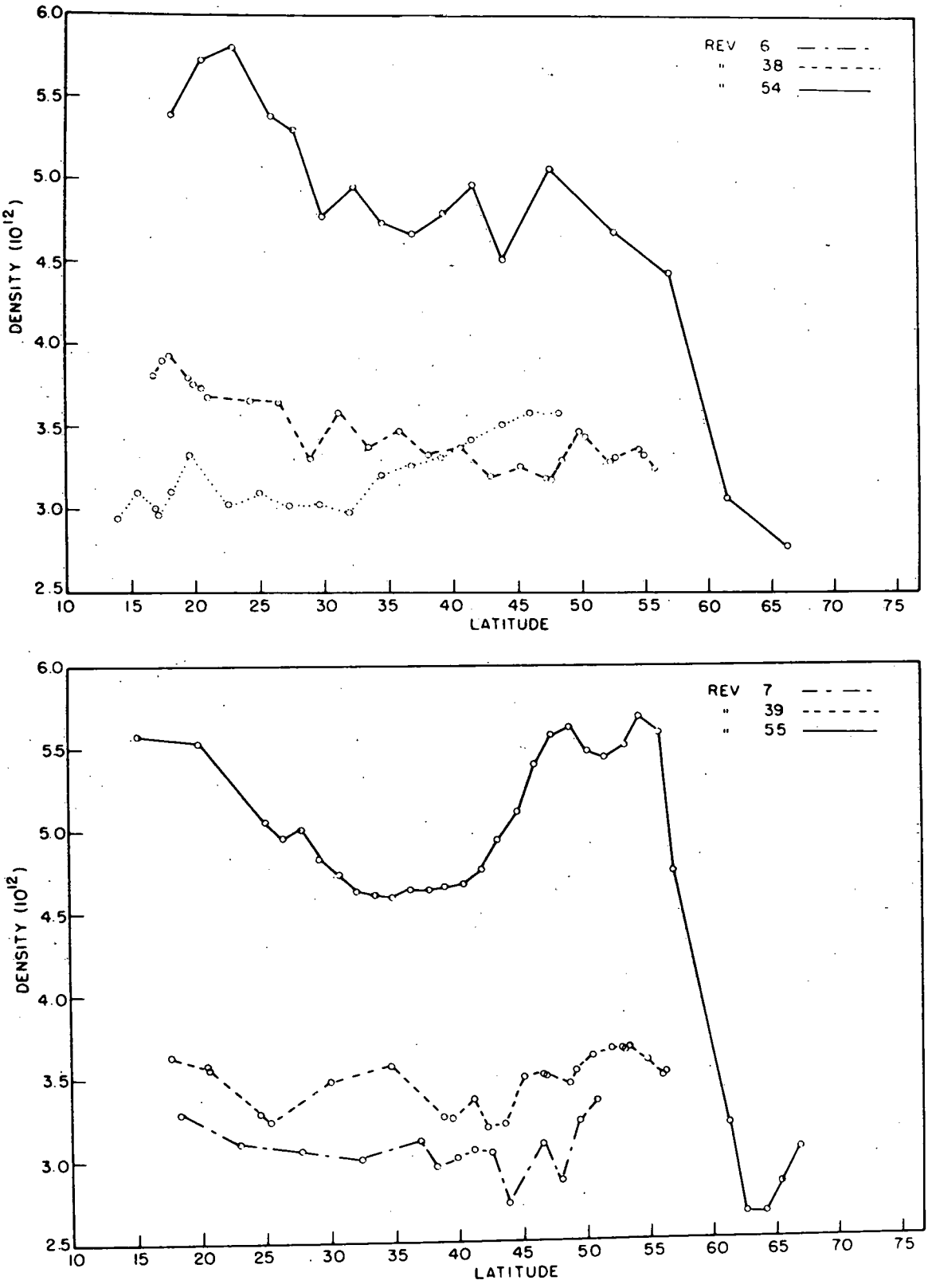

Figure 2b (top) and 2c (bottom)

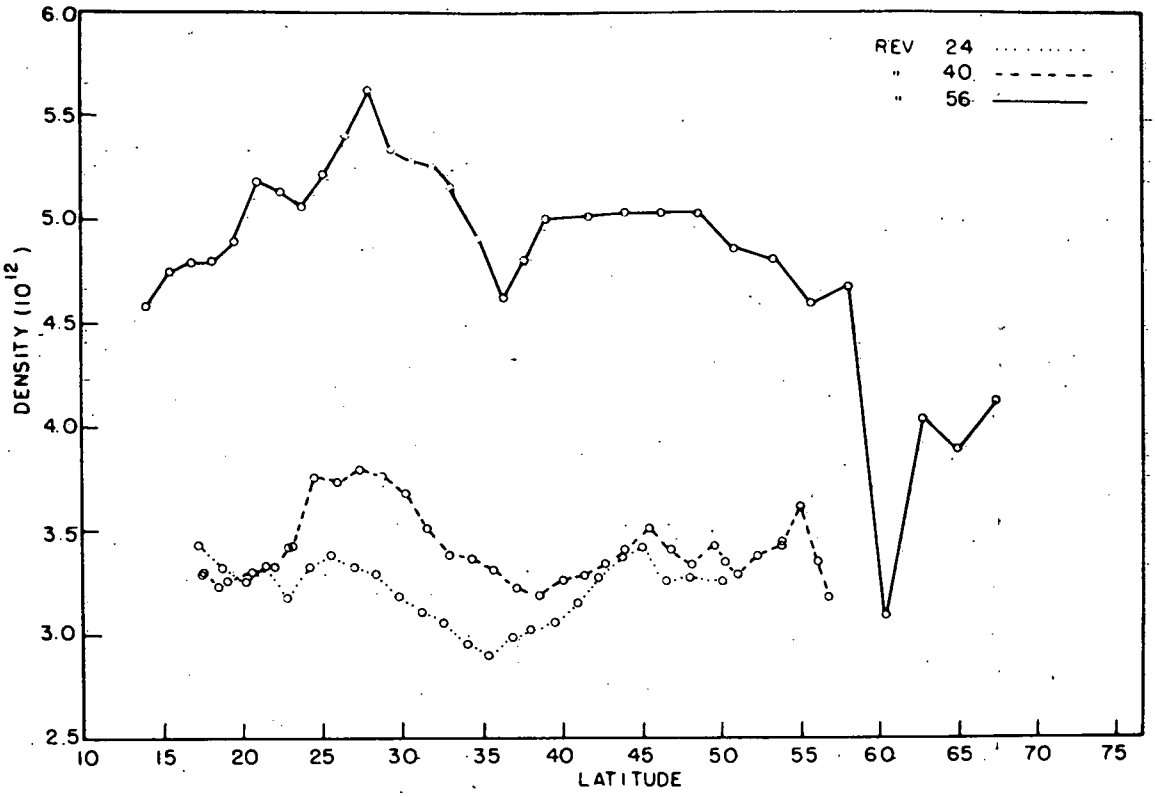

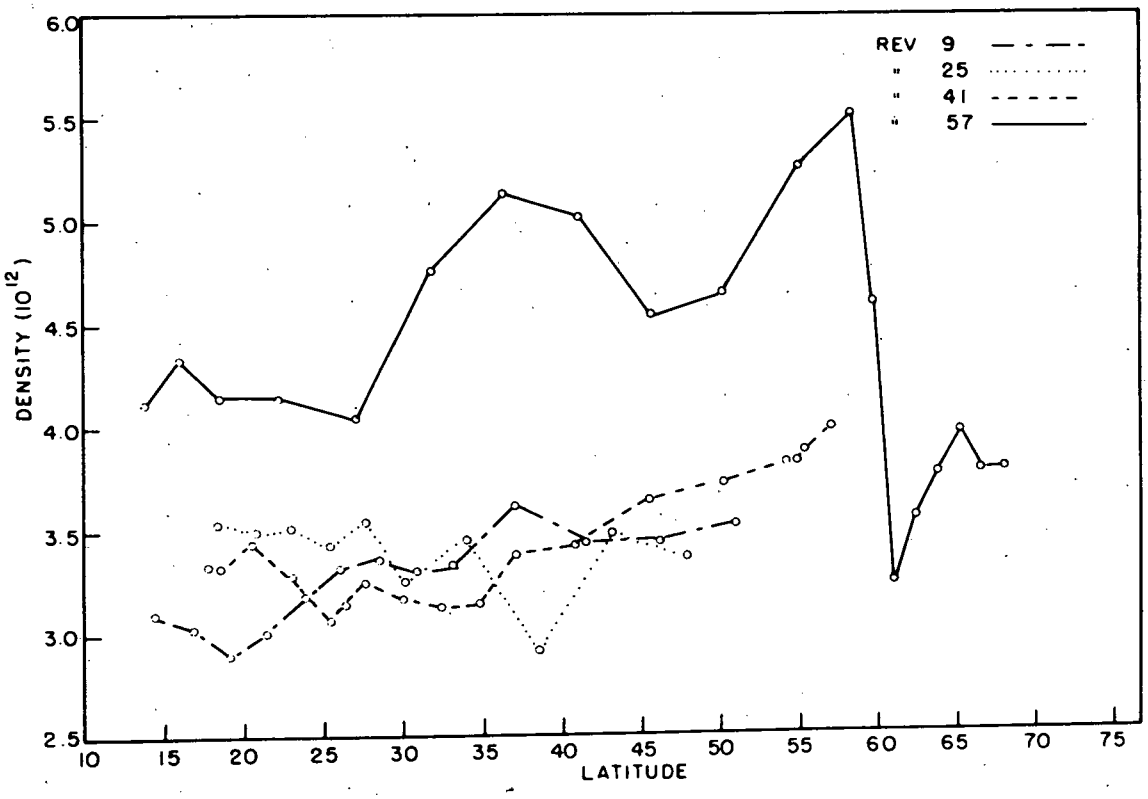

Figure 2d (top) and 2e (bottom)

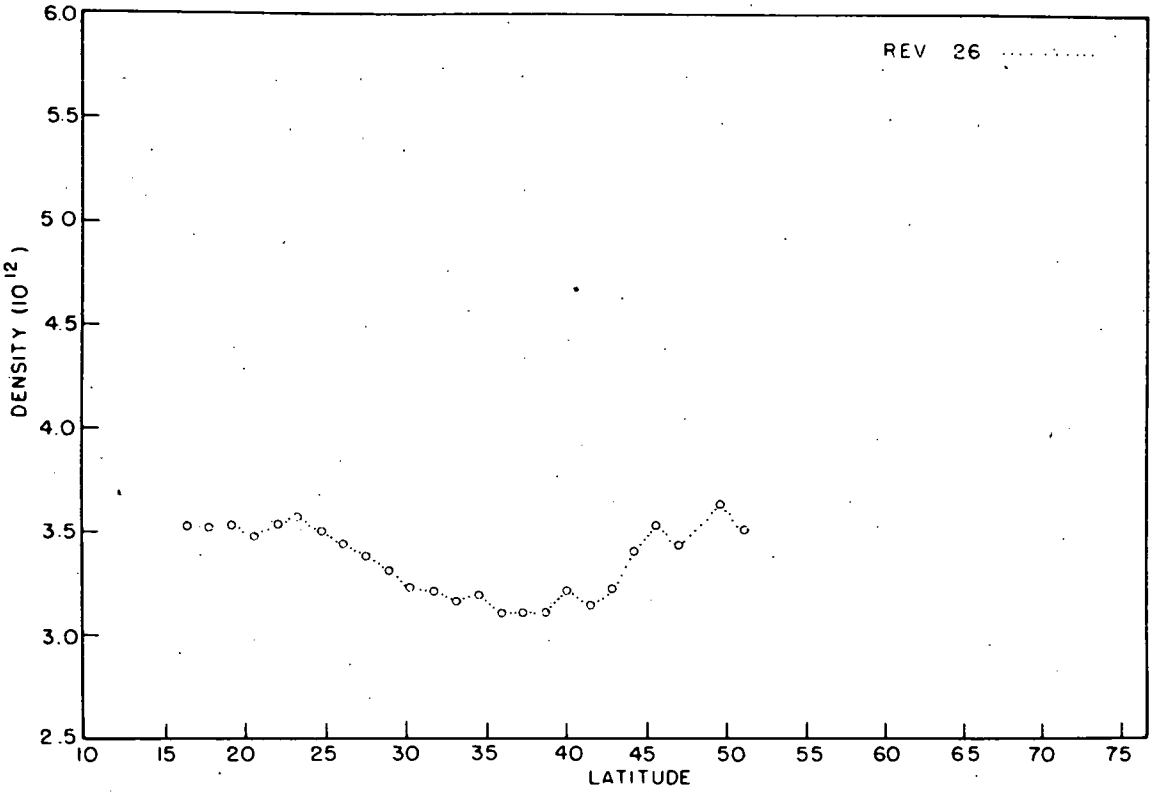

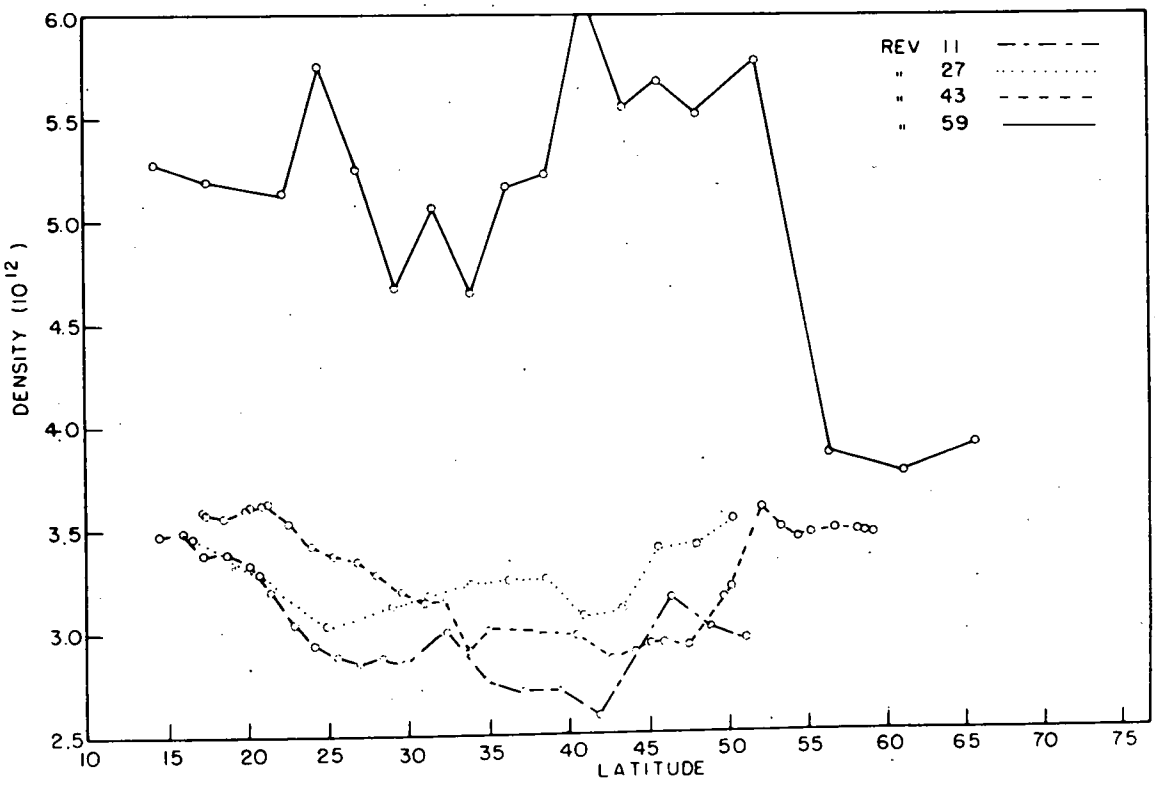

Figure 2f (top) and 2g (bottom)

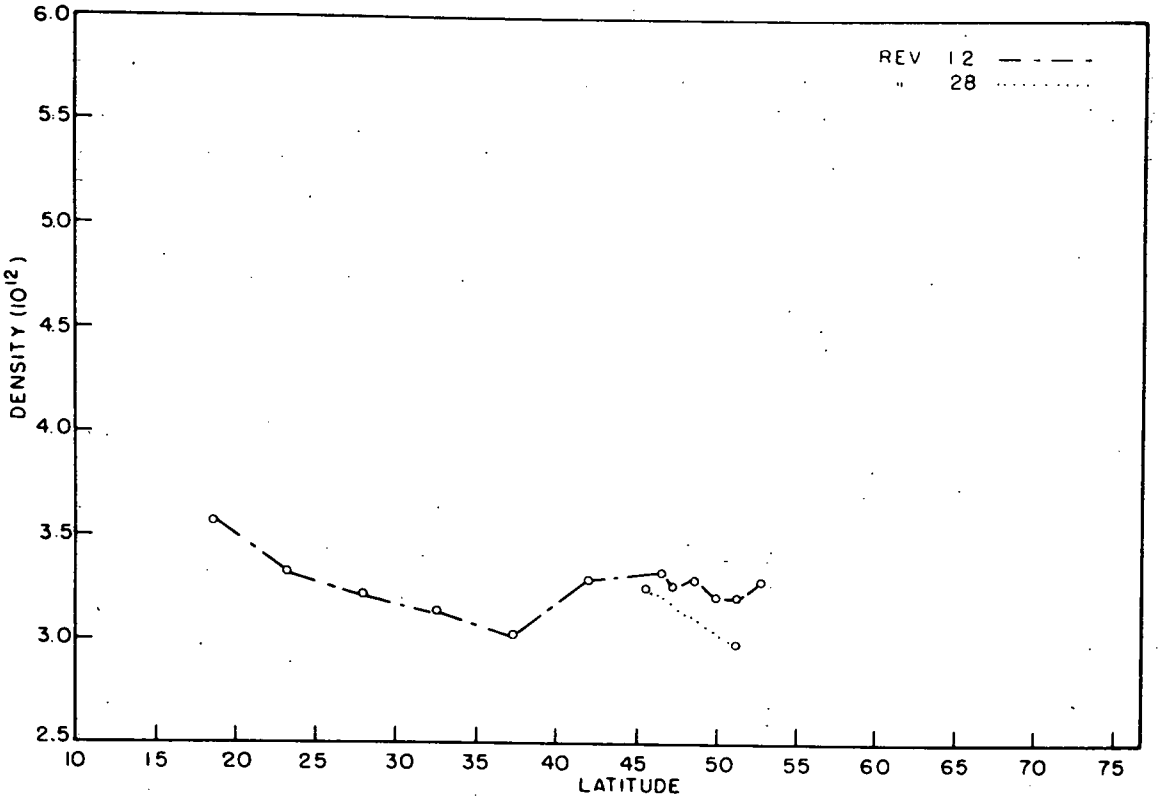

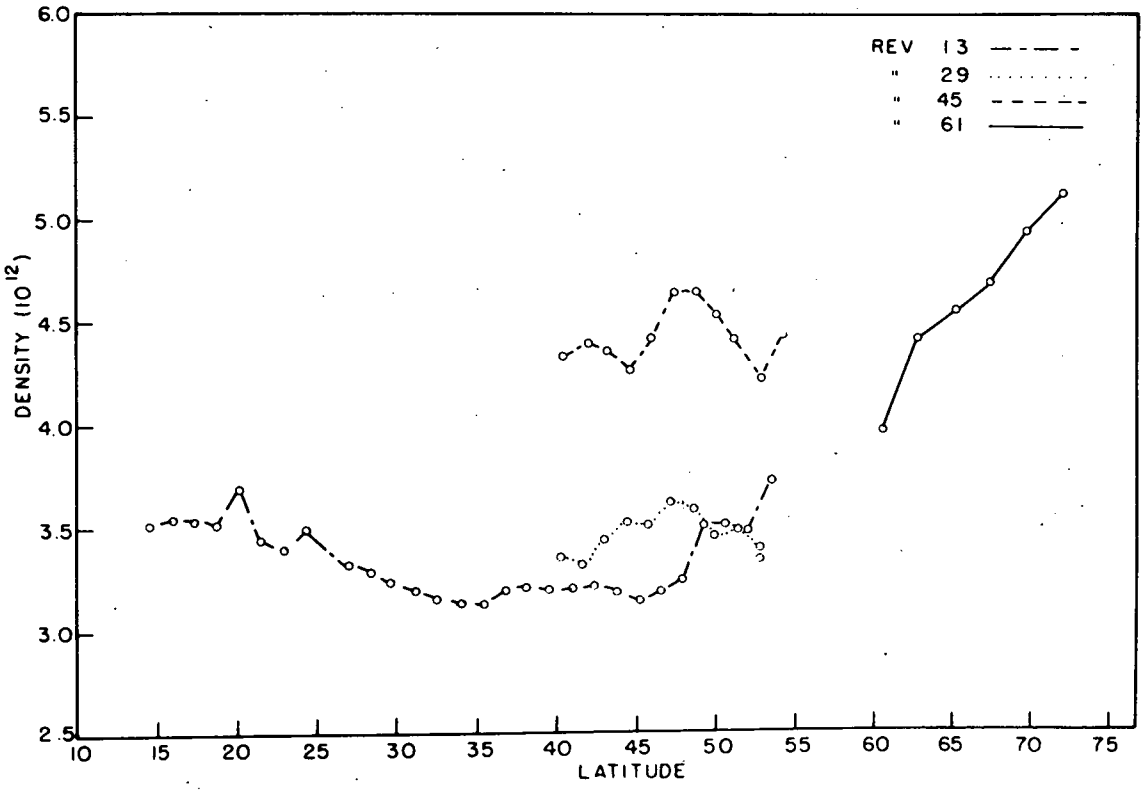

Figure 2h (top) and 2i (bottom)

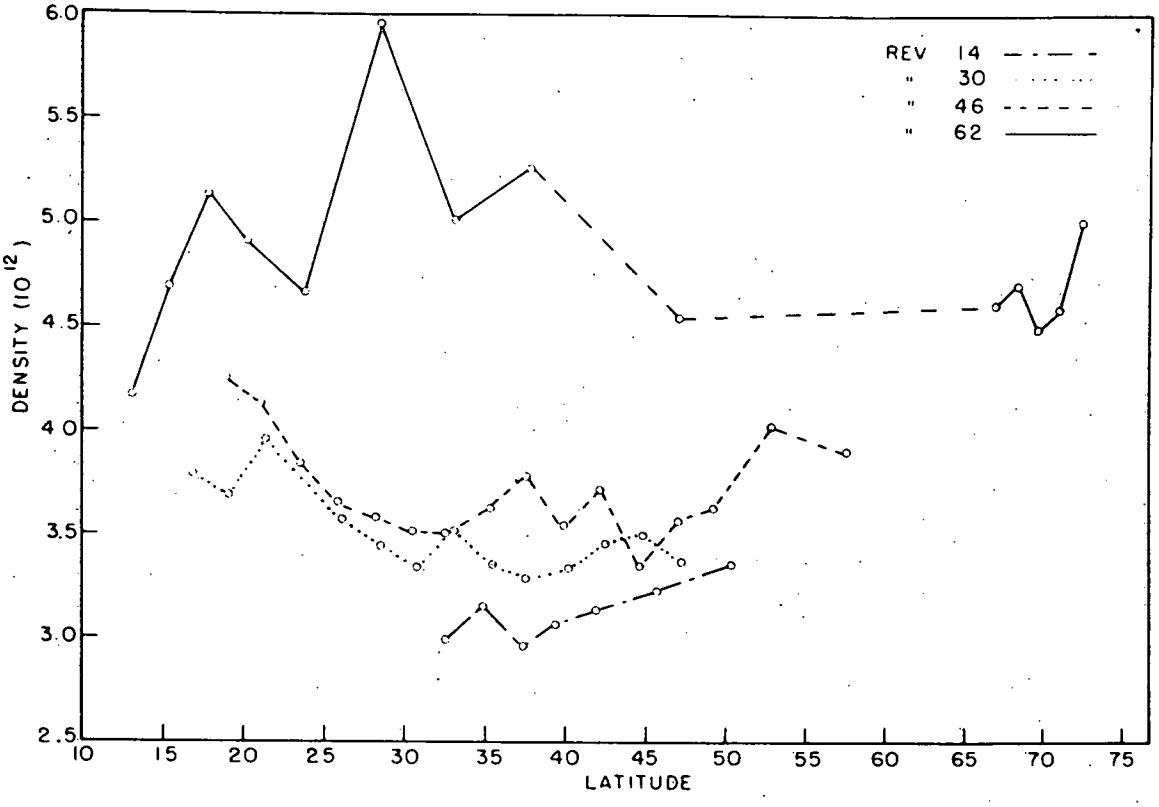

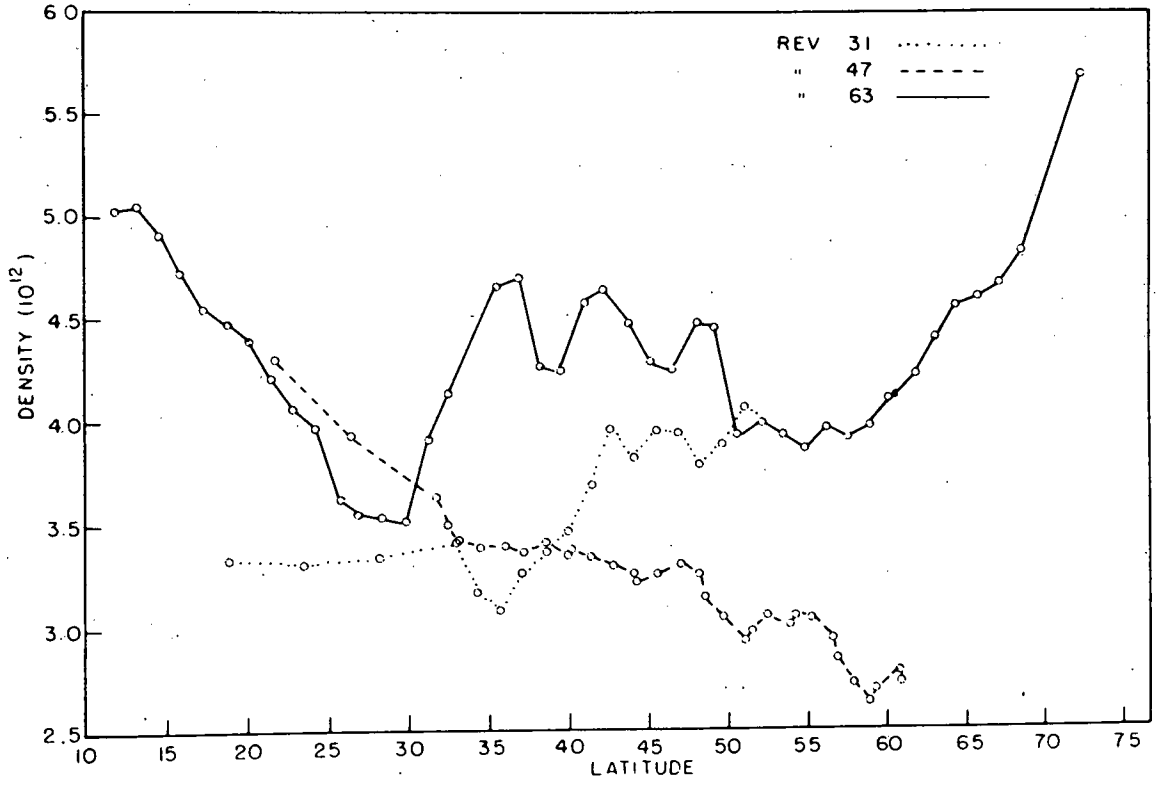

Figure 2j (top) and 2k (bottom)

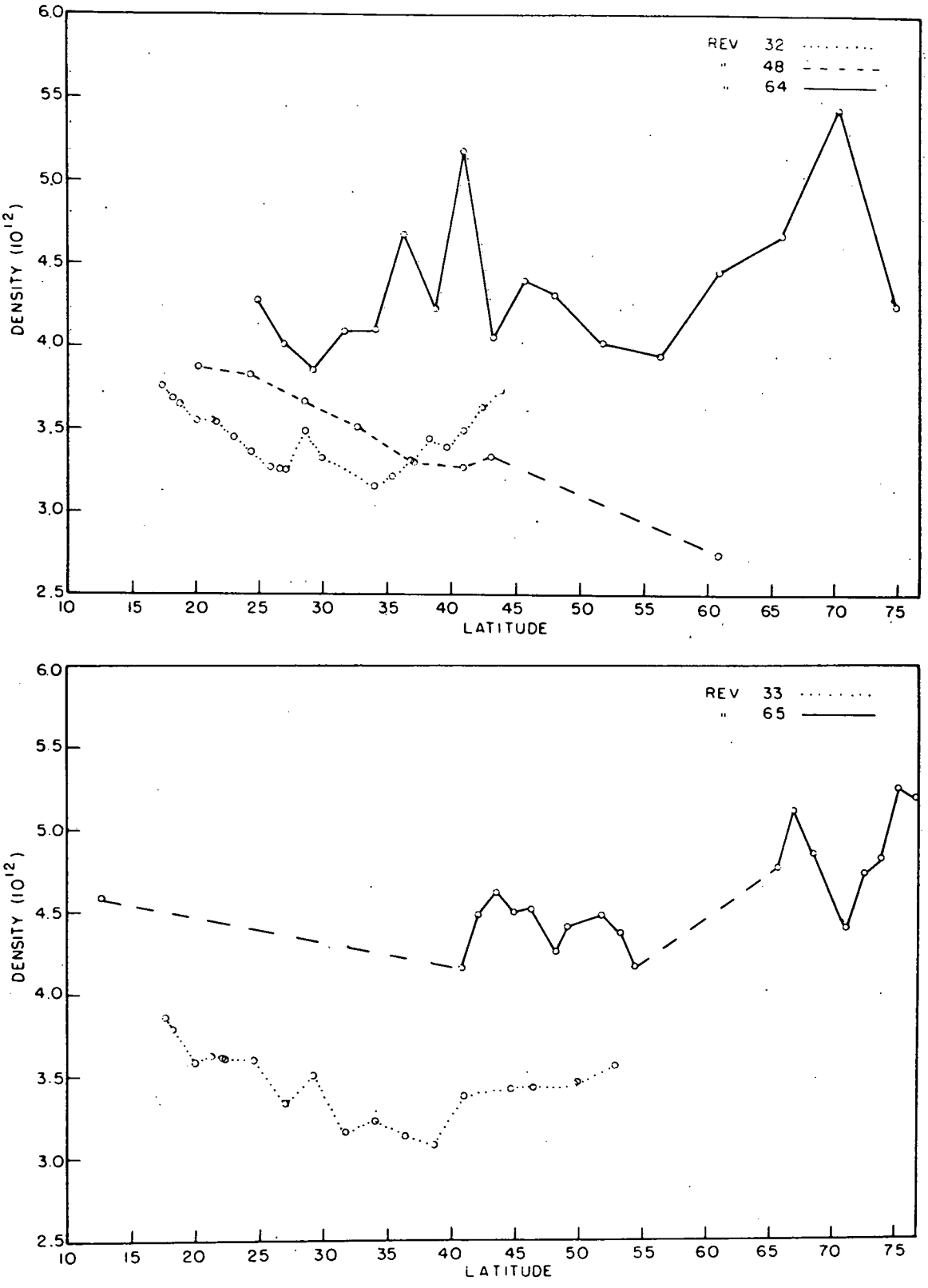

Figure 21 (top) and 2m (bottom)

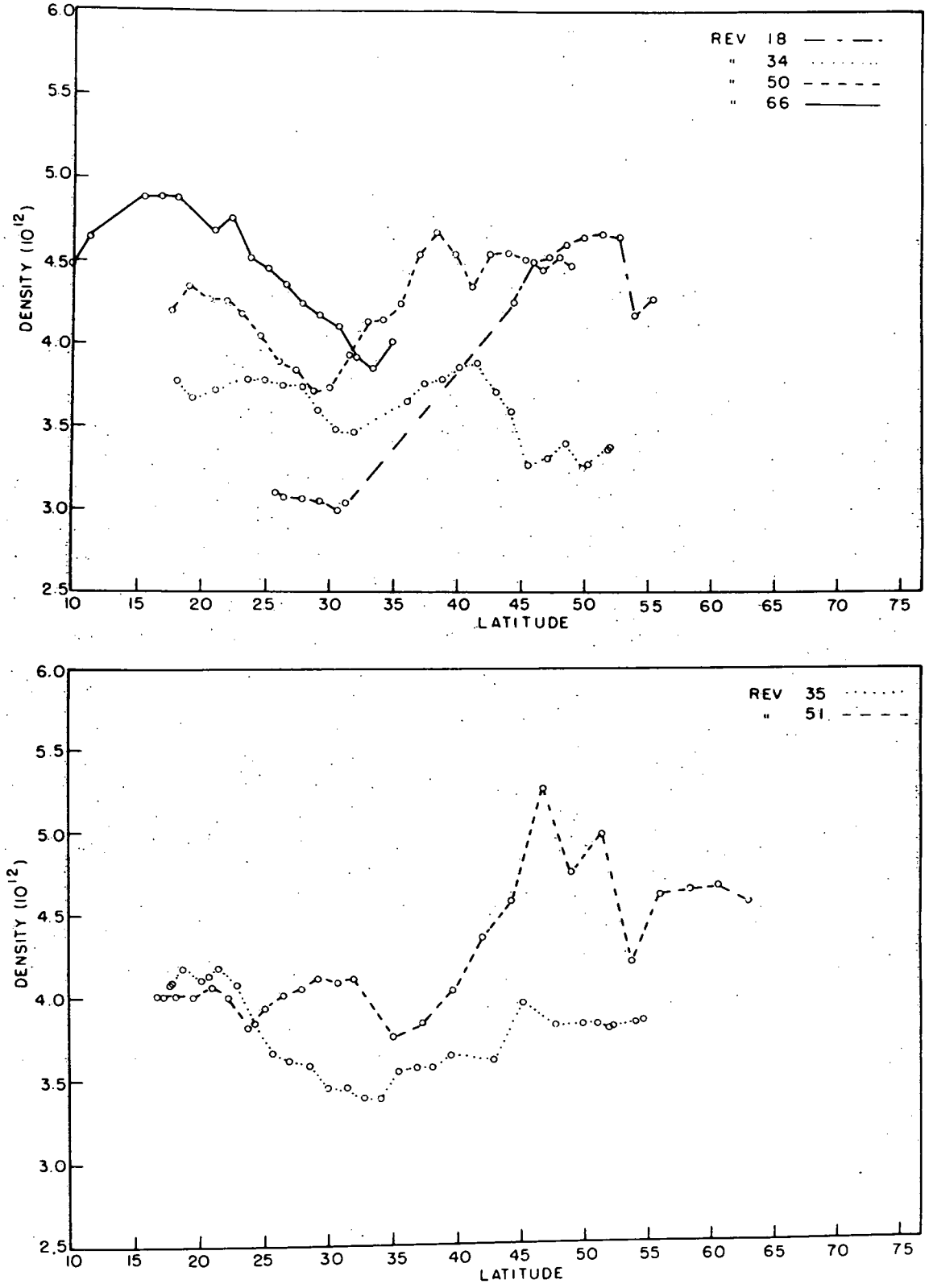

Figure 2n (top) and 2o (bottom)

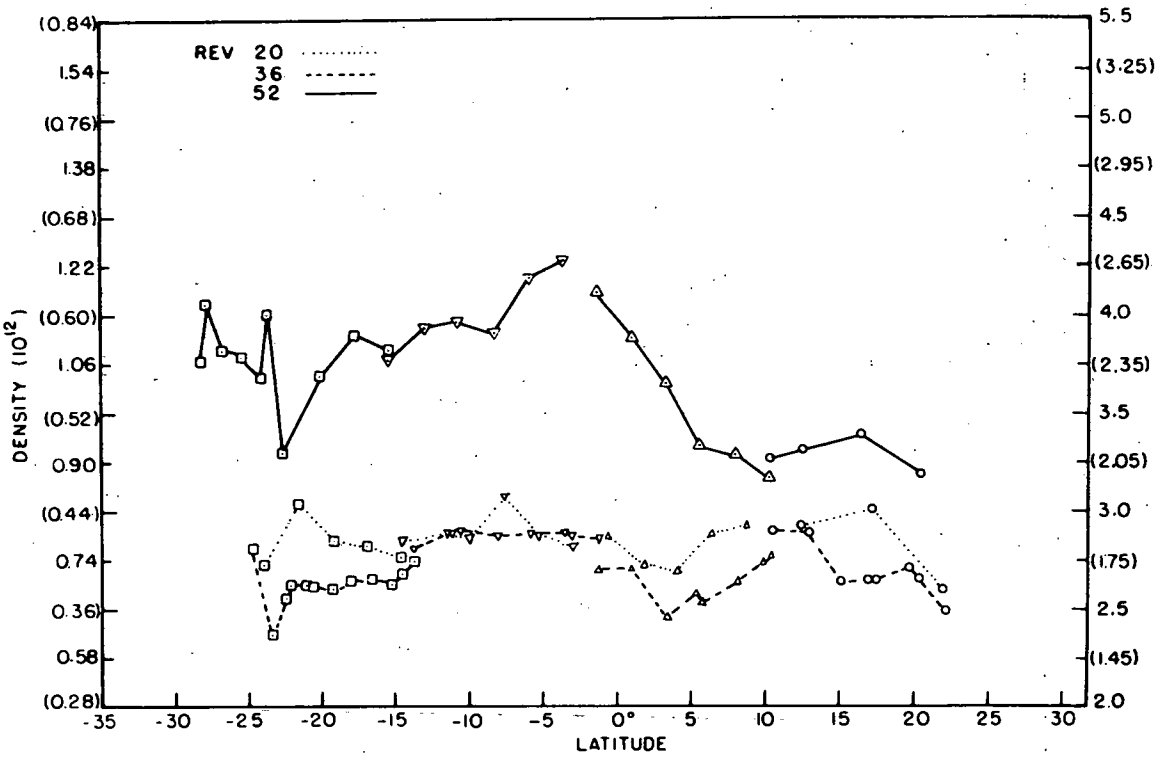

Figure 3a

Figure 3. LOGACS upleg densities, normalized to 150, 160, 180, and 200 km. The circles (o), triangles (Δ), upside-down triangles (∇), and squares (□) refer to density values normalized to 150, 160, 180, and 200 km respectively. The scales for the 150 and 160 km density are interposed on the right with the 160 km scale in parentheses. The scales for the 180 and 200 km density are interposed on the left with the 200 km scale in parentheses. All density values are in units of gm/cm^3 and scaled by 10^{12}.

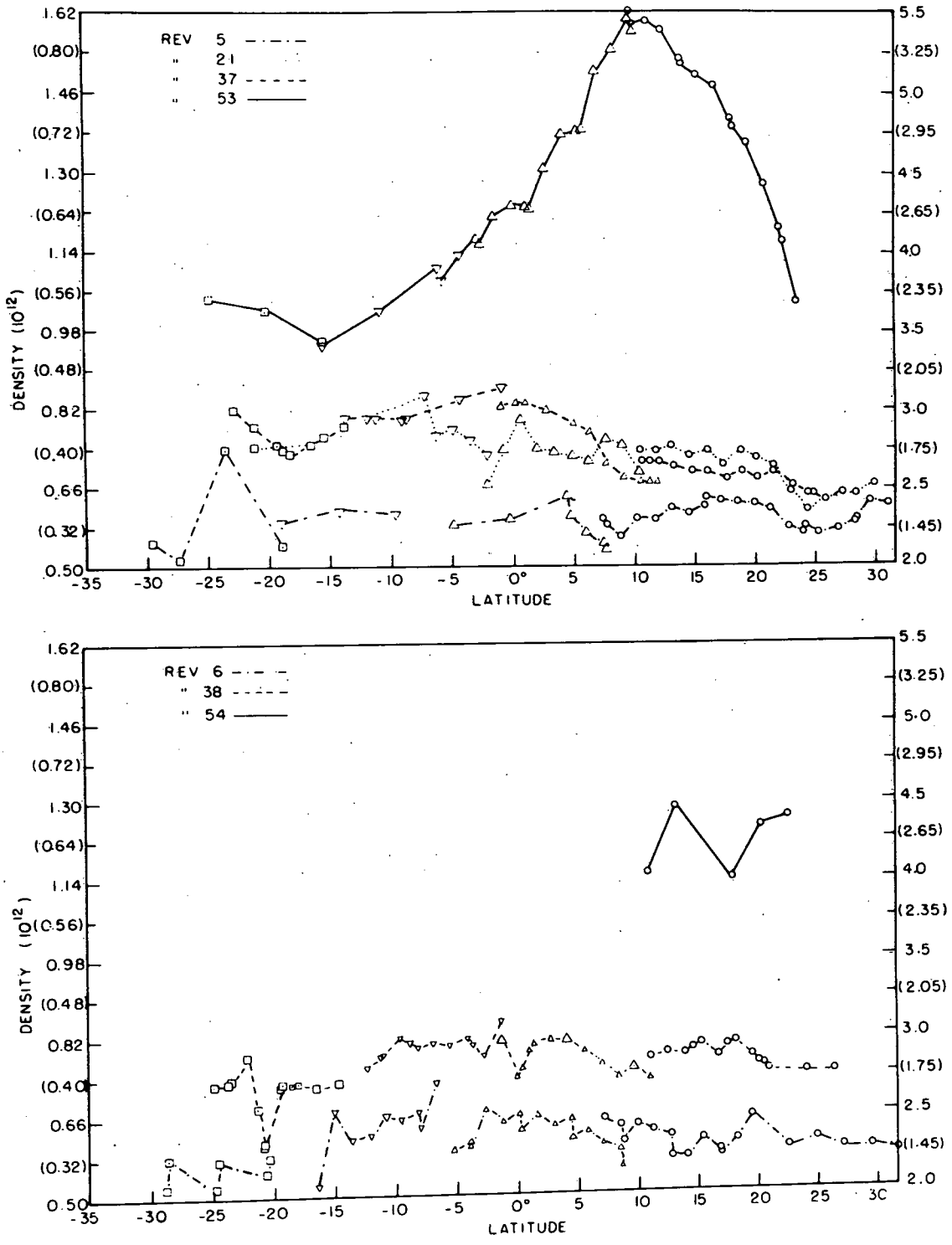

Figure 3b (top) and 3c (bottom)

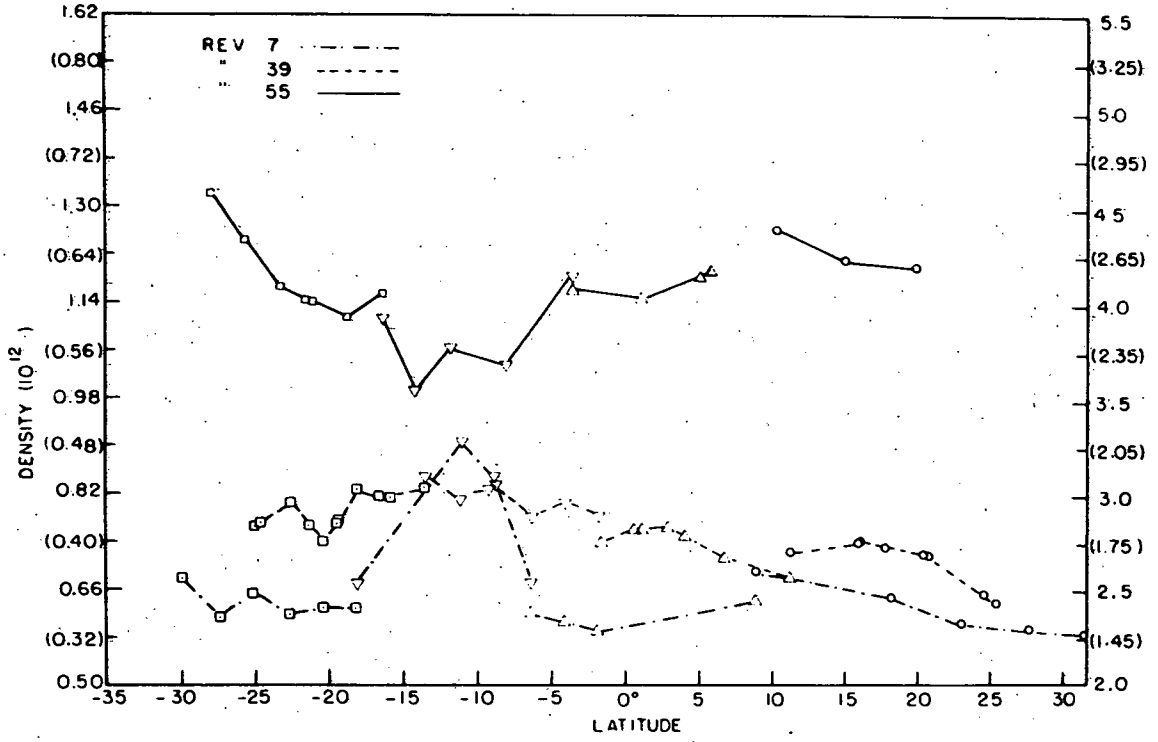

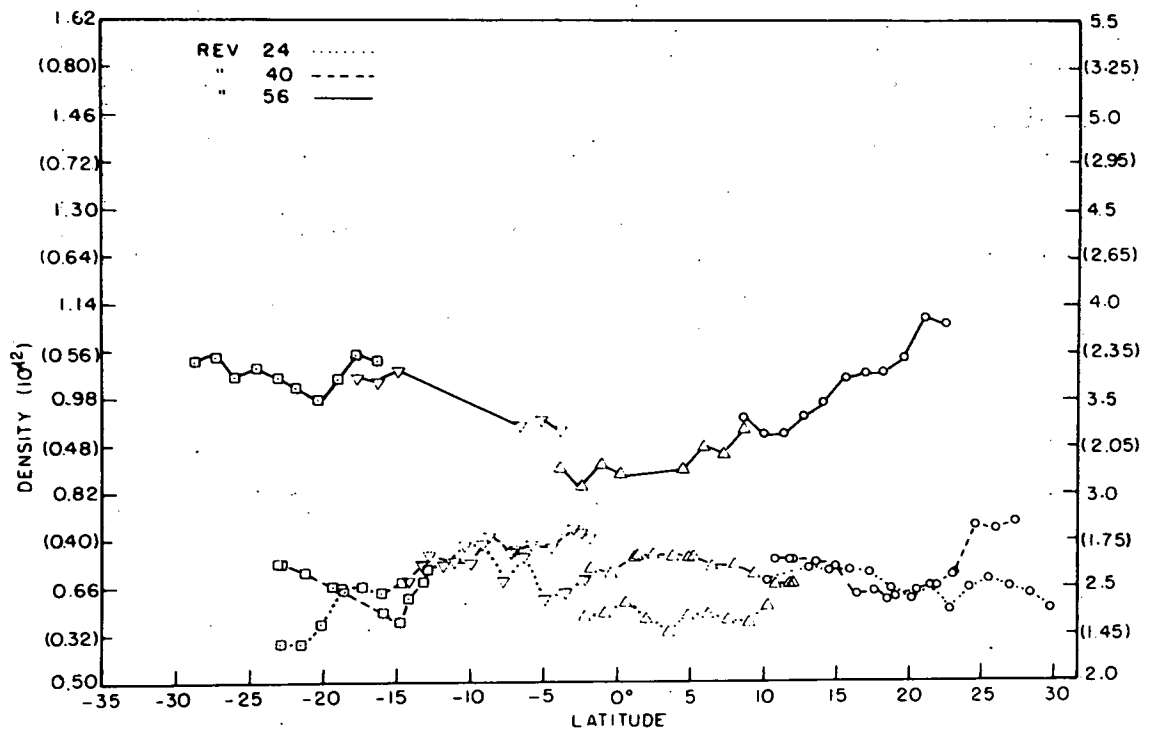

Figure 3d (top) and 3e (bottom)

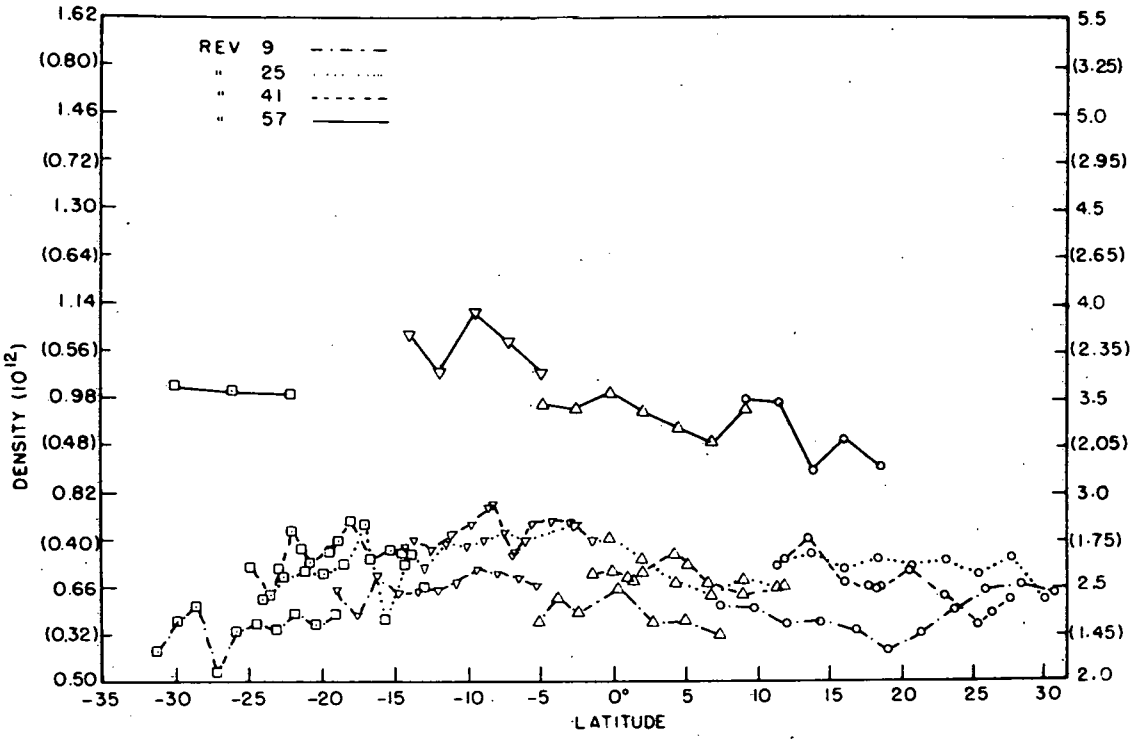

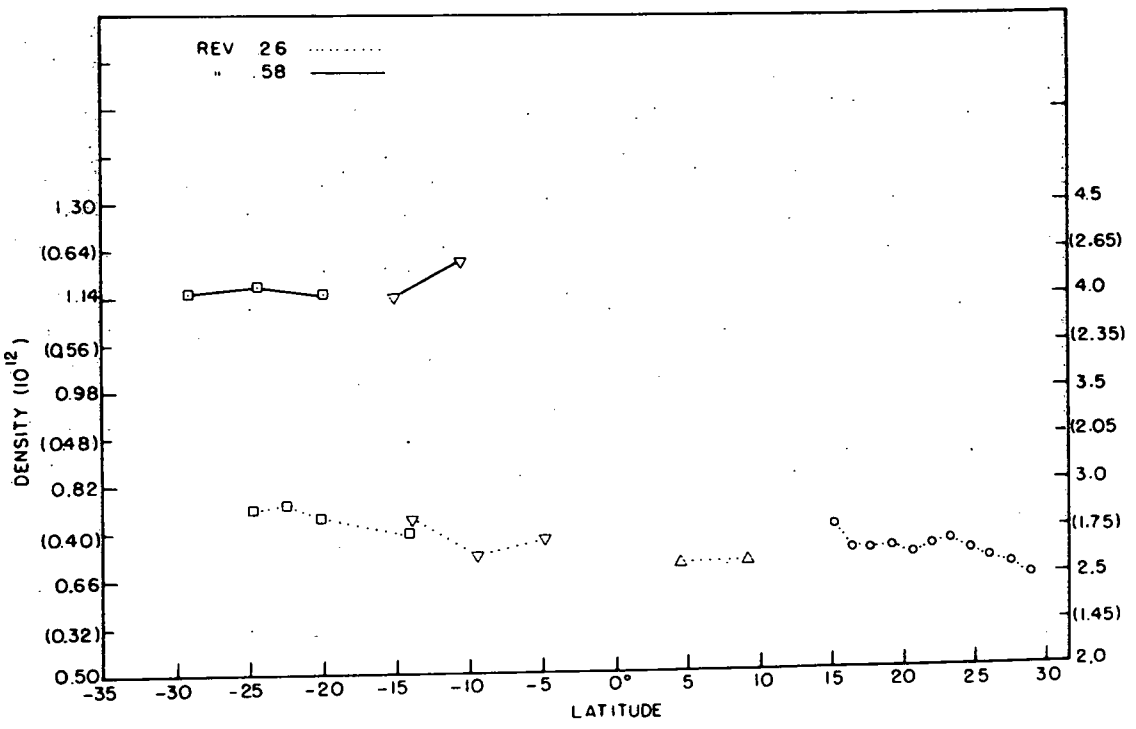

Figure 3f (top) and 3g (bottom)

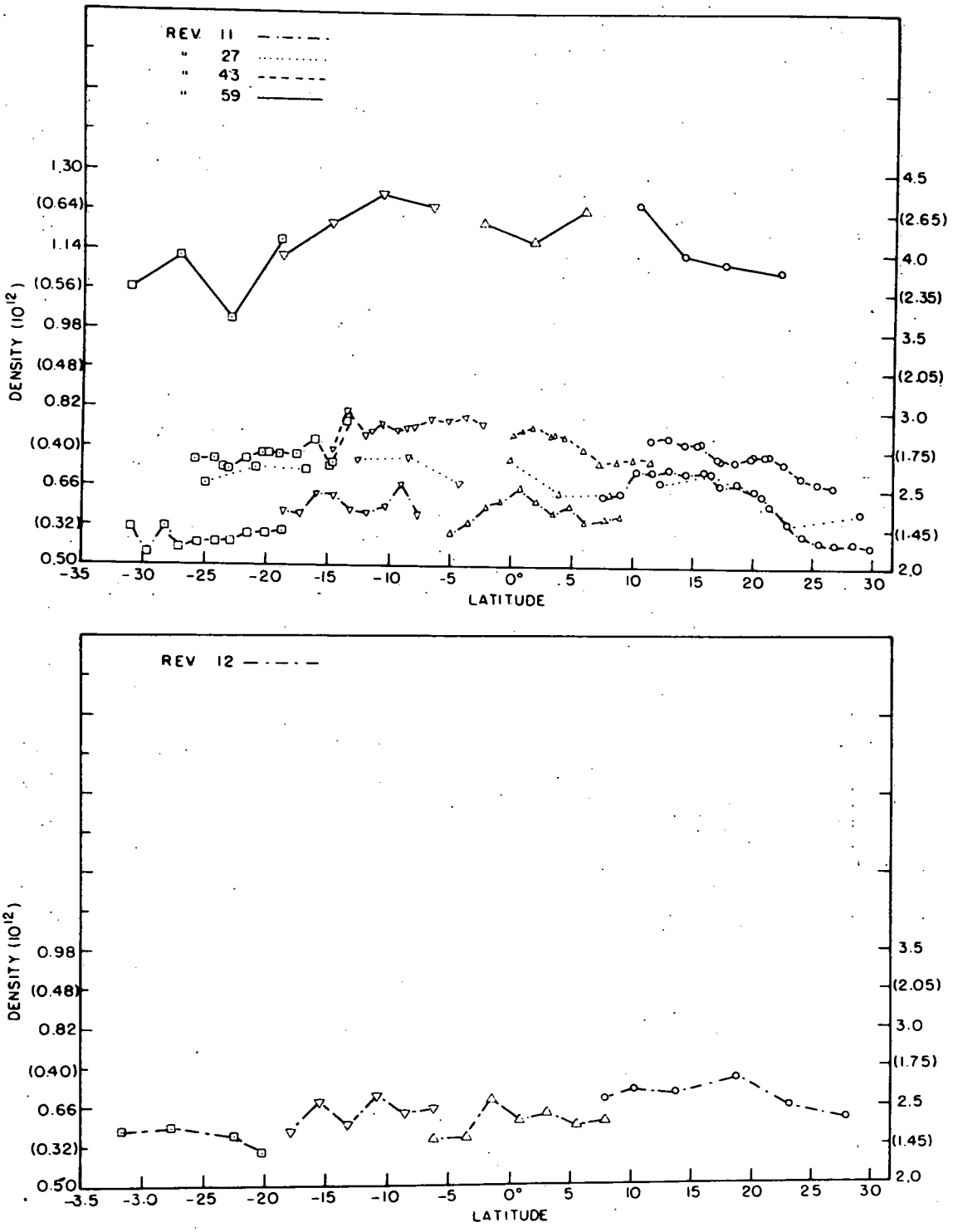

Figure 3h (top) and 3i (bottom)

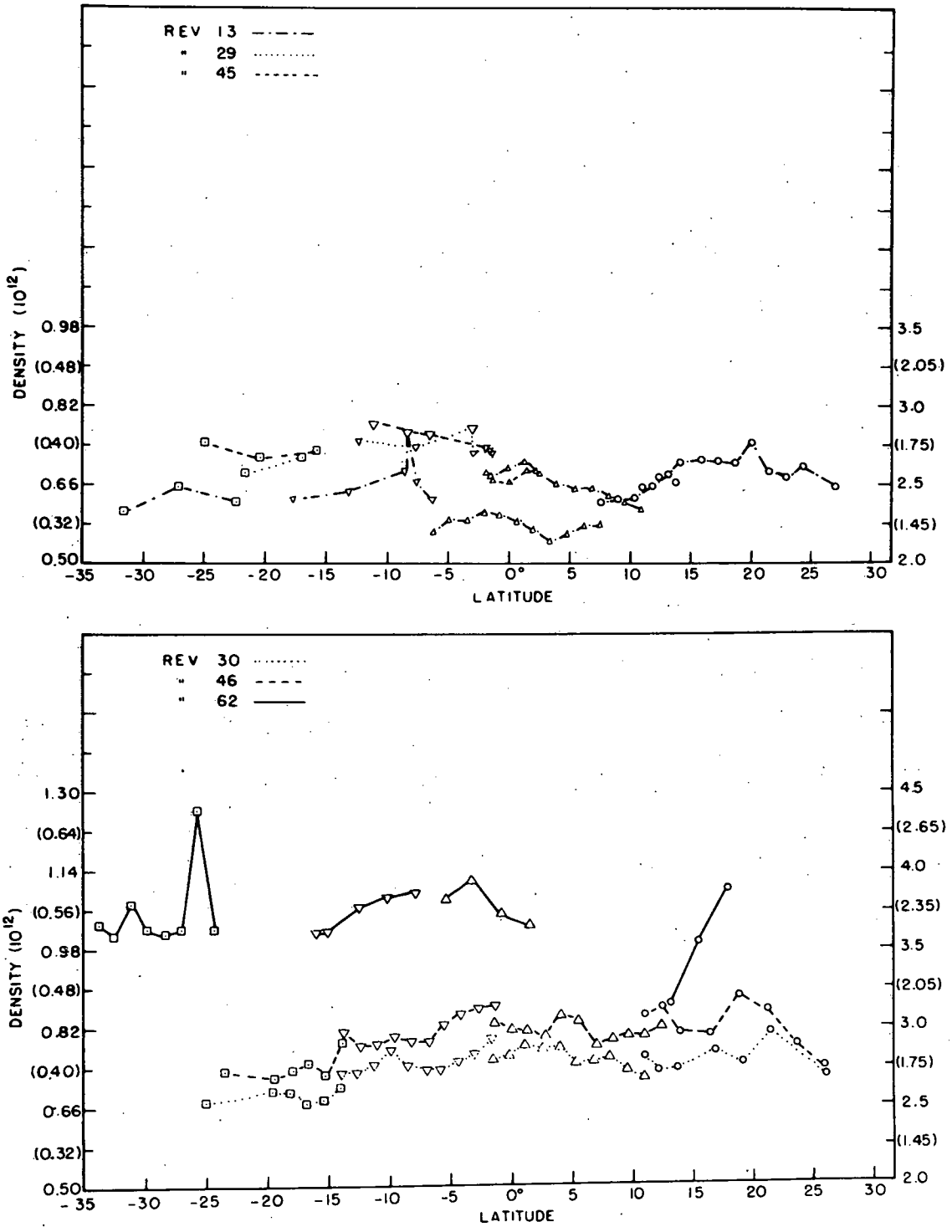

Figure 3j (top) and 3k (bottom)

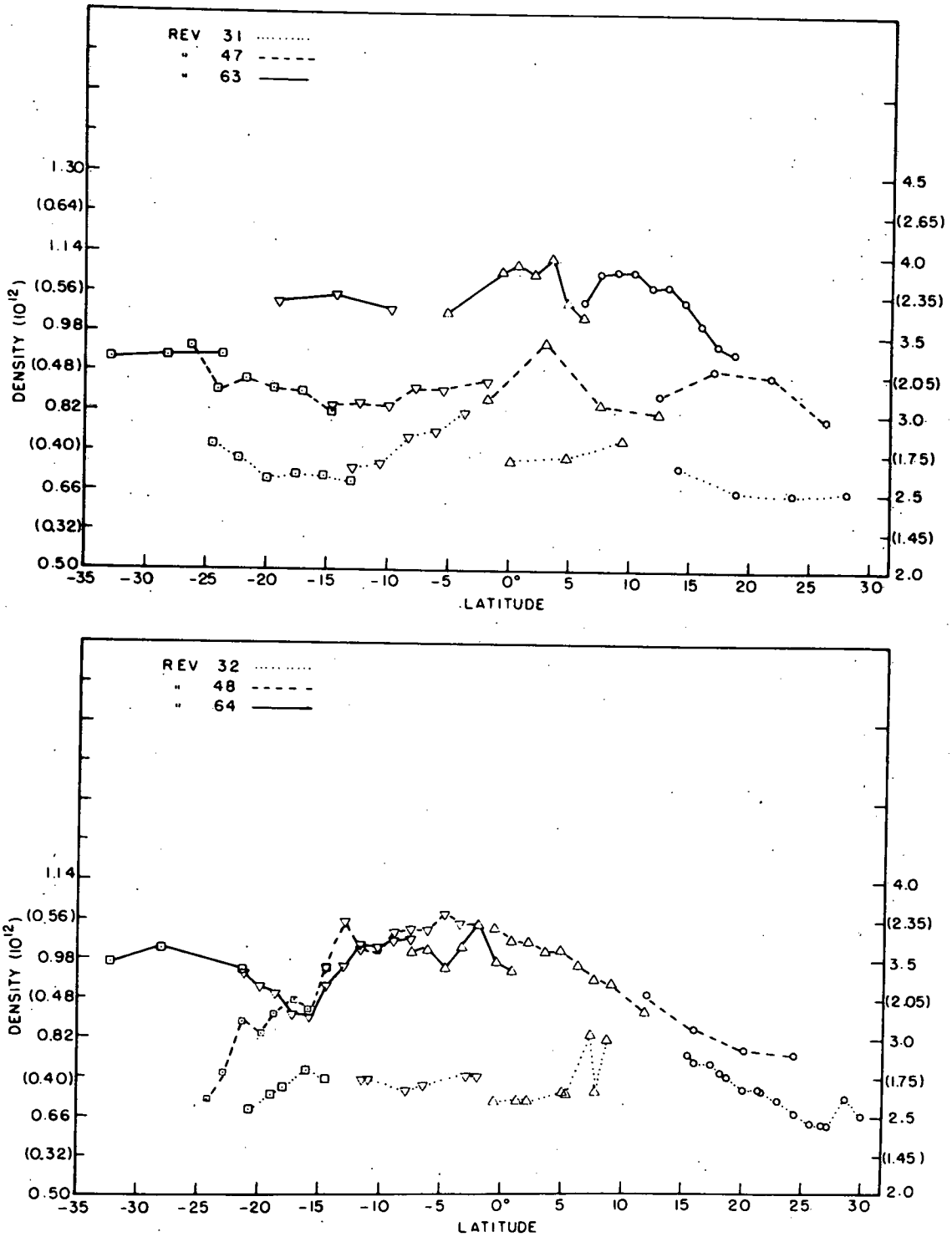

Figure 31 (top) and 3m (bottom)

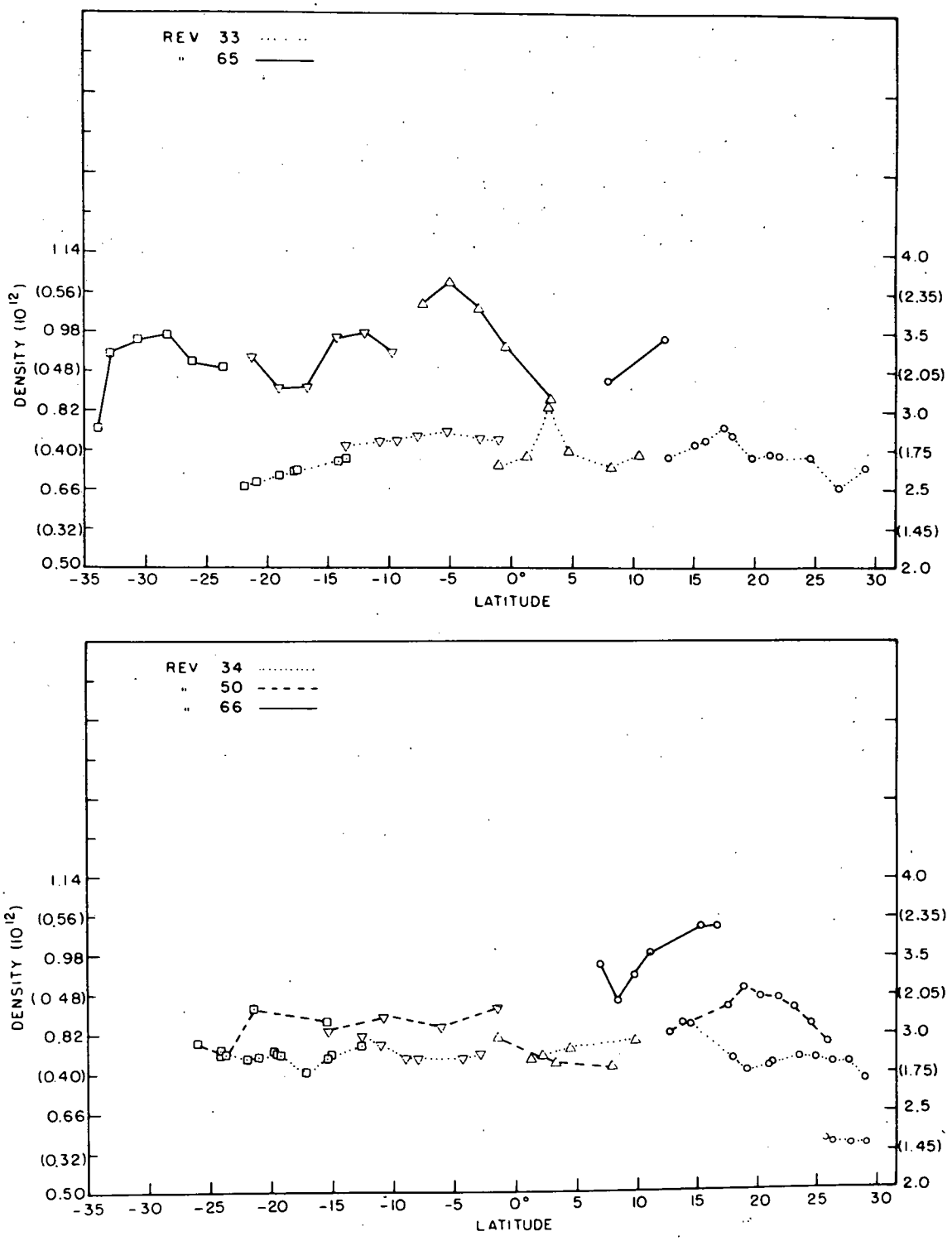

Figure 3n (top) and 3o (bottom)

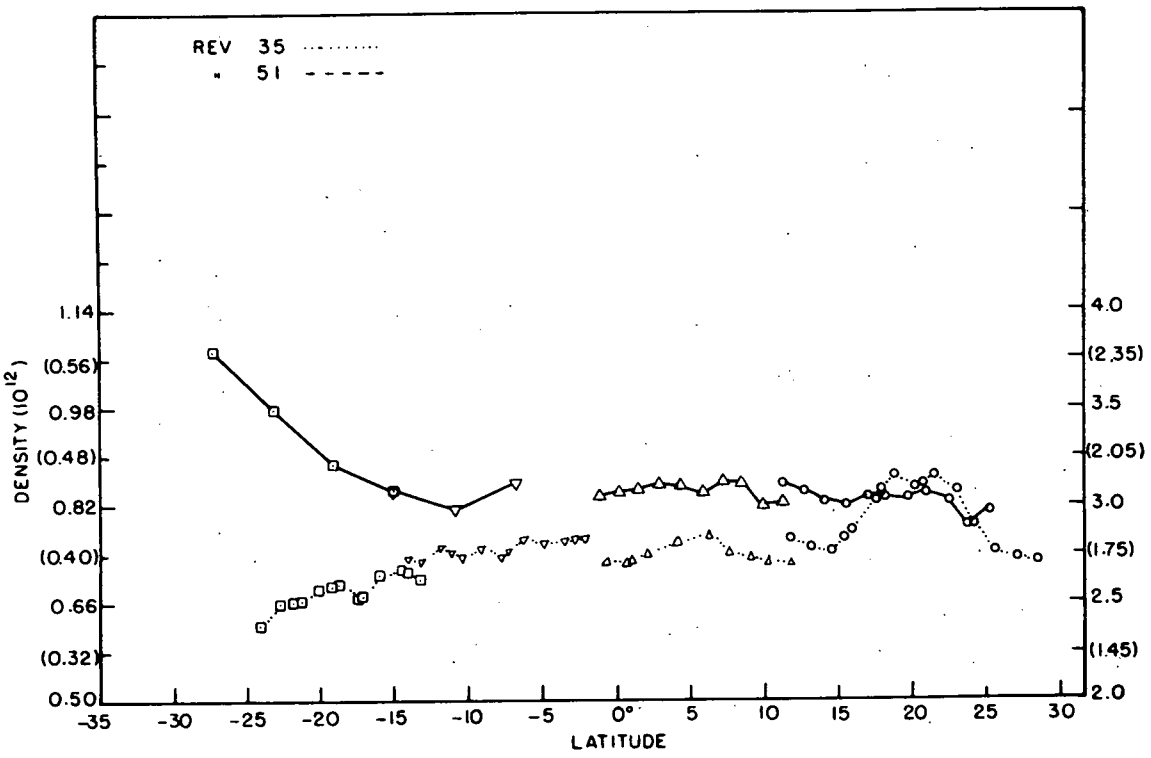
REV 35
51
DENSITY (10^{12})
1.14
(0.56)
0.98
(0.48)
0.82
(0.40)
0.66
(0.32)
0.50
4.0
(2.35)
3.5
(2.05)
3.0
(1.75)
2.5
(1.45)
2.0
-35 -30 -25 -20 -15 -10 -5 0° 5 10 15 20 25 30
LATITUDE

Figure 3p

displayed in Figure 2. Densities obtained as LOGACS was leaving perigee are shown in Figure 3. Here again the circles, triangles, upside down triangles, and squares are used to indicate densities normalized to 150, 160, 180, and 200 km respectively. The revolution numbers in the figures were grouped according to similarity of satellite ground track. For example revs 5, 21, 37, and 53 in Figure 1a had longitudes of the descending node at 126°E, 128°E, 129°E, and 130°E. All the LOGACS revolutions for which density observations were obtained are grouped in a similar fashion. This grouping is maintained throughout Figures 1, 2, and 3. Thus on any single figure the only density variations are due to latitude and time for a given standard altitude. In Figures 1 and 3 some overlap frequently occurs in the density curves for the same revolution between adjacent standard altitudes (revs 10 and 26 in Fig. 1f for example). The overlap was caused by normalizing those density values at heights within a kilometer of the division levels (i.e., 155, 170, and 190 km) to the standard altitudes above and below those heights. This was done to show the relative difference between the successive standard altitude plots and thus indicate the relative density variation over the entire latitude span covered in the figures. The separate density scales for 150, 160, 180, and 200 km were adjusted as closely as possible to give the same amplitude of relative variation and the same

level of the plotted density values. Maintenance of a convenient scale for plotting and keeping the density variation within reasonable bounds on the figures without smothering the significant density variations were additional factors in the choice of scale. Even so, the density variation occasionally exceeded the limits of the figure and the data had to be plotted against an auxiliary scale insert (rev 53, Fig. 1a and 2a; rev 62, Fig. 1j). The frequency of data from LOGACS varied considerably. Changes in the turntable spin rate, data recording rate, low vehicle-to-ground data transmission quality, control jet firings, and instrument anomalies all contributed to a reduction in data frequency at various times throughout the LOGACS flight. Large stretches of no data are indicated by a dashed line for rev 18 in Fig. 2n, rev 62 in Fig. 2j, and rev 65 in Fig. 2m. In general the normalized densities vary in a fairly smooth manner. Occasional density spikes due to interference from control jet firings or other vehicle dynamical effects are noted. Rev 14 in Fig. 1j at 78°N, rev 52 in Fig. 3a at 24°S, rev 5 in Fig. 3b at 5°N, rev 13 in Fig. 3j at 8°S, and rev 32 in Fig. 3m at 8°N are clear examples of such induced data noise.

The normalized density data derived from the SPADES accelerometer readings are shown in Figures 4 - 7. In all cases the circles, triangles, and upside down triangles represent densities normalized to 160, 180, and 200 km

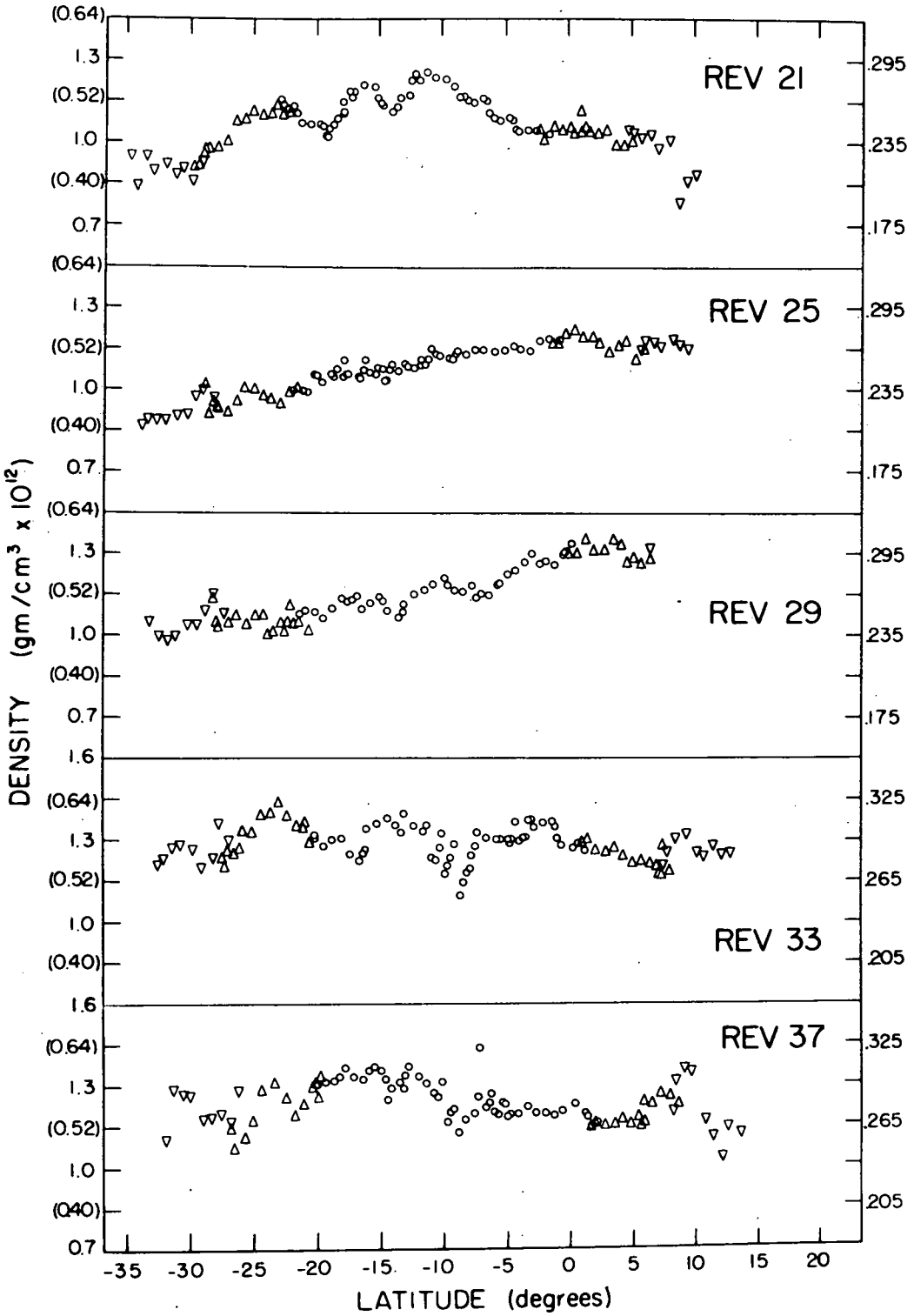

Figure 4a-e (top to bottom)

Figure 4. SPADES Densities for revs 21-57, normalized to 160, 180, and 200 km. The circles (o), triangles (Δ), and upside-down triangles (∇) refer to density normalized to 160, 180, and 200 km. The 200 km scale is on the right. The 160 and 180 km scales are interposed on the left. The 180 km scale is in parentheses.

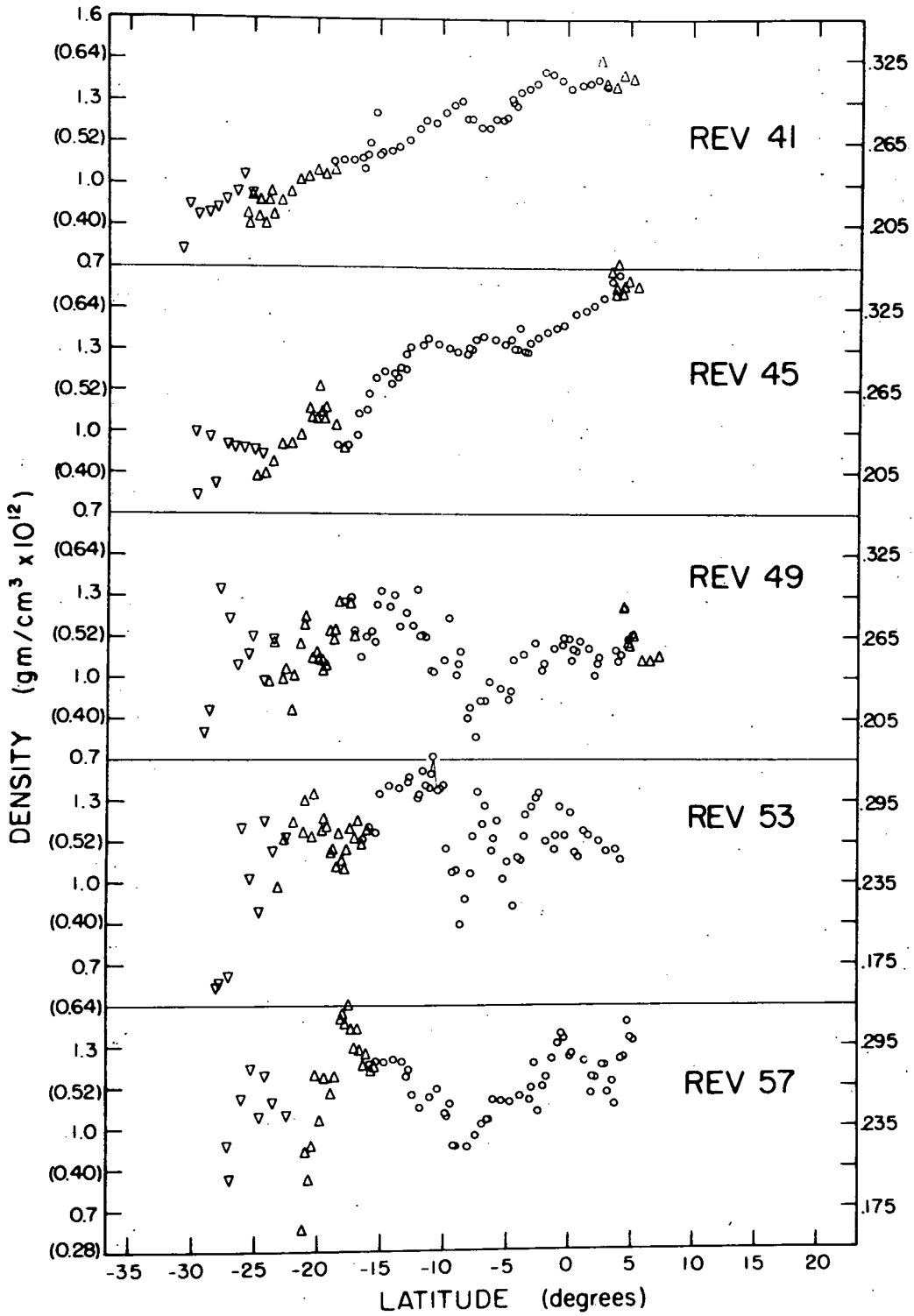

Figure 4f - j (top to bottom).

Figure 5a-e (top to bottom)

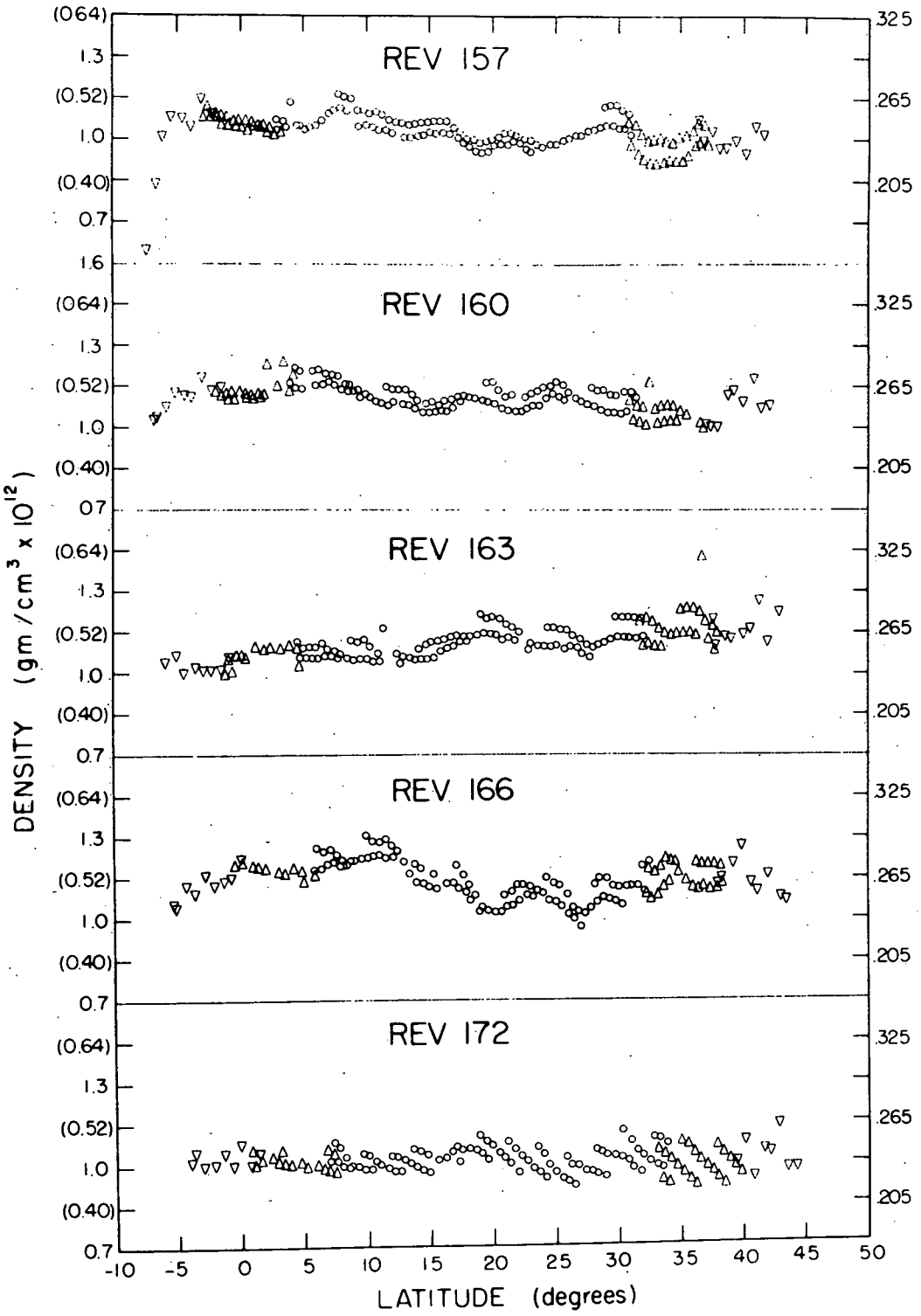

Figure 5. SPADES Densities for revs 157-208, normalized to 160, 180 and 200km. The circles(o), triangles(Δ) and upside-down triangles(∇) refer to density at 160, 180, and 200km. The 200km scale is on the right. The 160 and 180km scales are interposed on the left. The 180km scale is in parentheses.

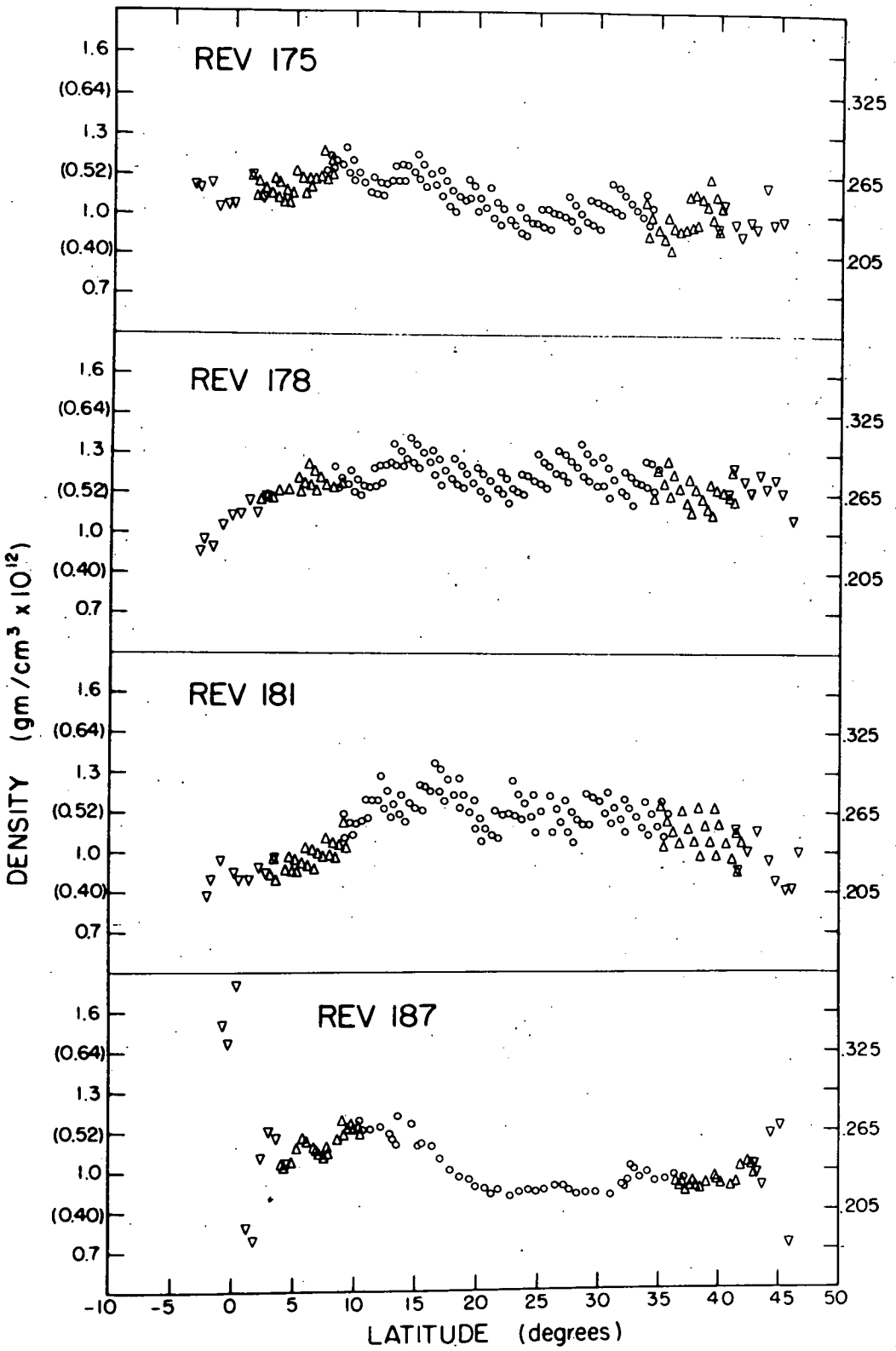

Figure 5 f-i (top to bottom)

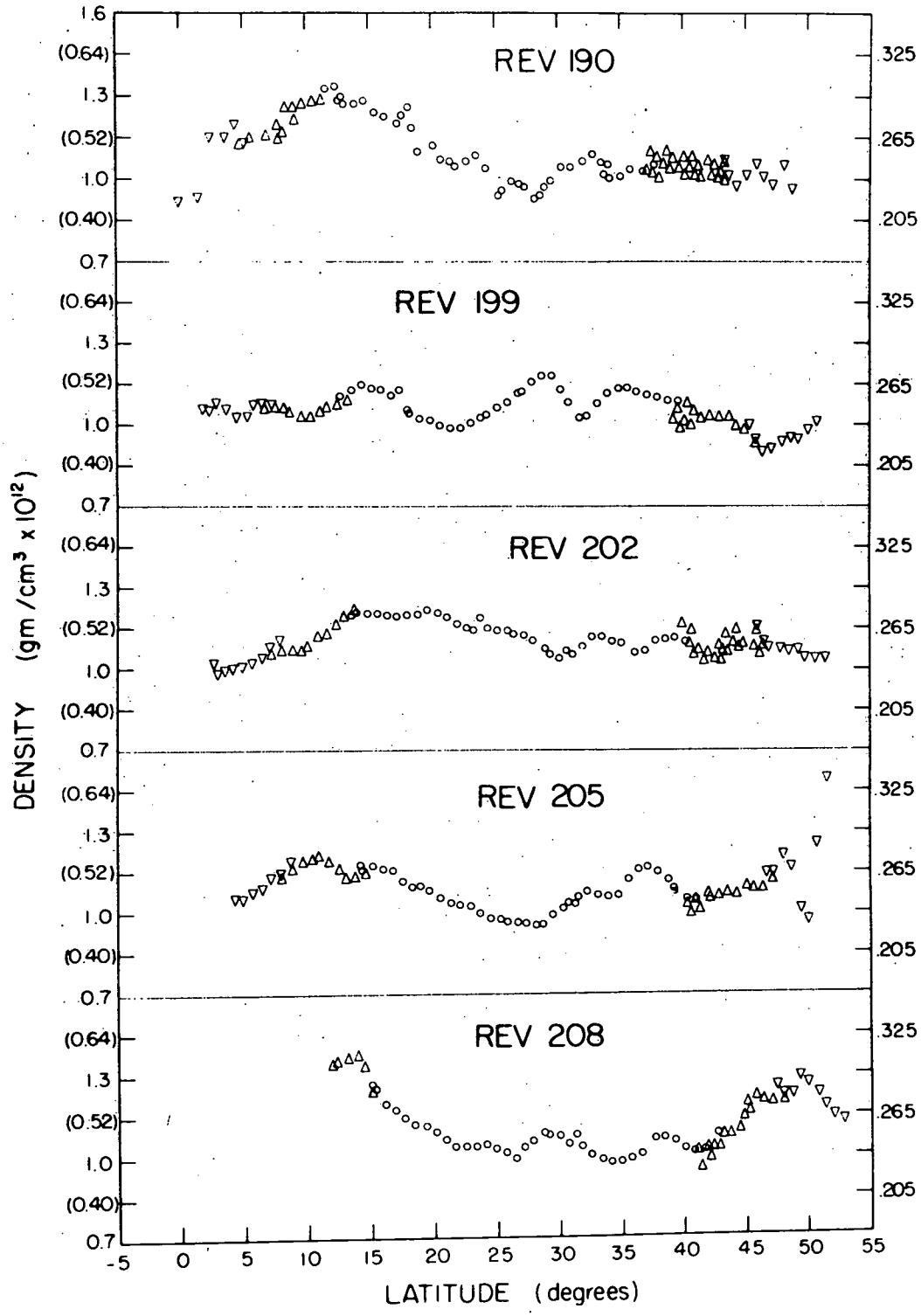

Figure 5 j-n (top to bottom)

Figure 6a-e (top to bottom)

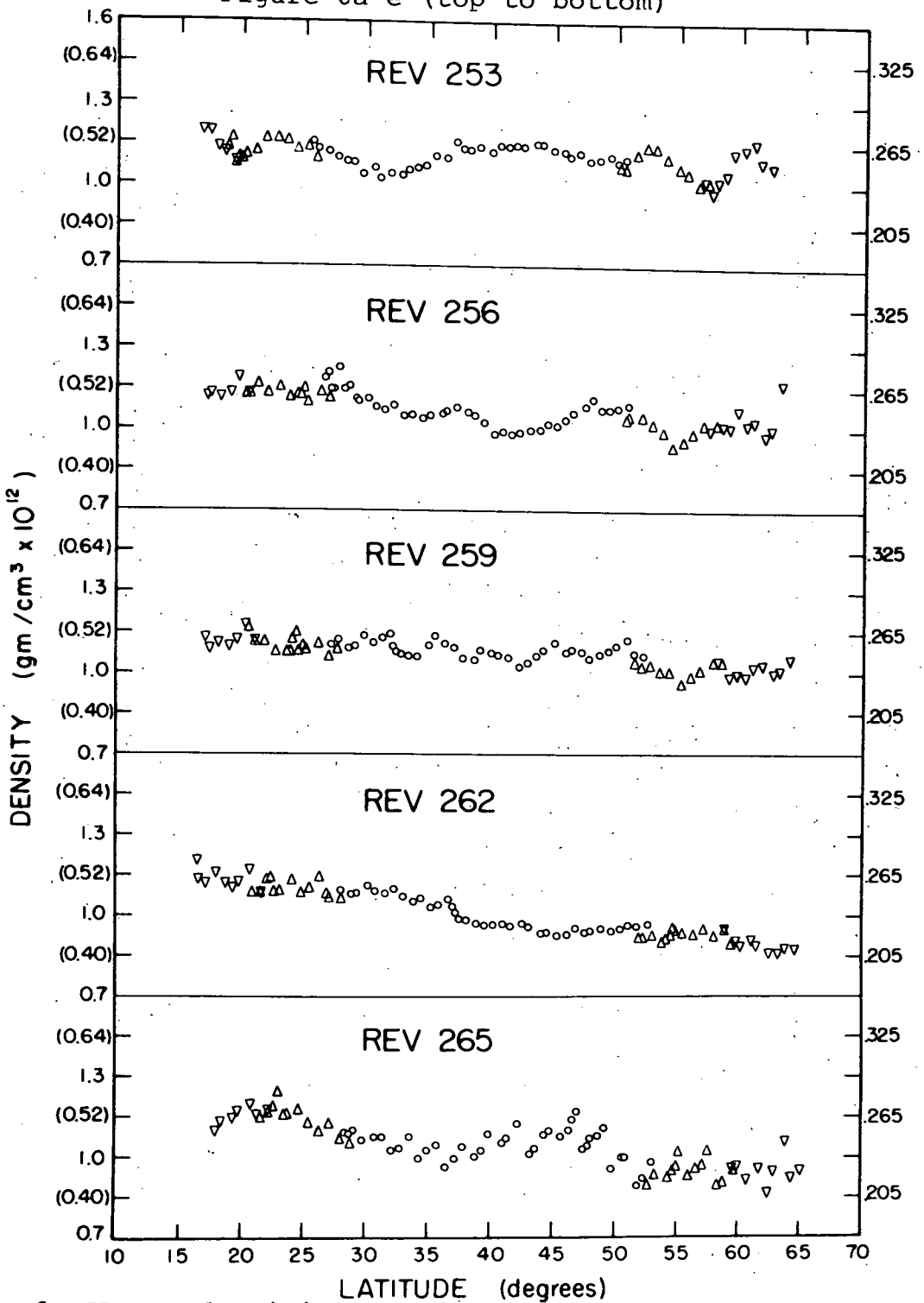

Figure 6. SPADES densities for revs 253-292, normalized to 160, 180 and 200km. The circles(o), triangles(Δ) and upside-down triangles(∇) refer to density at 160, 180, and 200km. The 200km scale is on the right. The 160 and 180km scales are interposed on the left. The 180km scale is in parentheses.

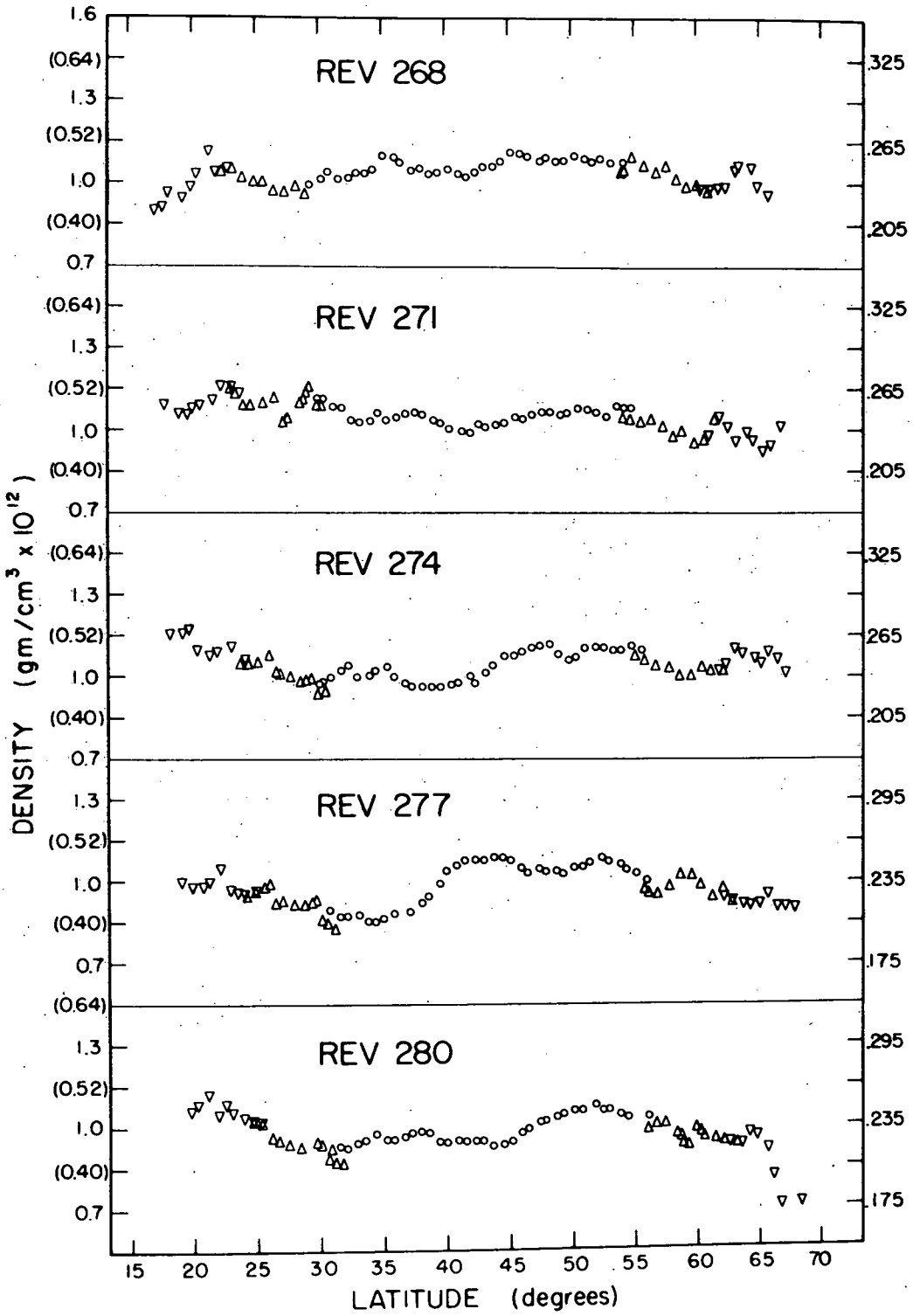

Figure 6 f-j (top to bottom)

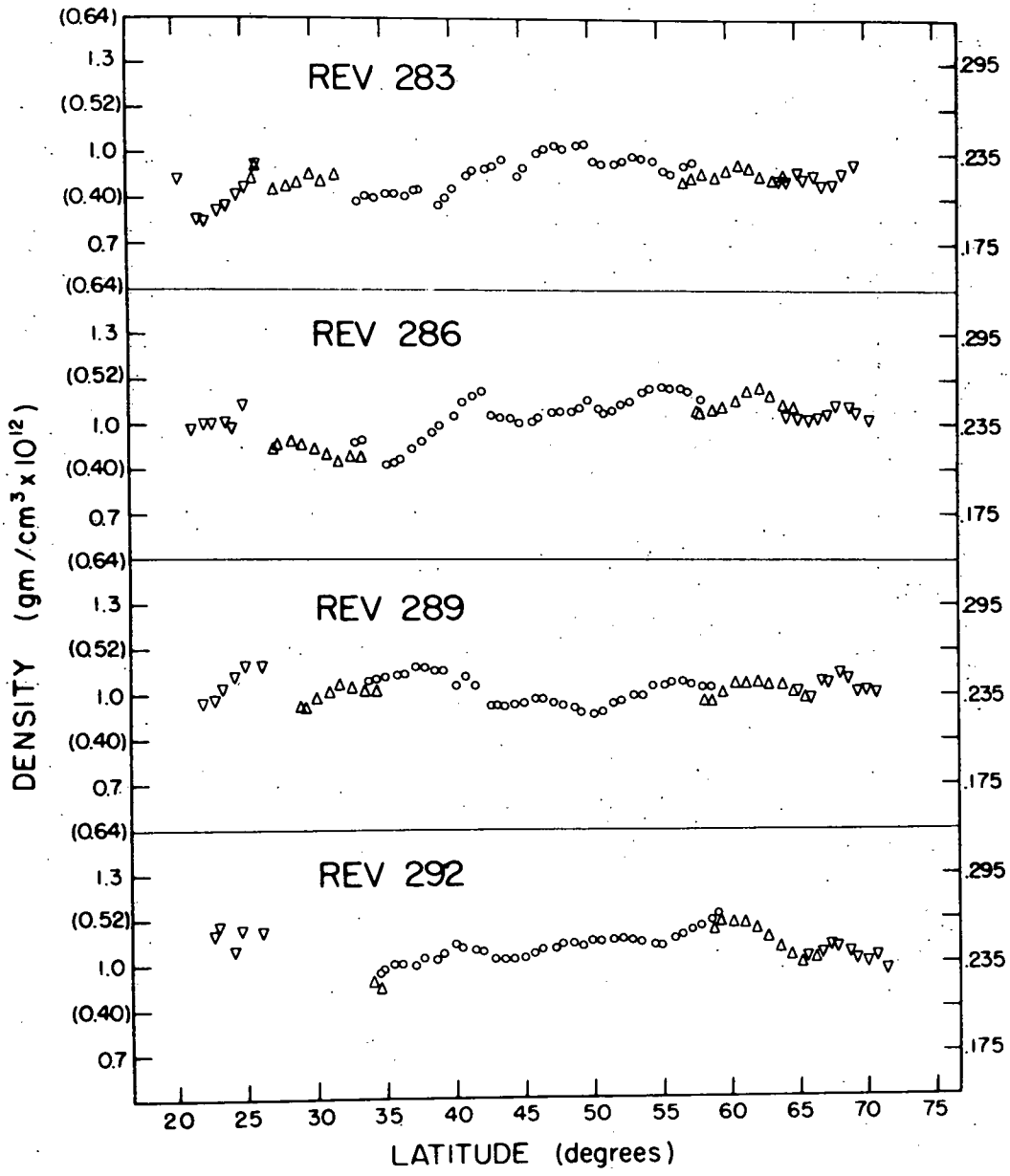

Figure 6 k-n (top to bottom)

Figure 7 a-d (top to bottom)

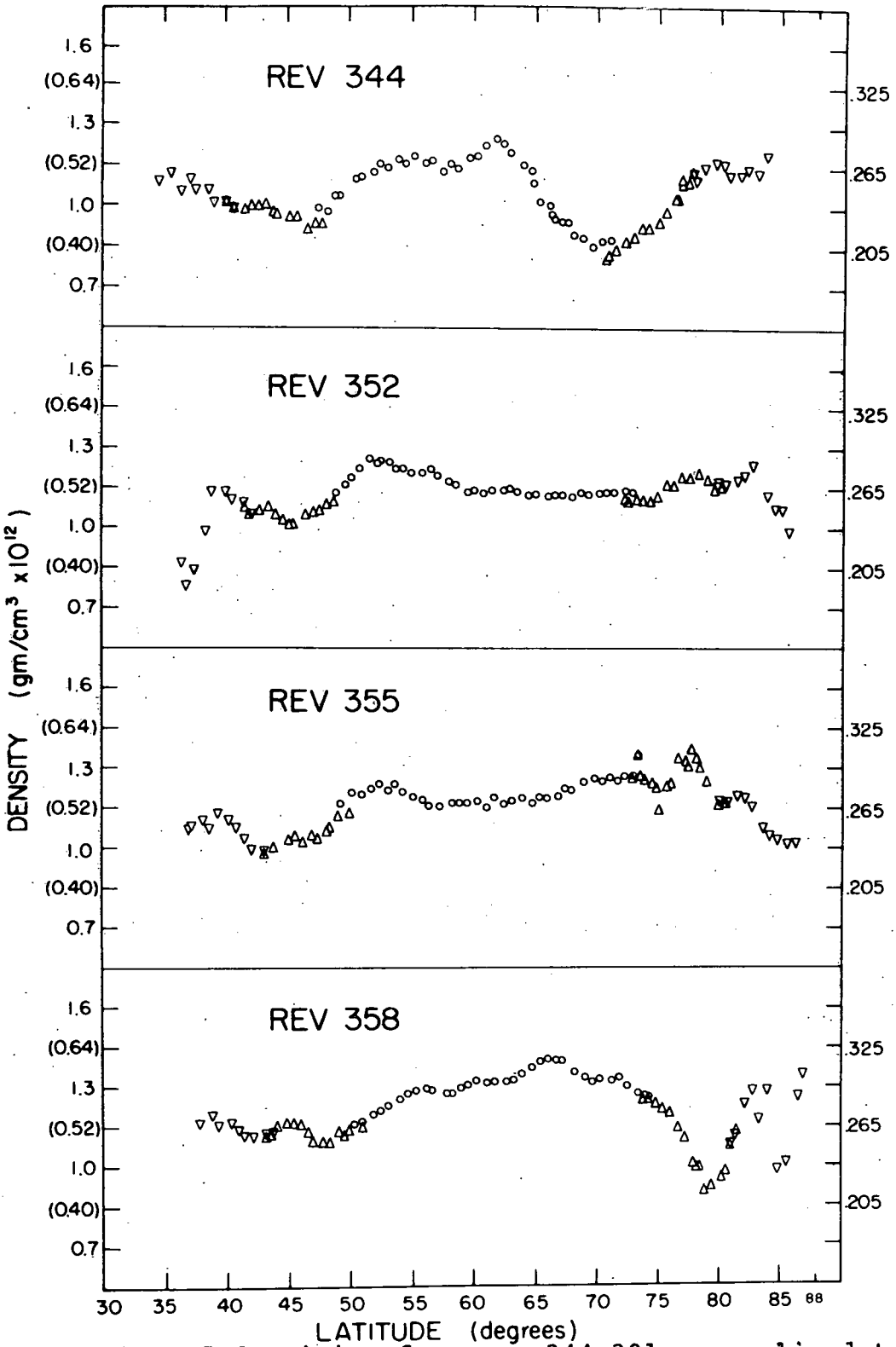

Figure 7.SPADES densities for revs 344-391, normalized to 160, 180 and 200km. The circles(o), triangles(Δ) and upside-down triangles(∇) refer to density at 160, 180, and 200km. The 200km scale is on the right. The 160 and 180km scales are interposed on the left. The 180km scale is in parentheses.

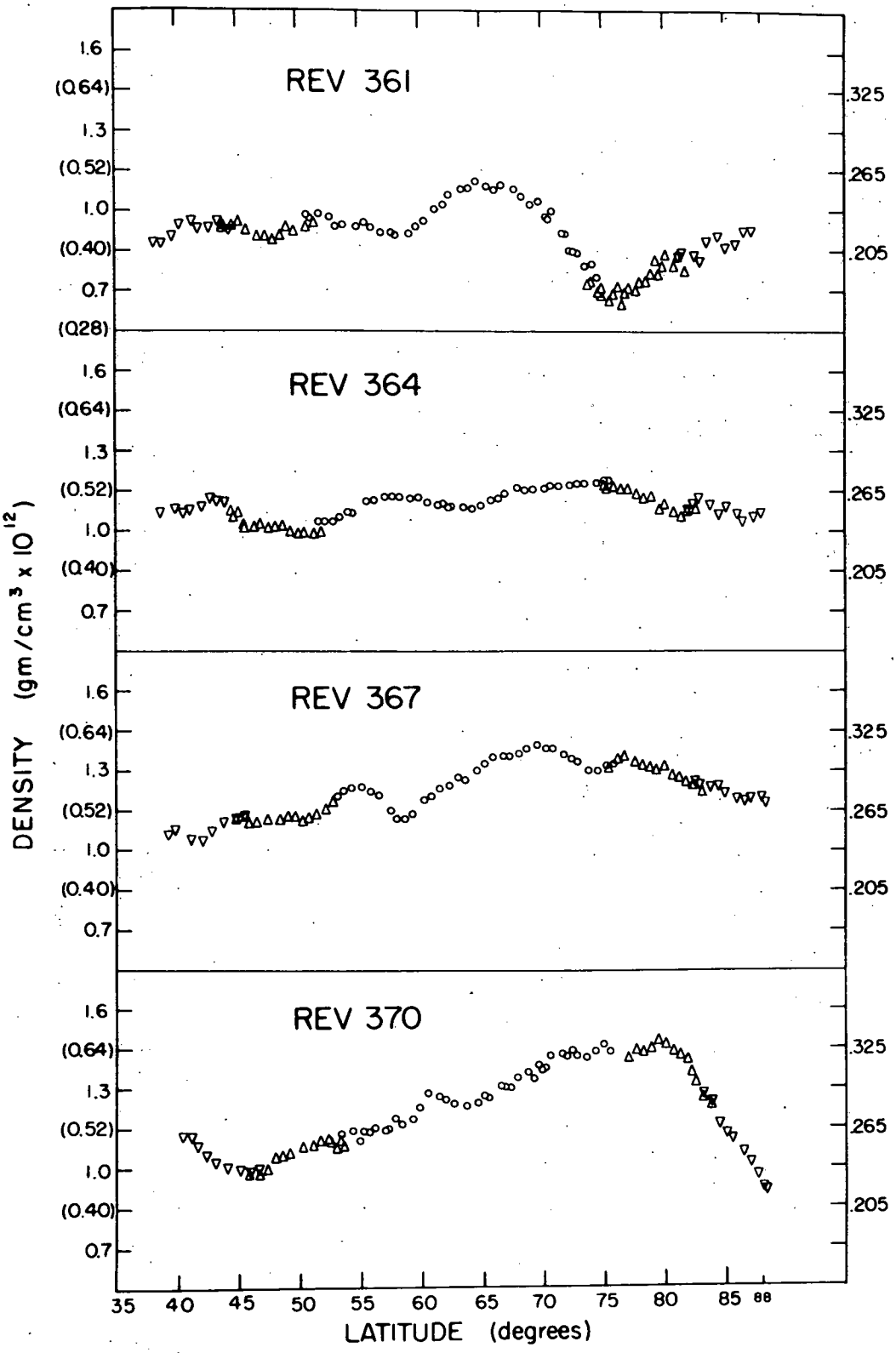

Figure 7 e-h (top to bottom)

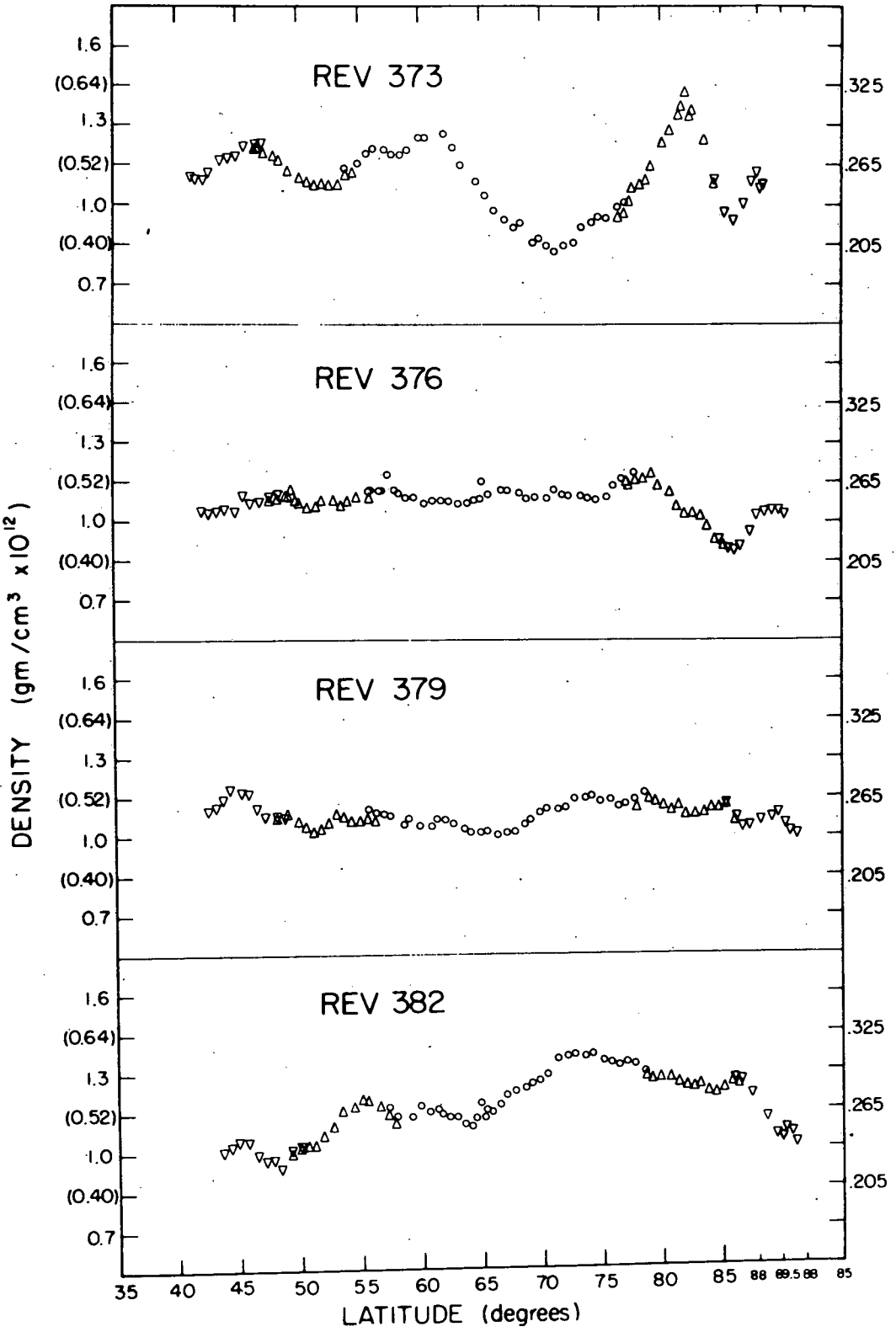

Figure 7 i-1 (top to bottom)

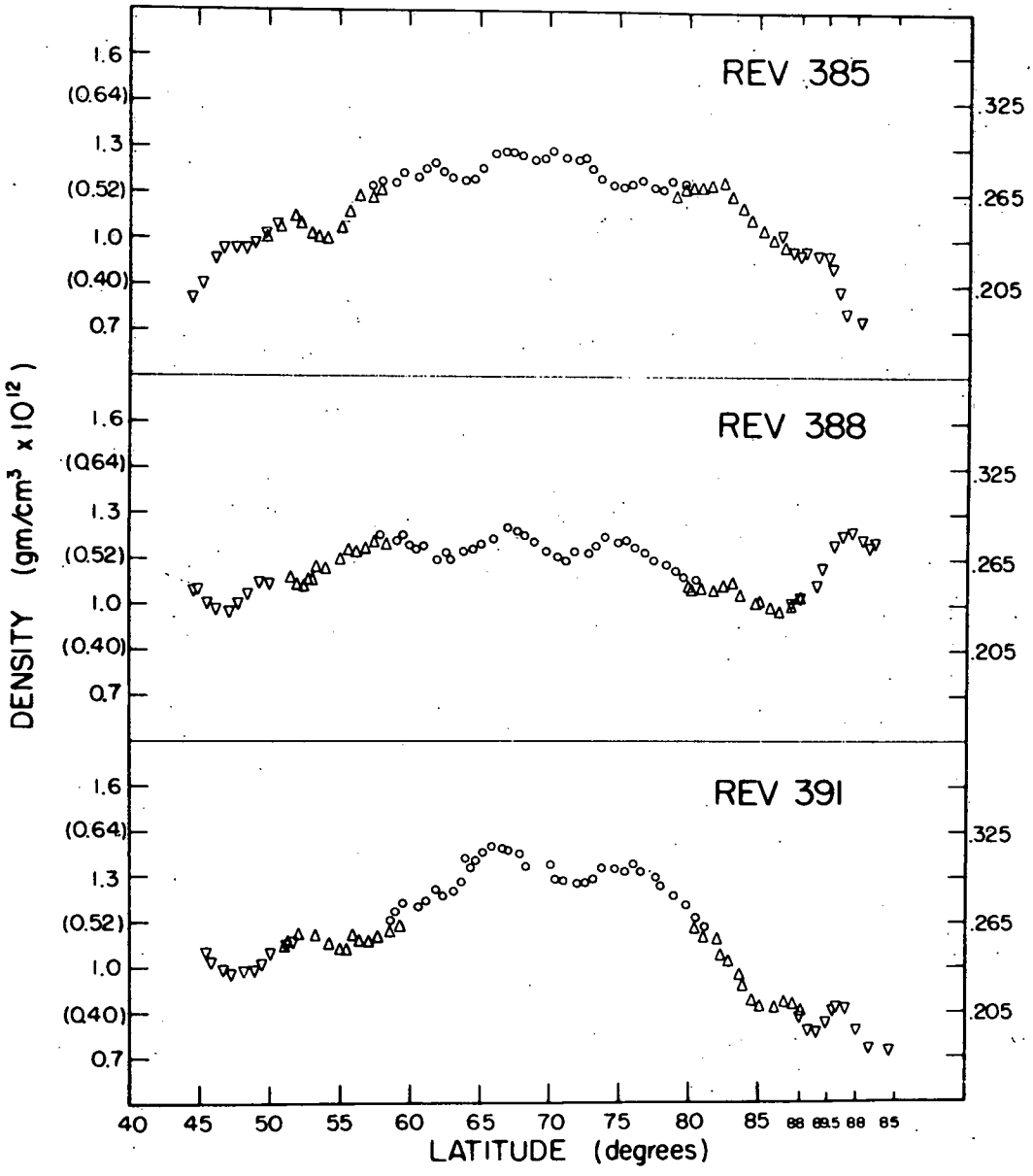

Figure 7 m-o (top to bottom)

respectively. The same considerations as for LOGACS were used in the choice of the density scales for the three standard altitudes. In this case the problem was considerably simplified by the smaller range of variation in the normalized densities (no intense geomagnetic storm) and the fact that only three scales required adjustment to each other. Data availability dictated the groupings into four figures for four distinct, separate time periods. Within the separate time periods only one case occurred where the data was obtained over nearly the same geographical locations, revs 344 and 373 in Fig. 7, but for consistency these data were plotted separately even though the density levels and latitudinal variation are remarkably similar. As with LOGACS there is intended overlap in the data plots for the different standard altitudes.

For SPADES the data frequency ranged between three and four seconds. Initially only one data point was used in every ten seconds. After these data were normalized and plotted the figures were checked for irregularities where use of some of the omitted intermediate data might be useful in confirming their validity. This was only done for the data normalized to 160 and 180 km. All the available data for revs 157 through 181 (Fig. 5a-h) were normalized and plotted in this procedure. During this period a combination of factors produced unreal scatter in the normalized data. These include apparent systematic

differences in the deduced densities when the accelerometer pointed into and away from the direction of motion as exhibited in Fig. 5a-d. Additional errors are apparent in Fig. 5e-h and Fig. 6e where it seems that improper periods and/or phases for the satellite spin rate and spin axis precession rate were input to the numerical filtering scheme used to process the accelerometer output. Similar filtering problems also appear to have affected the results for revs 33, 37, 49, 53, and 57 (Fig. 4d, e, h, i, and j). Atmospheric drag caused a decrease in the vehicle spin rate during the flight and magnetic torques from the operation of on-board electrical equipment also affected the spin axis orientation and precession rate. These effects were apparently not taken into account sufficiently in the inputs to the filtering scheme. The densities normalized to 200 km were generally more erratic due to the lower level of density and instrument sensitivity limits. Data for the 200 km altitude were frequently unavailable as in Fig. 4f-j for revs 41-57. Outside of these problems the density plots are remarkably smooth and completely justify the omission of over one-half the available intermediate data points. Even at 160 km there are occasional spikes due to vehicle or instrumental anomalies such as at 7°S on rev 37 in Fig. 4e and 15°S on rev 41 in Fig. 4f.

With the exception of high latitudes, the latitude scale is the same throughout Figs. 1-7. Latitude scale

differences occur only above 85° in Fig. 1 and above 87° in Fig. 7. These differences were brought about by the difference in the orbital inclination between LOGACS and SPADES and the fact that in neither case was the inclination exactly 90°. The latitude scales were stretched at high latitudes so that the horizontal spacing in the figures correspond to the actual distance covered by the satellite subpoint.

Much of the density variation shown in Figs. 1-7 is due to geomagnetic activity. The geographic coordinates of each observation point were converted to corrected geomagnetic coordinates to test whether the density variation might be more ordered in a coordinate system related to geomagnetic heating. The corrected geomagnetic coordinate system was chosen because it has been the most successful in organizing auroral and related phenomena (Whalen, 1970). The transformation from geographic to corrected geomagnetic coordinates was made using the method described by Hakura (1965). The spherical harmonic displacements from the dipole lines (Hultqvist, 1958) were used to correct the geomagnetic coordinates. A FORTRAN program for computing the coordinate transformation was written and thoroughly checked. The program was run on M.I.T.'s IBM 360 computer system. Correction terms were not available between ±30° geomagnetic latitude (Hultqvist, 1958). A linear interpolation was made between geomagnetic coordinates at the

geomagnetic equator and fully corrected geomagnetic coordinates at ±30° geomagnetic latitude. All the normalized densities shown in Figs. 1-7 were replotted against the corrected geomagnetic latitude. Due to space limitations these figures are not included here.

The density variation with latitude is readily seen in Figs. 1-7 for each individual satellite revolution. However, it is difficult to observe any longitude/time variation from the density data presented in this manner. The most natural solution to this difficulty is to enter the density values on a latitude-time cross-section chart and analyze isolines of constant density. Drawbacks to this approach are the regression of perigee around the satellite orbit and the latitudinal separation of the two sections of the normalized densities for all but the lowest standard altitudes. The perigee regression rate ranged from 3° to 3 1/2° per day for LOGACS and SPADES. This severely reduces the amount of latitudinal overlap in the normalized density plots over the period of observation. An additional difficulty is the interpretation of the density variation at the breakpoint between two standard altitudes. To overcome these problems all densities were normalized to 150 km for LOGACS and 160 km for SPADES. The respective altitudes were chosen to minimize any possibile additional normalization error for the greatest bulk of the density data. Only those observations obtained on

the day-side of the maximum latitude of each revolution were converted to 150 or 160 km.

The factors used to convert the normalized densities at the various standard altitudes to a single altitude are given in Table 6. These factors were derived by taking appropriate ratios of the densities listed in Table 6 of J71 (Jacchia, 1971). For example the densities for T_∞ of 1000°K at 150 and 180 km are listed as 2.064E-12 and 5.443E-13 gm/cm^3 in J71. The ratio $\frac{\rho 150}{\rho 180}$ is 3.7920. This is the conversion factor listed in Table 6 for 1000°K and 180 km. Assuming the density profile in J71 is valid, the multiplication by this factor of any normalized density value at 180 km and a T_∞ of 1000°K yields the equivalent density at 150 km. The listed differences between the factors at a given altitude in Table 6 for the successive 100°K increments of T_∞ are used for linear interpolation of intermediate values of T_∞. For LOGACS the maximum normalization interval is 60 km (210 km to the 200 km standard altitude and then to 150 km via Table 6). A 100°K error in T_∞ at 1000°K would result in a 7% error in the density reduced to 150 km over the 60 km interval. This would be the maximum possible error during undisturbed geomagnetic conditions. During the great storm of May 25-26, an error of 400°K at high latitudes is possible. A 400°K underestimation of T_∞ at 1300°K gives a 5.5% overestimation of the density converted from 180 km to 150 km.

TABLE 6

Conversion Factors for Reducing Standard Altitude Densities to a Single Altitude

NORMALIZATION TO 150 km

Alt. (km)	1000°	Δ	1100°	Δ	1200°	Δ	1300°	Δ	1400°
145	0.7459	0.0041	0.7500	0.0029	0.7529	0.0025	0.7555	0.0026	0.7580
160	1.6645	-0.0169	1.6476	-0.0140	1.6336	-0.0111	1.6226	-0.0085	1.6141
180	3.7920	-0.1242	3.6679	-0.0956	3.5722	0.0738	3.4984	-0.0588	3.4396
200	7.4325	-0.4263	7.0062	-0.3206	6.6885	-0.2458	6.4397	-0.1940	6.2457

NORMALIZATION TO 160 km

	900°	Δ	1000°	Δ	1100°	Δ	1200°
180	2.3484	-0.0702	2.2782	-0.0520	2.2262	-0.0395	2.1866
200	4.7537	-0.2884	4.4652	-0.2129	4.2524	-0.1600	4.0924

The use of 180 km in this comparison is due to the fact that by the time of the geomagnetic storm, the northward shift of perigee and the orbital decay had combined to reduce the altitude of the satellite to 180 km by the time it reached the maximum latitude point and began travelling southward. Thus during the storm no densities were reduced to 150 km from altitudes greater than 180 km at high latitudes where such large errors in the T_∞ computed from J71 would be expected to occur. Including errors due to differences in the shape of the temperature profile and the assumption of static equilibrium, the latitude-time plots of density from LOGACS converted to 150 km have a worst possible error of 10% at the lowest latitudes where the vehicle is passing upward above 200 km. For over 80% of the converted densities the worst possible error is at most 5%. A 100°K error at 1000°K would cause a 6.5% error in the density converted from 210 km to 160 km. Since no major geomagnetic storms occurred during the period of accelerometer-derived density observations from SPADES, 6.5% would be the worst possible error in the densities converted to 160 km.

The latitude-time analysis of the LOGACS densities converted to 150 km is shown in Fig. 8. The nearly vertical straight lines represent those portions of the latitude/time track of the satellite revolutions over which density observations were obtained. The figures at the

ends of the lines indicate the revolution numbers. All the density data below 85°N in Figs. 1-3 were read off at 1° latitude increments from Figs. 1-3, converted from their standard altitudes to 150 km (if necessary), and plotted for analysis. Obviously bad data points were smoothed out and linear interpolation was used to fill in gaps of up to 6° latitude in the LOGACS data. The solid isolines are drawn at intervals of 0.5×10^{-12} gm/cm^3. The centers of highest and lowest density are delineated by shading. A unique and most useful feature of Figure 8 is that the time of all the density values is between 1020 and 1145 LT. Below 80°N all density values are before 1106 LT. Thus there is a minimal effect of any diurnal variation in density thoughout range of Fig. 8. The same density data are shown in corrected geomagnetic latitude-time coordinates in Fig. 9. The location of the auroral oval is shown by the hatched area near 75°. Due to the offset of the corrected geomagnetic pole from the north pole the maximum latitude of density observations varies from one revolution to another.

Similar analysis of the densities from the SPADES accelerometer converted to 160 km are shown in Figs. 10-13 for geographic latitude and Figs. 14-17 for corrected geomagnetic latitude. As before, the nearly vertical straight lines represent the loci of the density observations and the figures at the ends, the rev numbers. The solid

isolines of density are drawn at intervals of 0.1×10^{-12} gm/cm^3. Density values were obtained over 1° increments from Figs. 4-7. For those revs where there was scatter in the density values normalized to the standard altitudes a smooth curve was drawn by eye through the points for pick-off of the 1° density values. No values were taken from the 200 km standard altitude plots where the scatter was judged to be too large. Fig. 4h below 27°S, Fig. 5i below 2°N and above 44°N, and Fig. 5m above 49°N are more prominent examples of such scatter. The factors in the lower portion of Table 6 were used to convert the 180 and 200 km density values to 160 km. In Figs. 10-13 and also Figs. 14-17 the local time ranges of the data were 1106 to 1117 LT, 1022 to 1037 LT, 0957 to 1010 LT, and 0923 to 0943 LT respectively. The hatched area in Figs. 16 and 17 indicates the location of the auroral oval.

The auroral oval location in Figs. 9, 16, and 17 was determined with the aid of the Auroral Oval Plotter (Whalen, 1970). The requisite geomagnetic local Q-indices were not available for either period of density observations. Q-indices are derived individually by geomagnetic observatories located at high latitudes. Basically the Q-index is a logarithmically scaled indicator of the total variation in the strength of the horizontal component of the geomagnetic field from that observed on a "quiet" day over a 15 minute interval. In Fig. 9 the K_p index was

used as a substitute for Q. The K_p index is a logarithmically scaled indicator derived from an average of the observations of the most disturbed component of the geomagnetic field at 12 subauroral (mid-latitude) stations over a 3 hour period. This gives a less accurate estimation of the auroral oval location but is an acceptable substitute (Feldstein and Starkov, 1967). For Figs. 16 and 17 a "planetary" Q index, Q_p, was derived from the auroral electrojet AU and AL indices given by Allen et al (1973). AU and AL represent the maximum upper and lower variation of the horizontal component of the geomagnetic field during a one hour period from the quiet day level as observed by geomagnetic observations located around the auroral oval. The extremes are not averages but the maximum or minimum value observed at any of the reporting stations. Both extremes may occur at the same station during a one hour period but more commonly one station records the largest excursion in the positive direction while another station supplies the extreme value in the negative direction. The hourly auroral electrojet index, AE, is the difference between the extreme values of AU and AL. Like Q, Q_p is a logarithmically scaled index of this total variation in the strength of the horizontal component of the geomagnetic field from that observation on a quiet day, but over a one hour interval. Although less acceptable than Q, Q_p is a far more acceptable substitute than K_p

(Feldstein and Starkov, 1967). The derived Q_p indices are given in Table 7.

TABLE 7

Q_p INDICES FOR SPADES

GMT Hour	July 1968			Aug. 1968			
DATE	30	31	1	5	6	7	8
01	4	5	3	4	4	6	7
02	4	5	3	4	5	7	7
03	3	4	3	4	6	7	7
04	4	4	3	4	7	5	4
05	3	4	4	7	7	5	7
06	3	4	4	4	5	6	6
07	3	4	3	3	6	6	6
08	3	5	4	3	4	5	7
09	3	4	6	4	4	6	6
10	3	3	6	6	5	5	3
11	3	5	5	7	4	5	3
12	3	6	3	5	4	7	3
13	3	4	3	6	5	7	3
14	2	4	3	7	5	6	5
15	4	4	4	6	4	6	4
16	4	4	5	6	4	6	3
17	5	3	5	6	2	6	3
18	4	3	4	4	5	4	4
19	5	3	3	3	6	4	3
20	4	4	3	3	6	4	3
21	6	4	4	4	6	4	5
22	6	4	4	5	5	4	5
23	5	4	4	5	4	5	6
24	5	3	3	6	5	5	6

IV. RESULTS

LOGACS

Perhaps the most obvious feature in Figs. 1-3 is the higher level of density at all standard altitudes following rev 47. This increase in density is in response to the great geomagnetic storm which began with strong sudden commencements at 1019 and 1236 UT on 25 May 1967. The density response to this storm is far from uniform. The density profile of rev 53 (Fig. 1a, 2a, 3b) is a prime example of the variation of density response with latitude. The minimum and near maximum normalized densities for the data sample both occur during this revolution. The most notable feature of rev 53 is the relative density maximum at about 10°N and the minimum at 66°N. This is completely contrary to what has been found at higher altitudes from orbital decay measurements. The maximum observed relative density occurred near the geographic pole on rev 62 (Fig. 1j) over 12 hours after the peak of the geomagnetic disturbance. The complicated nature of the density response can be seen more clearly in Figs. 8 and 9. The planetary geomagnetic range index, a_p, is shown at the bottom of the figures. Storm effects become apparent beginning with rev 45, about 1300 UT on 25 May. Peaks in the 150 km converted density appear at the highest latitudes, at mid-latitudes near 45°N, at low latitudes near the equator, and in the southern hemisphere near 30°S. Exact locations will

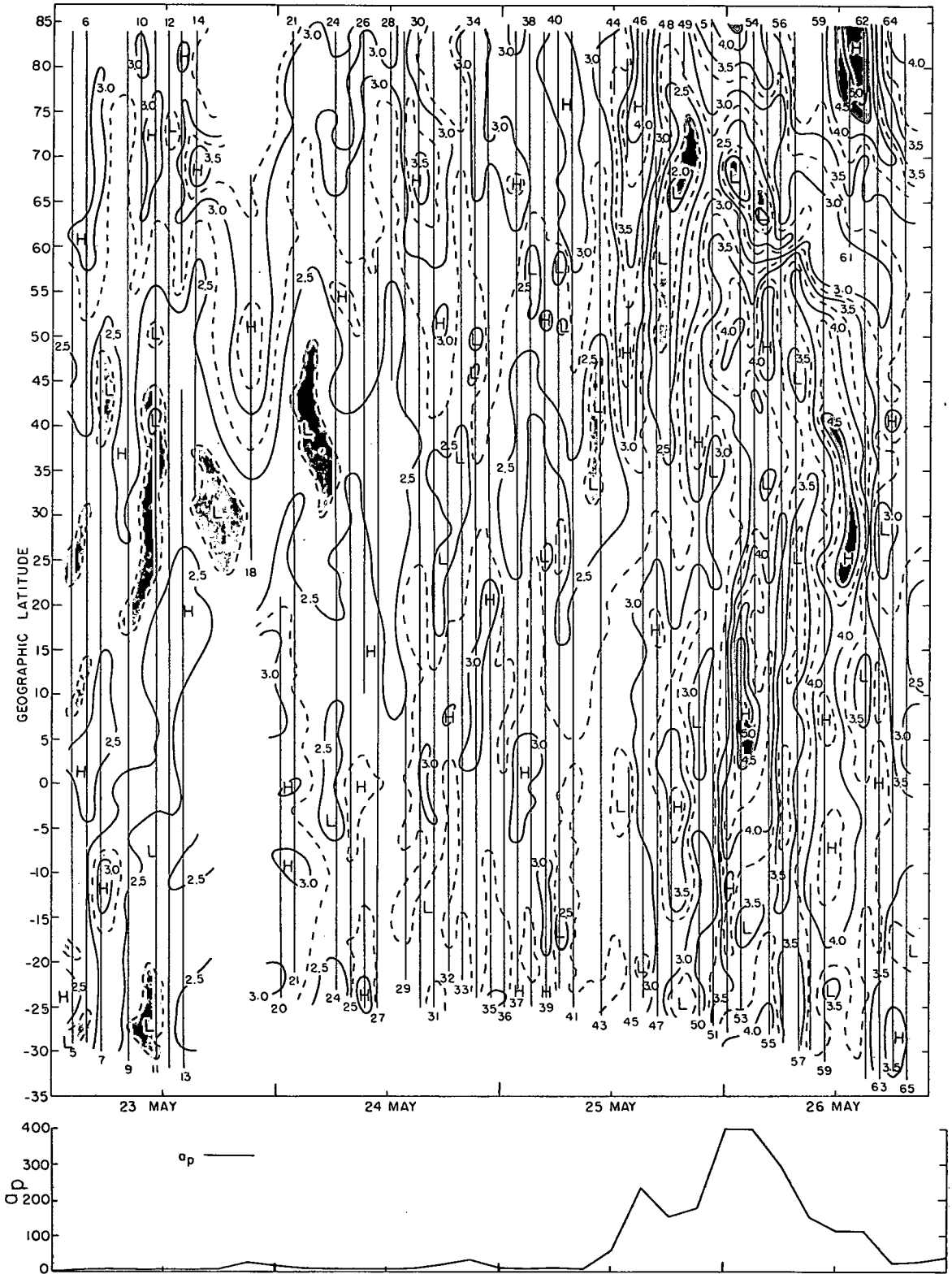

Figure 8. Time-geographic latitude analysis of LOGACSdensities converted to 150km. The density isolines are in units of gm/cm^3 scaled by 10^{12}.

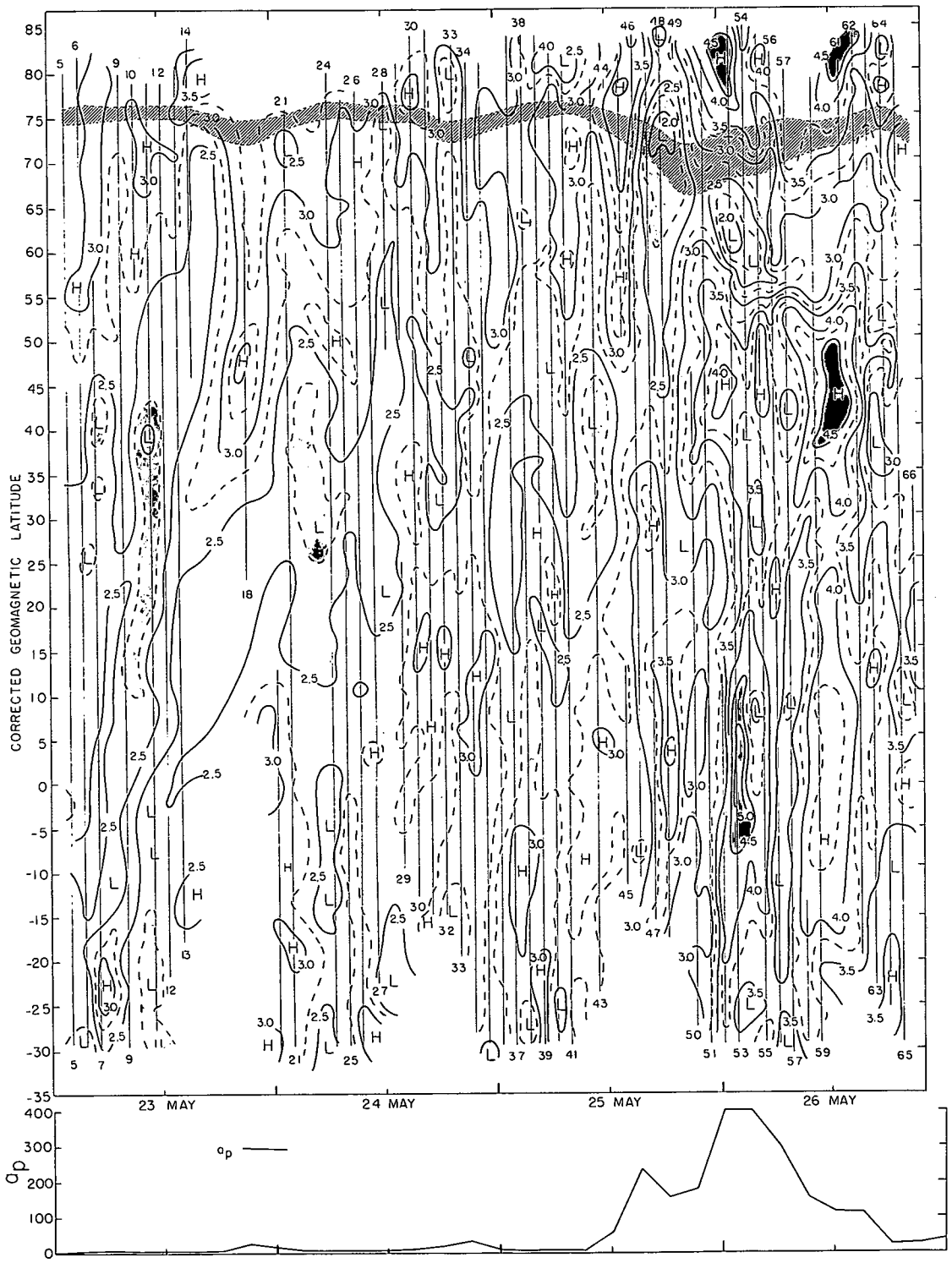

Figure 9. Time-Corrected Geomagnetic latitude analysis of LOGACS densities converted to 150km. The density isolines are in units of gm/cm^3 scaled by 10^{12}.

differ in Fig. 9 due to the differences in the coordinate systems. A deep low center appears initially at 65°N or 72° Corrected Geomagnetic (C.G.) latitude. During the course of the storm this low density region deepens to a minimum near 67°N (+61° C.G.) at about 0000 UT on 26 May, the peak of the geomagnetic storm. In the C.G. coordinate system this low density region occurs initially in the auroral oval but later moves equatorward of the auroral oval location even though the oval location itself expands and moves equatorward with increasing storm intensity. In Fig. 9 the center of the density trough reaches its southernmost position at about 0600 GMT on 26 May and then recedes poleward as it continues to fill. Prior to the storm, for revs 5-43, the average of the density converted to 150 km was 2.70×10^{-12} gm/cm^3. During the storm period, revs 45-66, the average converted density was 3.40×10^{-12} gm/cm^3. The density given by J71 for the pre-storm conditions is about 2.3×10^{-12} gm/cm^3.

Less dramatic, but equally significant, variations of density occur during the non-storm period of LOGACS observations. The density varies with latitude in a most unexpected manner. A very frequent feature of the density plots in Fig. 2 is the occurrence of a relative density minimum between 25°N and 40°N. There is also a tendency for a similarly located minimum in the southern hemisphere data (Fig. 3). A relative maximum in density occurs near

the equator as can be seen in Fig. 3. In Fig. 1 there is an obvious trend toward an increase of density with an increase in latitude. A careful examination of Fig. 8 reveals a series of high density centers near 70°N, and generally low density at 30°N, and higher density near the equator.

For each revolution, 5° latitude averages were calculated from the 1° latitude values of density converted to 150 km (used to make the analysis of Fig. 8). For each 5° latitude band these averages were then averaged over all revolutions. Separate averages were also made for the storm and non-storm periods. This process was repeated for the data converted into C.G. coordinates. Periods when data were unavailable resulted in a data set that was not fully homogeneous with respect to sampling frequency. The results are summarized in Table 8. The data in the bottom row of Table 8 are the columnar averages of the mean density in each 5° latitude band and the standard deviations of the latitudinal means from the columnar averages. In all cases, geographic or C.G. latitude, storm or non-storm, there is a definite minimum in the density structure between 25° and 40°. During undisturbed conditions the minimum appears to be better defined in geographic latitude. The minimum is relatively deeper and the standard deviations about the means between 30° and 40° are smaller in geographic coordinates. There is some

TABLE 8

Zonal Means of LOGACS Density Data Converted to 150 km

Lat. Band	Geographic Latitude									Corrected Geomagnetic Latitude								
	Total			Non-storm			Storm			Total			Non-storm			Storm		
	$\bar{X}$	σ	N	$\bar{X}$	σ	N	$\bar{X}$	σ	N	$\bar{X}$	σ	N	$\bar{X}$	σ	N	$\bar{X}$	σ	N
-25 - -20	2.90	.42	43	2.65	.23	27	3.32	.33	16	Insufficient Data								
-20 - -15	2.92	.45	43	2.65	.21	27	3.36	.37	16	Insufficient Data								
-15 - -10	2.98	.47	43	2.71	.22	27	3.46	.41	16	2.99	.51	43	2.70	.19	26	3.47	.51	16
-10 - -5	3.02	.50	43	2.72	.20	27	3.52	.44	16	3.00	.53	43	2.71	.20	27	3.50	.54	16
-5 - 0	3.06	.53	42	2.74	.19	27	3.60	.48	16	3.02	.60	43	2.68	.19	27	3.59	.63	16
0 - 5	3.05	.51	43	2.76	.20	27	3.55	.49	16	3.05	.62	44	2.69	.19	27	3.63	.64	17
5 - 10	3.02	.57	43	2.70	.21	27	3.56	.58	16	3.04	.59	45	2.68	.20	27	3.58	.56	18
10 - 15	3.03	.60	44	2.68	.19	27	3.59	.61	17	3.00	.56	44	2.64	.21	27	3.56	.49	17
15 - 20	3.00	.57	43	2.64	.19	26	3.55	.51	17	2.94	.53	40	2.59	.23	25	3.52	.35	15
20 - 25	2.91	.54	42	2.57	.18	26	3.46	.46	16	2.85	.51	42	2.52	.19	27	3.43	.36	15
25 - 30	2.81	.53	41	2.48	.16	25	3.31	.51	16	2.78	.48	42	2.46	.16	27	3.34	.31	15
30 - 35	2.74	.50	42	2.43	.13	26	3.26	.43	16	2.81	.49	41	2.46	.17	25	3.34	.32	16
35 - 40	2.76	.54	41	2.43	.17	26	3.33	.47	15	2.83	.54	40	2.49	.21	25	3.38	.45	15
40 - 45	2.84	.55	43	2.51	.21	27	3.39	.49	16	2.88	.60	40	2.53	.23	25	3.47	.58	15
45 - 50	2.89	.56	43	2.57	.24	27	3.42	.54	16	2.91	.56	42	2.60	.23	27	3.48	.54	15
50 - 55	2.90	.50	42	2.65	.21	27	3.35	.57	15	2.89	.44	43	2.67	.22	27	3.31	.45	15
55 - 60	2.88	.38	40	2.74	.20	26	3.15	.50	14	2.82	.31	43	2.78	.21	28	2.90	.44	15
60 - 65	2.90	.33	43	2.89	.18	28	2.92	.51	15	2.83	.31	42	2.84	.18	27	2.80	.47	15
65 - 70	2.99	.43	41	2.98	.27	26	3.01	.63	15	2.92	.30	42	2.89	.16	26	2.96	.45	16
70 - 75	3.10	.43	42	2.95	.19	25	3.32	.59	17	3.06	.38	41	2.94	.15	25	3.25	.53	16
75 - 80	3.23	.63	43	2.92	.15	25	3.66	.79	18	3.25	.45	42	3.03	.23	25	3.59	.48	17
80 - 85	3.31	.63	43	2.95	.15	25	3.81	.71	18	Insufficient Data								
	2.96	.14	22	2.70	.16	22	3.40	.21	22	2.94	.12	19	2.68	.16	19	3.37	.24	19

$\bar{X}$, σ, and N are the mean, standard deviation, and number of cases in the latitude band.

indication in both coordinate systems that the latitude of the minimum shifts equatorward during the storm. As expected, the variation is less random in C.G. latitude during the storm. This is evidenced in Table 8 by the markedly lower variation about the latitudinal means poleward of 15°.

The equatorial maximum and the trend toward a minimum poleward of 20°S are evident at all times in geographic coordinates. The density fall-off with latitude in the southern hemisphere is absent in C.G. coordinates during the non-storm period. For storm conditions the variation about the latitudinal means is 20 to 30% larger for C.G. latitude between -15° and +5°.

During the non-storm period there is a 20% increase of the density from the mid-latitude minimum to about 80°. In geographic coordinates this increase occurs between 40° and 70°N with nearly level density above 70°N. For C.G. latitude this increase continues to 80°, the highest latitude with an adequate data sample. During the storm period this poleward increase of density from the mid-latitude minimum is interrupted by an even deeper minimum between 60° and 65° in both coordinate systems. The maximum storm density occurs above 80°N geographic latitude. Insufficient data were available to determine whether a similar polar maximum occurs in C.G. latitude. Between -25° and 55° there is a density increase of 25 to 37% between quiet

and storm conditions. In the 60°-65° band the density is substantially unchanged. Above 80°N the density increase was nearly 30%.

Intense density gradients are important features of Figs. 1 and 2. These strong gradients are associated with the geomagnetic storm. They form first at high latitudes on rev 51 (Fig. 1o) and increase in intensity on either side of the 60° to 65°N storm density trough (revs 53-55 in Fig. 1a-c, 53-59 in Fig. 2a-g, and revs 61-64 in Figs. 1 and 2i-1). Strong gradients also occur at low latitudes on revs 53 and 63 (Figs. 2a, 3a, and 2k). Intense gradients are also created in time/longitude as can be seen in Figs. 8 and 9. Most notable are the strong gradients at about 0100 UT and 10°N and at 1600 UT at 28°N and 82°N on Fig. 8.

SPADES

For convenience the four data intervals from SPADES will be discussed separately. The first interval includes 10 revolutions of data spaced 4 revolutions apart beginning with rev 21 on July 13 and ending with rev 57 on July 15, 1968. During this period the perigee latitude moved from 12°S to 4°S. The latitudinal coverage of the density data was between 33°S and 13°N. A moderate geomagnetic disturbance began with a sudden commencement at 1612 UT on July 13 and lasted till about 0600 UT on July 14. At first glance the density profiles at the standard altitudes of 160, 180, and

200 km in Fig. 4 show no strong response associated with the geomagnetic activity. With a six hour delay time the densities on revs 29, 33 and 37 would be expected to exhibit some response to the geomagnetic storm. Examination of the profiles of revs 25, 41, and 45 before and after the storm shows that the density is indeed enhanced on revs 29, 33, and 37, particularly between 30°S and 10°S during the latter two revolutions. This effect can be seen clearly in Fig. 10 where a high density region forms between -30° and -10° and 0000 UT and 1500 UT on July 14. This high interrupts the general trend of lower density near 25°S. The indices at the bottom of Fig. 10 are the planetary geomagnetic range index, a_p, with the scale given on the right and the auroral electrojet index, AE, with the scale given on the left. a_p is a scaled antilog of the K_p, 3 hour geomagnetic index. AE and a_p are plotted without any time lag. The same data are displayed against C.G. latitude in Fig. 14. There does not appear to be any particular advantage to the use of C.G. coordinates at these low latitudes.

With the exception of revs 33 and 37 during the geomagnetic disturbance and revs 49, 53, and 57 where excessive noise appears in the data there is a decided trend toward an increase in density from 30°S to the equator in Fig. 4. This trend can also be seen in Fig. 10. Density values were read off each plot in Fig. 4 over 1° latitude

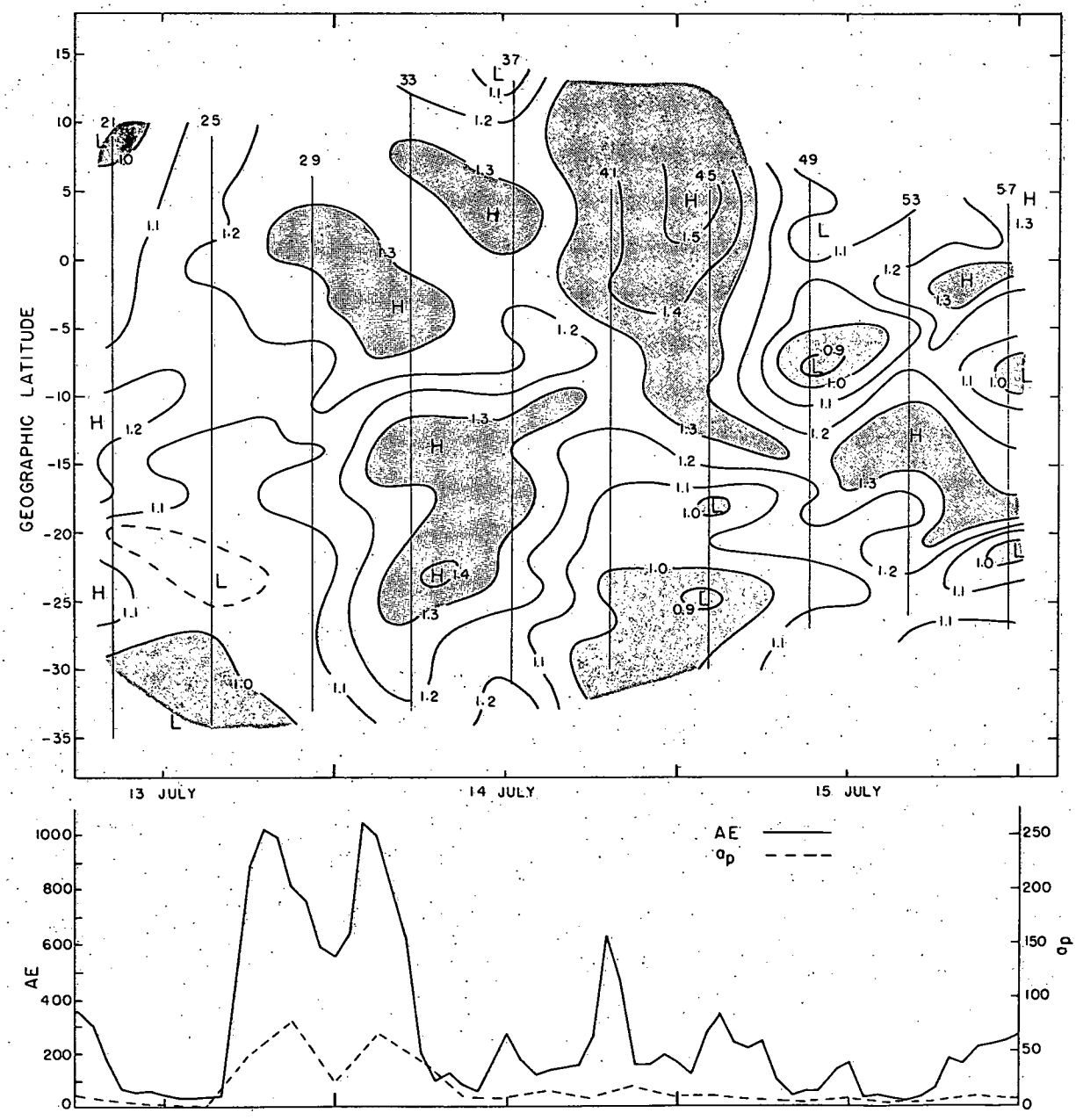

Figure 10. Time-geographic latitude analysis of SPADES densities converted to 160km, revs 21-57. The density isolines are in units of gm/cm^3 scaled by 10^{12}.

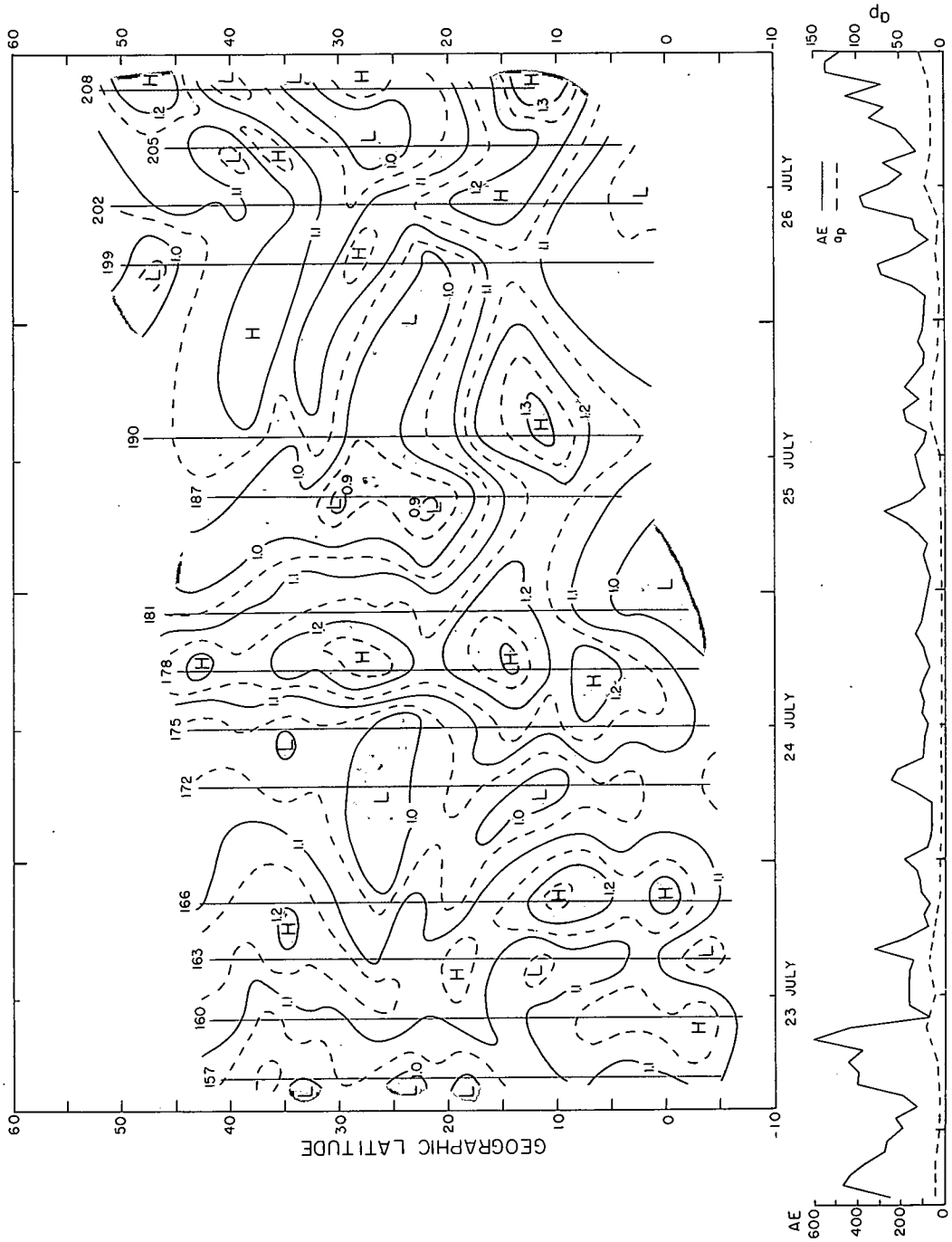

Figure 11. Time-geographic latitude analysis of SPADES densities converted to 160km, revs 157-208. The density isolines are in units of gm/cm^3 scaled by 10^{12}.

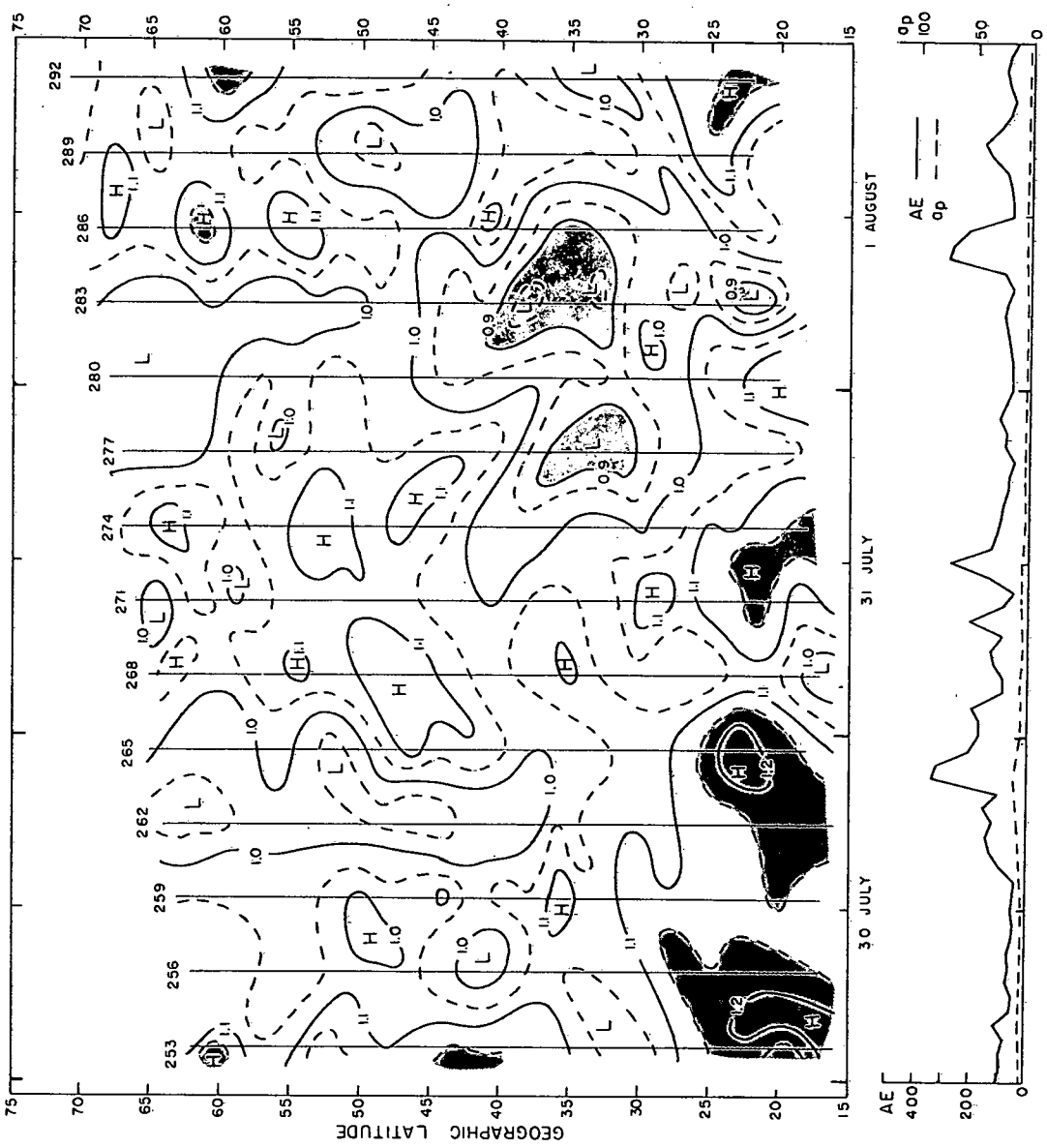

Figure 12. Time-geographic latitude analysis of SPADES densities converted to 160km, revs 253-292. The density isolines are in units of gm/cm^3 scaled by 10^{12}.

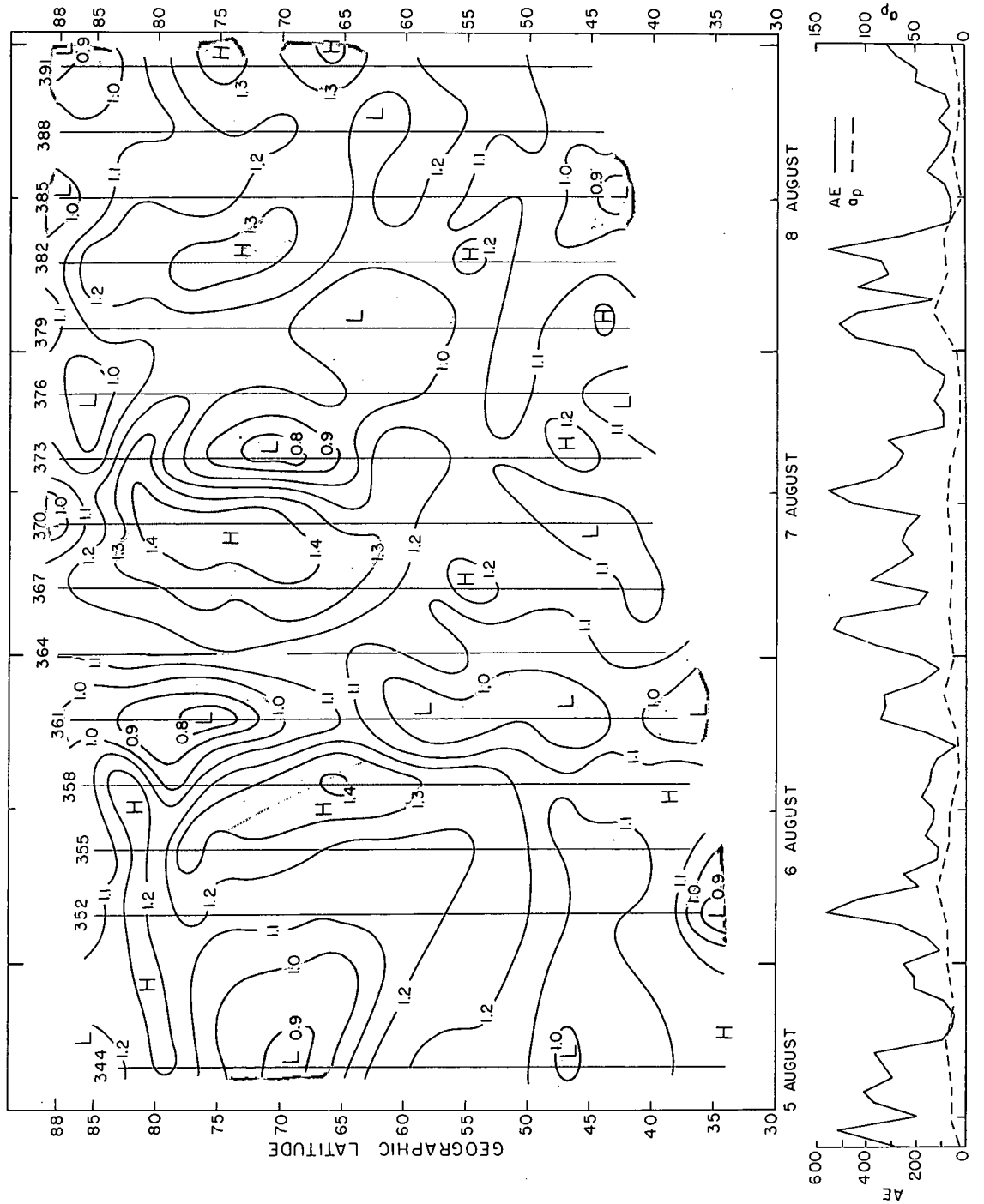

Figure 13. Time-geographic latitude analysis of SPADES densities converted to 160km, revs 344-391. The density isolines are in units of gm/cm^3 scaled by 10^{12}.

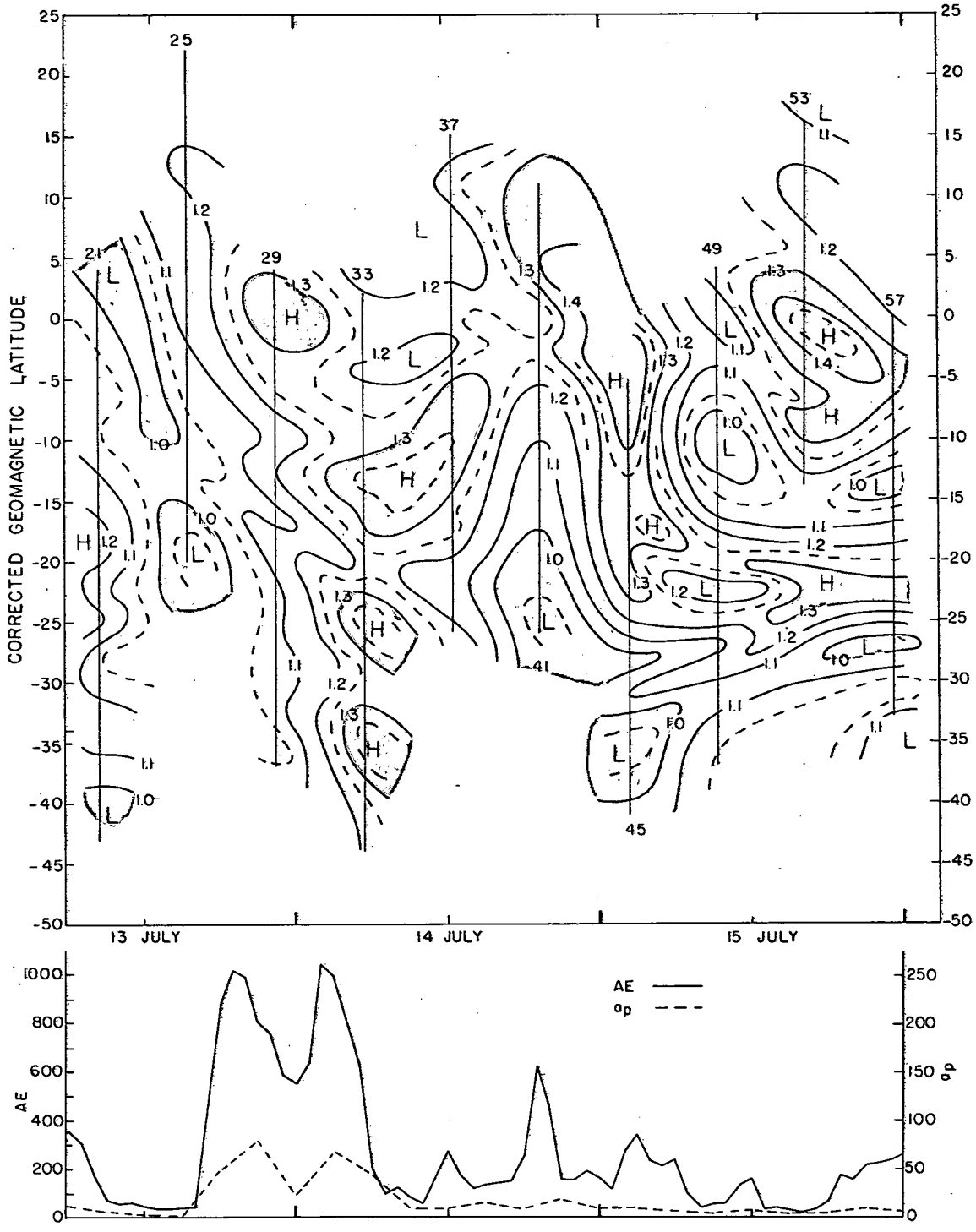

Figure 14. Time-Corrected Geomagnetic latitude analysis of SPADES densities converted to 160km, revs 21-57. The density isolines are in units of gm/cm^3 scaled by 10^{12}.

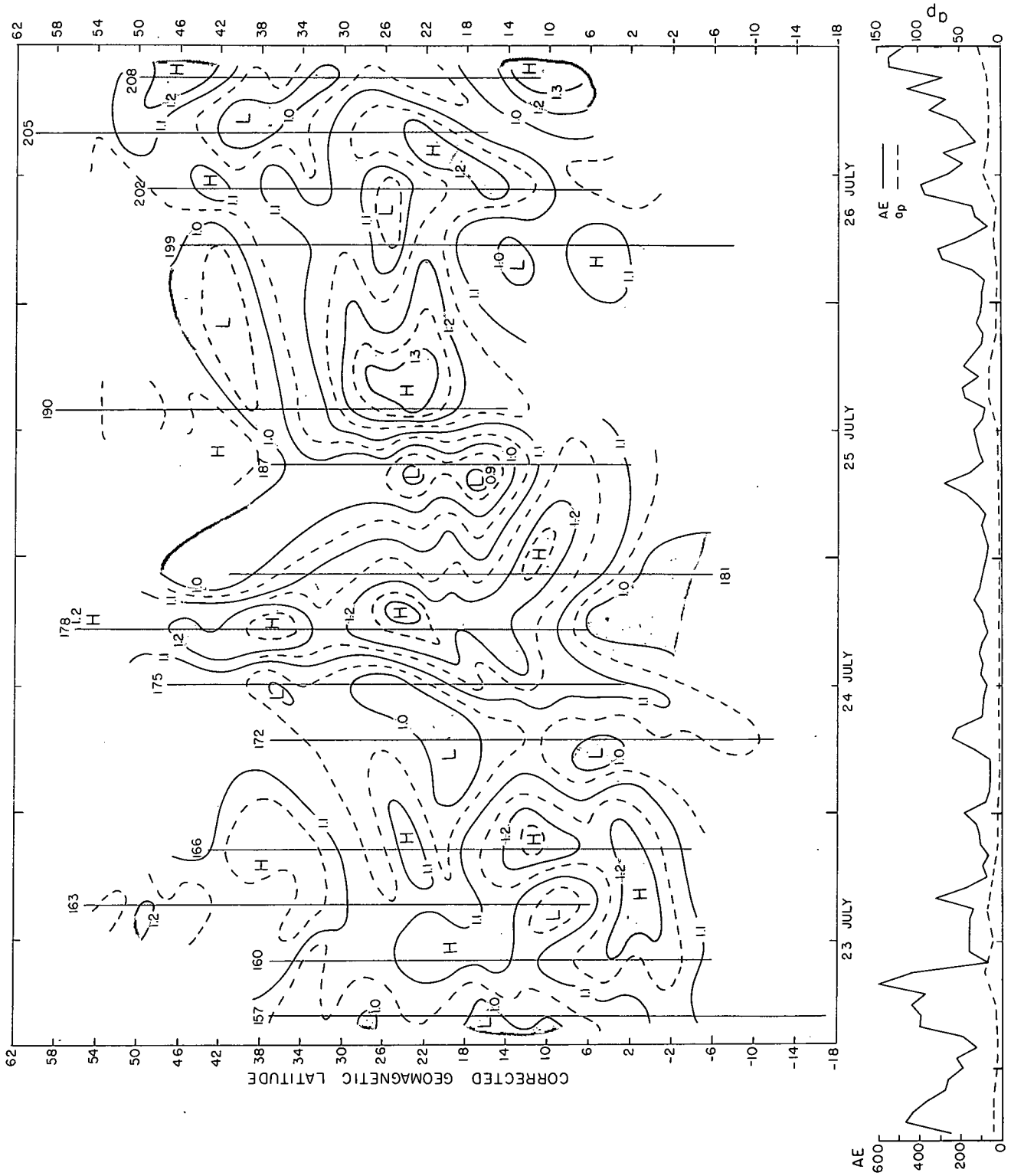

Figure 15. Time-Corrected Geomagnetic latitude analysis of SPADES densities converted to 160km, revs 157-208. The density isolines are in units of gm/cm^3 scaled by 10^{12}.

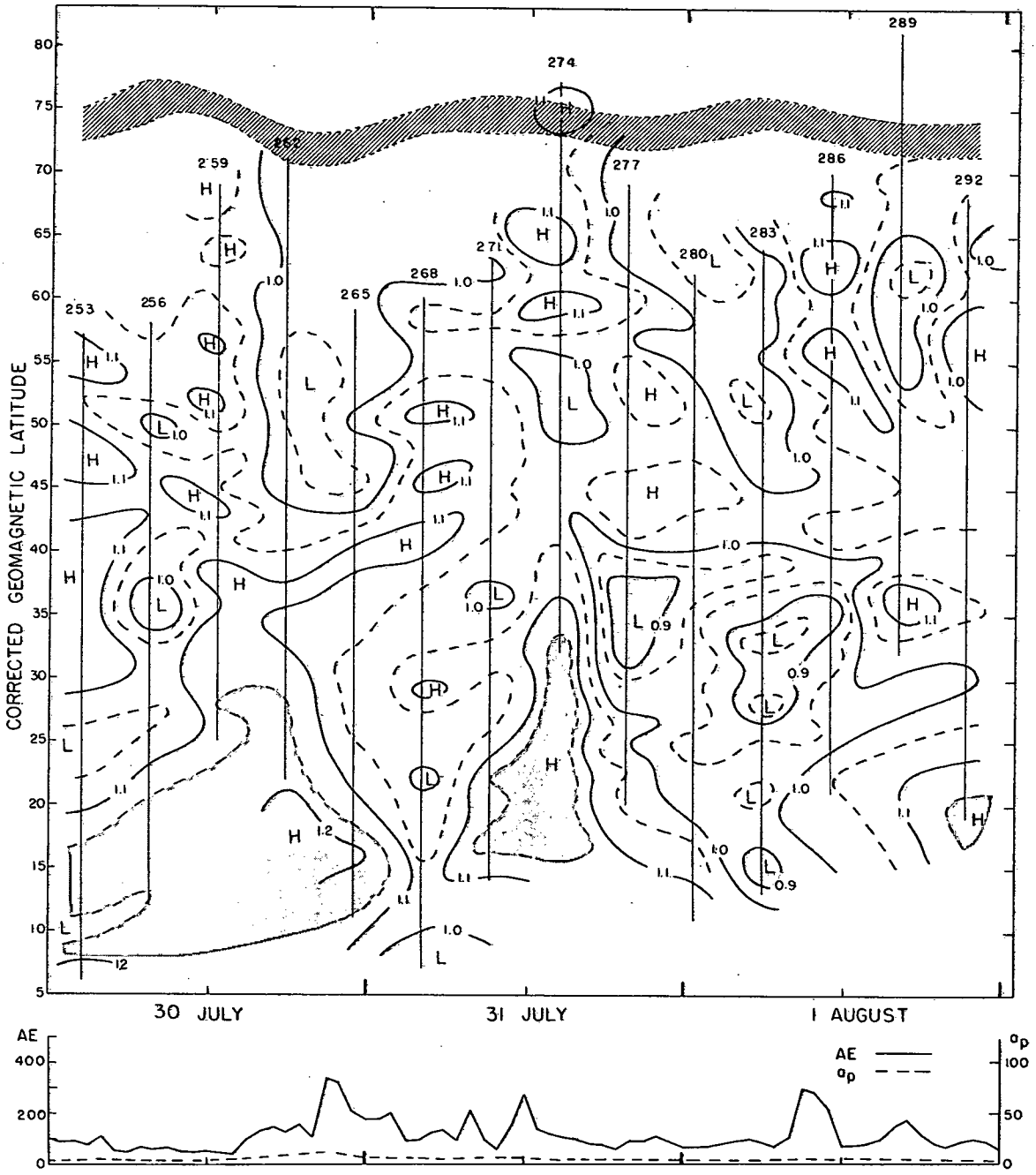

Figure 16. Time-Corrected Geomagnetic latitude analysis of SPADES densities converted to 160km, revs 253-292. The density isolines are in units of gm/cm^3 scaled by 10^{12}.

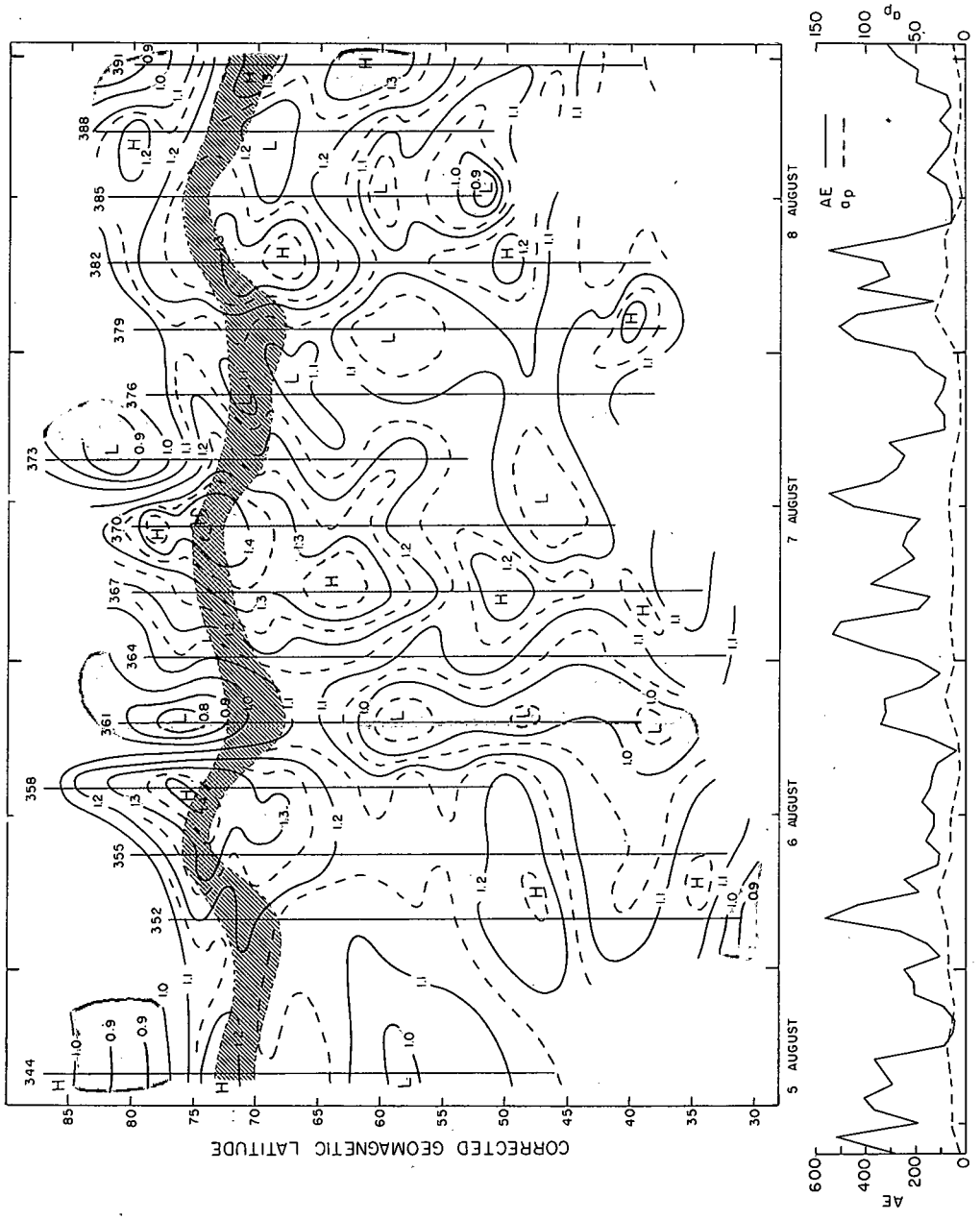

Figure 17. Time-Corrected Geomagnetic latitude analysis of SPADES densities converted to 160km, revs 344-391. The density isolines are in units of gm/cm^3 scaled by 10^{12}.

increments and where necessary converted to 160 km. These values were used to make the analysis in Fig. 10. As with LOGACS, 5° latitude averages were calculated from these 1° values for each revolution over the latitude span of the data and then averaged over all revolutions for each 5° latitude band. The results are given in Table 9. They include the storm period as well as a smoothed profile for revs 49, 53, 57. Even so, there is a clear, significant density increase of 12% between 25-30°S and the equator. The data set for Table 9 is completely homogeneous except for incomplete coverage in three of the 25-30°S averages. The results using C.G. latitude are shown in Table 10. The same trend exists with C.G. latitude but is less definite and there is more scatter about the latitude band means. The average 160 km density for the 13-15 July period is 1.17×10^{-12} gm/cm^3 vs. 1.26×10^{-12} gm/cm^3 given by J71.

The second data span from SPADES encompasses the period of July 23-26, 1968 and includes 14 revolutions during which density data were obtained. The nominal data frequency was one revolution out of every three but the data gathering revolutions were occasionally canceled due to an insufficient power supply. The density data is displayed in Fig. 5. The perigee latitude increased from 17°N on rev 157 to 28°N on rev 208. Data were obtained between 6°S and 52°N. This period was free of any significant

TABLE 9

Zonal Means of SPADES Density Data Converted to 160 km

Geographic Latitude

Lat. Band	Revs 21-57			Revs 157-208			Revs 253-292			Revs 344-391		
	$\bar{X}$	σ	N	$\bar{X}$	σ	N	$\bar{X}$	σ	N	$\bar{X}$	σ	N
-30 - -25	1.09	.09	10									
-25 - -20	1.12	.12	10									
-20 - -15	1.18	.11	10									
-15 - -10	1.22	.09	10									
-10 - -5	1.16	.11	10									
-5 - 0	1.22	.11	10									
0 - 5	1.23	.13	10									
5 - 10				1.13	.07	14						
10 - 15				1.19	.13	14						
15 - 20				1.13	.07	14						
20 - 25				1.07	.08	14	1.10	.08	14			
25 - 30				1.06	.09	14	1.06	.06	14			
30 - 35				1.08	.07	14	1.01	.07	14			
35 - 40				1.09	.06	14	1.01	.07	14			
40 - 45				1.09	.05	14	1.03	.06	14			
45 - 50							1.05	.05	14	1.08	.06	15
50 - 55							1.05	.05	14	1.13	.07	15
55 - 60							1.04	.05	14	1.15	.08	15
60 - 65							1.04	.06	14	1.17	.08	15
65 - 70										1.18	.15	15
70 - 75										1.17	.17	15
75 - 80										1.18	.15	15
80 - 85										1.16	.11	15
85 - 89										(1.06	.09	11)
	1.17	0.05	7	1.10	.04	8	1.04	.03	9	1.15	.03	8

$\bar{X}$, σ, and N are the mean, standard deviation, and number of cases in the latitude band.

TABLE 10

Zonal Means of SPADES Density Data Converted to 160 km

Corrected Geomagnetic (C.G.) Latitude

Lat. Band	Revs 21-57			Revs 157-208			Revs 253-292			Revs 344-391		
	$\bar{X}$	σ	N	$\bar{X}$	σ	N	$\bar{X}$	σ	N	$\bar{X}$	σ	N
-25 - -20	1.18	.11	8									
-20 - -15	1.17	.12	9									
-15 - -10	1.15	.14	10									
-10 - -5	1.19	.14	10									
-5 - 0	1.22	.13	10									
0 - 5	1.19	.11	9									
5 - 10				1.10	.06	11						
10 - 15				1.13	.10	13						
15 - 20				1.10	.08	14						
20 - 25				1.11	.10	14						
25 - 30				1.09	.09	14	1.03	.07	12			
30 - 35				1.08	.06	14	1.03	.09	14			
35 - 40				1.07	.08	14	1.03	.08	14			
40 - 45							1.05	.03	14			
45 - 50							1.04	.05	14			
50 - 55							1.03	.05	14	1.11	.07	15
55 - 60							1.04	.06	14	1.12	.09	15
60 - 65										1.17	.10	15
65 - 70										1.21	.08	15
70 - 75										1.23	.12	15
75 - 80										1.14	.15	15
	1.18	.02	6	1.10	.02	7	1.04	.01	7	1.16	.05	6

$\bar{X}$, σ, and N are the mean, standard deviation, and number of cases in the latitude band.

geomagnetic activity. There were mild disturbances on July 23 and 26. Data filtering problems, previously discussed, affected the derived densities on the first eight data revolutions. A number of the revolutions exhibit some smaller scale wave structure that could either be natural or a result of incomplete filtering of the accelerometer output.

There is a general trend in Fig. 5 for density maximum near 10°N and minima near 30°N. This is readily seen in Fig. 11. The density appears to increase poleward of 30°N. The same data is analyzed in C.G. coordinates in Fig. 15. The latitudinal structure is less ordered in Fig. 15. Five degrees latitude averages of the 160 km densities were calculated as before. The results are given in Tables 9 and 10. The latitude variation observed between revs 157 and 208 was obtained from a homogeneous data sample except that data were not obtained as scheduled on revs 169, 184, 193, and 196. Table 9 indicates a definite density maximum at 10-15°N, a minimum at 25-30°N, and a slight density increase poleward of 30°N. The data obtained equatorward of 5°N indicates a further decrease of density from the 5-10°N average. Similar results are seen in Table 10 but as before the latitudinal variation is less definite with C.G. latitude. The density for revs 157-208 averaged $1.10 \times 10^{-12} gm/cm^3$. For the same average location and condition a value of $1.21 \times 10^{-12} gm/cm^3$ is given by J71.

The third SPADES data period occurs during a quiet geomagnetic period, July 30 to August 1 (see Table 4). The density data were obtained every three revolutions in this period. Fig. 6 contains the plots of these data. The density structure and variation is much less definite in Fig. 6. Perigee ranges from 38°N to 47°N on revs 253 and 292. The latitude span of the data is 17°N to 71°N. Time-latitude analyses of the density are given in Figs. 12 and 16 for geographic and corrected geomagnetic (C.G.) coordinates. In Fig. 12 there is a predominance of low density near 32°N and a slight trend toward increasing density above and below that latitude. The results of 5° latitude averaging are given in Tables 9 and 10. A minimum in density occurs between 30° and 40°N. Equatorward of 30°N the average density increases significantly while only a slight rise is observed poleward of 40°N. Conversion to C.G. coordinates smears out any significant latitudinal variation (Table 10). The average observed density converted to 160 km is 1.04×10^{-12} gm/cm^3 vs a value of 1.17×10^{-12} gm/cm^3 from J71.

The fourth data period from SPADES runs from rev 344 to rev 391 on Aug. 5-8, 1968. Data were obtained on revs 344, 352, and every 3 revolutions after rev 352. During this period data were obtained from 35°N up to 89.5°N, the maximum latitude, and back down to 86°N. Plots of the normalized density observations are shown in Fig. 7.

The perigee point ranged from 59° to 70°N. In the Aug. 5-8 time period the geomagnetic activity level was neither excessively quiet nor were any significant disturbances indicated by the K_p index. Throughout the period the activity level was somewhat enhanced above normal levels, particularly the auroral electrojet index, AE.

The individual density plots of Fig. 7 exhibit a variety of latitudinal variations. Equatorward of 55°N the density is generally lower. At about 70° or 75°N there is considerable fluctuation between high and low density. Latitude-time analyses of the density field are shown in Figs. 13 and 17. In Fig. 13 there is generally lower density at the lower latitudes. Between 65° and 80°N the variation is manifested in a series of alternating high and low centers. These high and low centers do not appear to have any consistent relation to the AE index level. In Fig. 17 these high and low centers are more nearly aligned along 75° to 80°, the auroral oval location (shown by the hatched area). Here the high centers appear to occur with or immediately follow enhancements of the AE index while lows are associated with intervals of low AE index. An alternating pattern of highs and lows appears between 45° and 55° in Fig. 17 but with the phase shifted somewhat from the 75°-80° pattern. Several areas exist in both Fig. 13 and 17 where strong density gradients occur in both space and time. The density decreases 45% at 76° between revs

358 and 361 in Fig. 17 and a 42% decrease occurs at 71°N between revs 370 and 373 in Fig. 13.

The 5° latitude band averages of the density converted to 160 km are given in Tables 9 and 10. In geographic coordinates the density increases from the 45°-50°N band to the 65°-70°N band. Above 80° the density begins to decrease. Data obtained poleward of 85°N (not included in the columnar summation) indicates a steep decline to a polar density minimum. In C.G. coordinates (Table 10) the maximum density occurs at the latitude of the auroral oval, 70°-75°. Between 65° and 75° the variance of the density from the zonal means is much smaller in C.G. coordinates. Data obtained equatorward of 50° C.G. indicates a further decrease of density in that direction. The average 160 km density over the rev 344-391 period was $1.15 \times 10^{-12} gm/cm^3$. J71 gives a value of 1.22×10^{-12} gm/cm^3 for the same average location and level of solar and geomagnetic activity.

The mean densities in each period of data from SPADES differ. This difference is due in part to the latitude, local time, and solar and geomagnetic activity differences. Using the inverse of the normalization factor for T_∞ of 1125°K from Table 6, the non-storm (revs 5-43) average density from LOGACS was converted to 160 km. This 160 km average density is compared with the observed average densities at 160 km from SPADES in Table 11 along with the densities given by J71 for the same average locations

TABLE 11

Seasonal Density Variation at 160 km

Vehicle	Rev Span	Period	Observed Density ($gm/cm^3 \times 10^{12}$)	Model Density (J71) ($gm/cm^3 \times 10^{12}$)
LOGACS	5-43	23-25 May	1.64	1.39
SPADES	21-57	13-15 July	1.17	1.26
SPADES	157-208	23-26 July	1.10	1.21
SPADES	253-292	30 July-1 Aug.	1.04	1.17
SPADES	344-391	5-8 Aug.	1.15	1.22

and solar and geomagnetic activity levels. The SPADES average densities are consistently lower than those from J71 but they do vary in a very similar manner. The LOGACS non-storm average density is considerably higher than that specified by J71 but in comparison with the SPADES results still indicates a seasonal/semiannual variation in the same sense as given by J71. The real amplitude of the seasonal/semiannual variation appears to be larger than that specified by J71 at 160 km for the data considered here.

LONGITUDINAL VARIATION

Even in the absence of geomagnetic activity there is a considerable variation of the density level with time at a given latitude. During a 24 hour period the earth makes almost one complete rotation underneath the satellite orbit. Thus, although the density observations are made at the same local time for a polar orbiting satellite, the longitude of the observations varies systematically through a 360° longitude cycle every 24 hours. At a given latitude density variations with time may also be treated as density variations with longitude. With density data available from one satellite at a time it is not completely clear whether to attribute density changes along a latitude circle to time variations or to longitude dependence. The only known short-term dependence of density is associated with either geomagnetic activity or, to a much smaller extent,

solar EUV flux changes. Given a relatively steady state of solar and geomagnetic activity, any 24 hour periodic variation would be due to a longitudinal density variation.

Figs. 8 and 10-13 give the geographic latitude-time variation of density for LOGACS and SPADES. Due to the intense geomagnetic storm, LOGACS density data on and after rev 45 will be excluded from analysis. Above 40°N in Fig. 8 there are high density centers on revs 14 and 30, 16 revolutions or 24 hours apart. Between 25° and 45°N low density regions are found on revs 11, 27, and 43, each 24 hours apart. The relatively strong high density center on rev 18 lacks an exact counterpart on rev 34 but high density is found on revs 31 and 35. Near 20°N high density areas are located on revs 20 and 34-35 and also revs 14, 30, and 46 (the latter is more enhanced, probably due to the storm). Near 15°S high centers are found on revs 7, 26, and 39 (data were missing on rev 23). Numerous other minor centers exist, most of which are not significant in terms of the relative density variation which they indicate. In Fig. 10 the effects of the geomagnetic disturbance on the rev 33 and 37 densities make it difficult to find "uncontaminated" longitudinal variations. Near the equator high centers are located at 0000 UT and low centers at 1200 UT. The exact locations of these centers are uncertain due to the low time resolution of the data. Low time resolution and missing data revolutions hinder analysis of

Fig. 11. Near 0600 UT low density is found on revs 157, 172, 187, and 199. For SPADES there are 13.7 revolutions each 24 hours. High density regions are located near 2000 UT from revs 166, 178, and 208. Data from revs 193 and 196 would have aided considerably in confirming the high density location. For the 30 July-1 Aug. period (Fig. 12) the generally small amplitude of the density variation made determination of any regular longitudinal variation rather difficult. Below about 40°N low density is generally at about 0600 UT from revs 256, 268, and 283. Low density on rev 277 interrupts the pattern of high density at about 2100 UT on revs 265 and 292. Poleward of 45° the phase of the longitudinal pattern is changed. Low density is located near 2000 UT by revs 262, 265, 277, 280, and 289. High centers are located near 1100 UT from revs 256, 259, 271, 274, and 286. At the higher latitudes in Fig. 13 a strong periodic density variation is readily apparent. This variation may be due in part to a forced response to auroral electrojet activity. High density regions are found near 0900 UT on Aug. 6-8 and low density near 1800 UT on Aug. 5-8. From the SPADES data there is a general trend at low latitudes for low density centers to occur near 0600 UT and highs near 2000 UT. At latitudes above 45°N highs occur near 1000 UT and lows near 1900 UT.

To confirm the above qualitative observations, averages were calculated from the 1° latitude values of

the densities converted to 150 km for LOGACS and 160 km for SPADES for each individual revolution. For LOGACS, three separate averages were calculated for the latitude ranges 25°S - 10°N, 10°N - 45°N, and 45°N - 85°N. The SPADES data from revs 253-292 were broken into two sections at 45°N. In order to compare the longitudinal density variation observed by the two satellites, the seasonal variation and the effects of differences in the general solar/geomagnetic activity levels had to be eliminated from the density averages for each revolution. This was done by dividing the revolution averages by the mean density for the period of the observations, i.e., the averages for revs 157-208 were divided by $1.10 \times 10^{-12} gm/cm^3$ (see Table 11). These normalized values for each revolution are plotted against their respective longitudes in Figs. 18-20. The values from the non-storm portion of LOGACS (revs 5-43) are plotted on the figures with the SPADES data. The plotted data show considerable scatter. Much of this scatter is attributable to changes in the level of geomagnetic activity. For the LOGACS results, a strong increase in the level of solar EUV flux as indicated by the 2800 MHz index (Table 3) occurred over the rev 5-43 period used to calculate the time density average for the normalization process. This results in all normalized values for revs 5-14 being less than 1.0 and almost all the values from revs 29-43 being greater than 1.0 due to the general

density increase over the rev 5-43 period caused by the increase in solar EUV flux. Even so, the general sense of the longitudinal variation should be maintained. In Figs. 18-20, averages of the plotted points in each 30° longitude sector are indicated by squares connected by a solid line.

The results for the 25°S - 10°N latitude band are given in Fig. 18. There does not appear to be any significant difference between patterns of variation of LOGACS and SPADES. The geomagnetic storm enhanced values for revs 33 and 37 of SPADES are located at 87° and 342°E respectively. High density prevails from 120°E to 290°E and low density from 290°E to 70°E. Maximum and minimum density occurred in the 180° - 210°E and 300° - 330°E sectors. However few data points occurred in these sectors (2 and 3) compared with those available for calculating the averages in the other sectors. Six points define both the secondary minimum between 30° and 60°E and the secondary maximum at 120° - 150°E. With SPADES data from two separate observational periods there are more points available to define the average curve for 10°N - 45°N in Fig. 19. A clear high density area lies between 150°E and 320°E. Low density predominates from 330°E to 90°E. Again only two values are available to define the maximum at 150° - 180°E. The scatter of points about the mean seems to be somewhat less. The minimum density average occurs in the 60° - 90°E

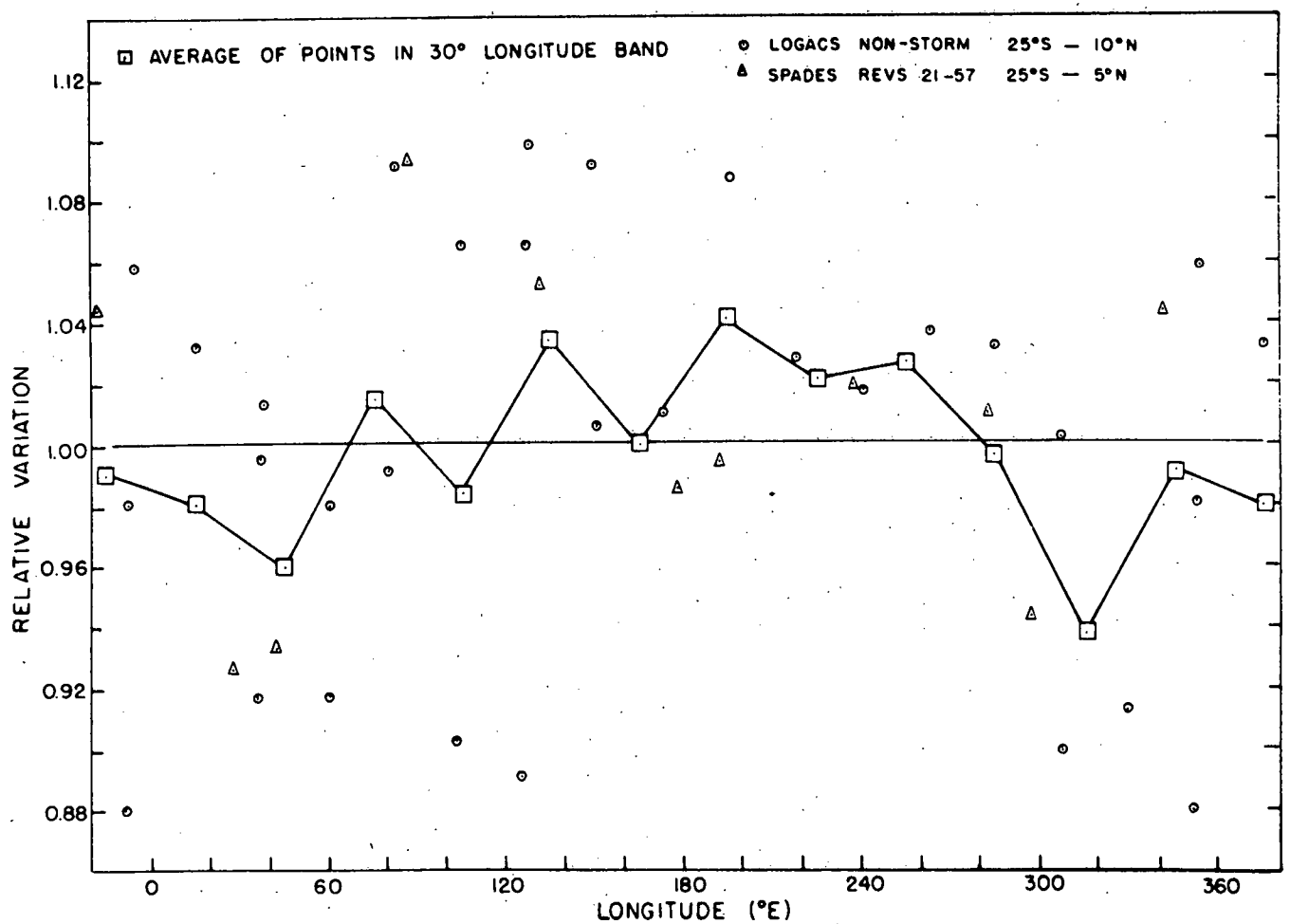

Figure 18. Density variation with longitude, 25°S - 10°N.

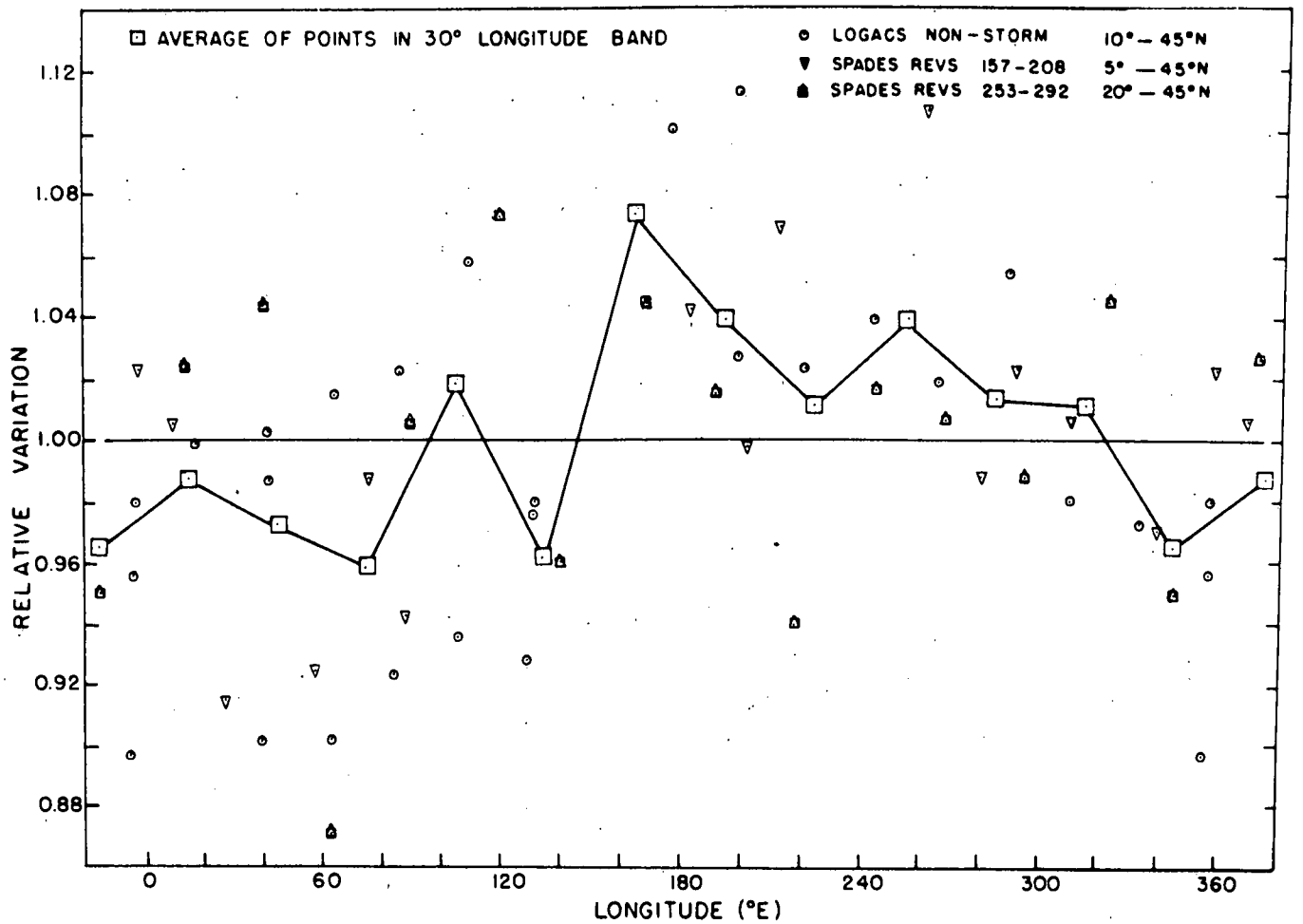

Figure 19. Density variation with longitude, 10°N - 45°N.

sector and is defined by eight values. Between 45° and 85°N (Fig. 20) there is a marked change in the longitudinal variation pattern. From about 340°E forward to 200°E the excursion of the means is rather small. A deep minimum occurs between 210° and 270°E and a less pronounced maximum lies between 270° and 330°E. Even without the very low value at 217°E the 210° - 240°E sector would still be near the low average at 240° - 270°. A weak maximum extends from 0° to 100°E and a secondary minimum lies between 110° and 160°E. The statistical significance of these latter features is rather low. In general the longitudinal density variation at 25°S to 10°N (Fig. 18) and 10°N to 45°N (Fig. 19) is the same with respect to the location of high and low density areas. The density variation with longitude above 45°N (Fig. 20) differs significantly in that the general location of high and low density regions is 180° out of phase with the variation at lower latitudes. It appears that the high and low density distribution is skewed and the extremes are less than 180° apart in Figs. 18-20. This is in agreement with the qualitative conclusions arrived at from examination of Figs. 8 and 10-13.

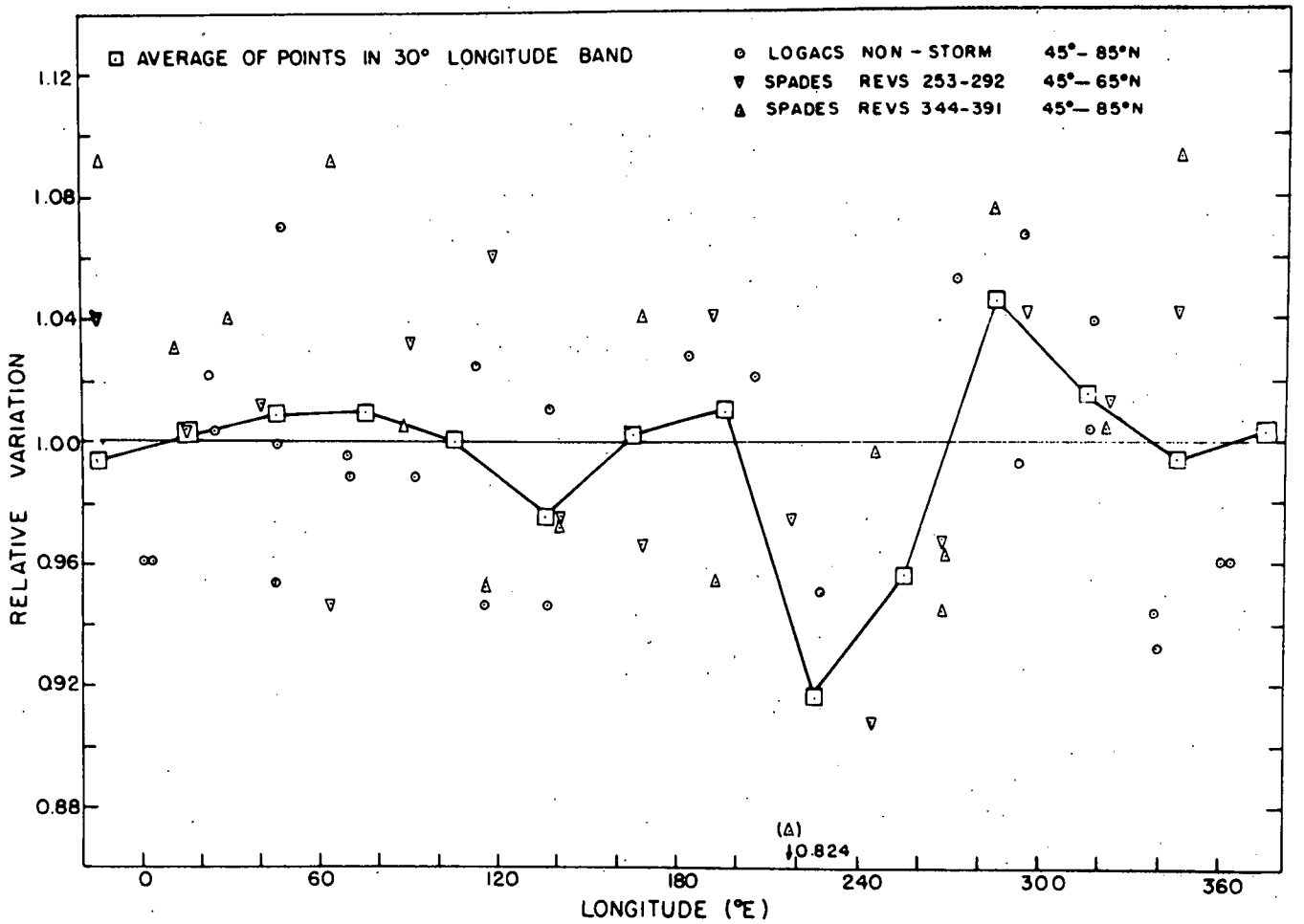

Figure 20. Density variation with longitude, 45°N - 85°N.

V. DISCUSSION

LATITUDE VARIATION

The latitudinal density variation given by J71 for the local time, solar declination, altitude, and T_∞ experienced during the flights of LOGACS and SPADES is less than 2.5%. According to J71 a very flat density maximum occurs near 30°N to 45°N for LOGACS and SPADES with a steady decline on either side of the maximum. The latitudinal density variation observed by LOGACS and SPADES is summarized in Tables 8-10. A density minimum is observed near 30°N in all observation periods covering that latitude. A density maximum occurs near the equator and the largest densities occur at high latitudes. The non-storm minimum density value for LOGACS of $2.43 \times 10^{-12} gm/cm^3$ occurs between 30°N and 40°N (Table 8). For convenience all further density values will be understood to have the units of gm/cm^3 and scaled by 10^{-12}. The standard deviations about the zonal means in these two latitude bands are 0.13 and 0.17. The standard deviation of the zonal means from their average of 2.70 is 0.16. The minimum value is thus deemed to be a significant, real feature of the latitudinal density structure. Similarly, the maximum density plateau poleward of 65°N is also a real feature of the 150 km density structure. The secondary maximum of 2.76 in the 0°-5°N band and the density fall-off in the southern hemisphere are of lesser significance. Never-the-less, the smooth variation

of the zonal averages from one band to the next lends considerable credence to the validity of the latitudinal variation.

The geographic SPADES density variation in Table 9 independently confirms the LOGACS results. The local times of nearly all observations are within ±40 minutes of 1040LT. Although observations from SPADES range from mid-July to early August and LOGACS observations are in late May a year earlier, the solar declination angle during these periods only varies from 16° to 20.7°N. Thus the two satellites obtained their density observations under very similar conditions. In Table 9 the 1.06 minimum at 25°-30°N in the rev 157-208 period, the 1.01 minimum between 30°N and 40°N in the rev 253-292 period, and the sharp fall-off to 1.08 at 45°-50°N from larger values at higher latitudes in the rev 344-391 period are all confirmations of a density minimum in or very near the 30°-35°N latitude band. All three aforementioned density values are at least one full standard deviation below the respective means of their zonal averages. The larger density values between 65° and 80°N in the rev 344-391 period confirm the findings of LOGACS. Both, with density values more than one standard deviation above the mean of the latitudinal averages, indicate that a density plateau in that latitude region is a real part of the density structure. One dark spot in this high-latitude aspect of the density structure is the

absence of any increase of density above 50°N during the rev 253-292 period. However this time period was noted for its lack of geomagnetic activity. High-latitude heating associated with geomagnetic activity is apparently the cause of the high-latitude density "bulge".

The increased density at the equator found by LOGACS seems to be confirmed by the SPADES data. The rev 21-57 results in Table 9 show a maximum of 1.23 between 0° and 5°N. This value and the 1.22 average for 0° to 5°S are both a full standard deviation above the mean of the zonal averages. Data from the rev 157-208 period also yield significantly higher density equatorward of 20°N to 5°N. However the fall-off at 5°-10°N is not consistent with the pattern established by the LOGACS data. Poleward of 15°S the density decreases as shown by the rev 5-43 LOGACS data (Table 8) and the rev 21-57 period of SPADES (Table 9), particularly the latter. This steeper drop-off found by SPADES is probably associated with the higher geomagnetic activity during the rev 21-57 time period. The storm period LOGACS data (revs 45-66) also indicate a more rapid decline of density away from the equator into the southern hemisphere.

Overall, with the exception of latitudes poleward of 65°, the density variation with latitude appears to be more sharply defined in geographic rather than C.G. coordinates. Comparison of Tables 9 and 10 show that for the

first three periods of SPADES data the latitudinal variation about the mean densities for these periods is much larger with geographic latitude, 0.05, 0.04, and 0.03 vs 0.02, 0.02 and 0.01 (standard deviations at the bottom of Tables 9 and 10). For these same periods the individual variations from the zonal means are slightly greater overall for C.G. coordinates. The difference between the equatorial maximum and the near 30° minimum is greater in geographic latitude for LOGACS. Up to about 65° the individual variations from the zonal means are somewhat less for the data referred to geographic latitude. Above 65° the data from LOGACS and the fourth SPADES period show a marked changeover in the relation of the latitudinal density variation to the coordinate system. For the non-storm portion of LOGACS there is a nearly flat density variation with geographic latitude while in C.G. coordinates the density continues to increase significantly to the poleward limit of the data (80°). The rev 344-391 SPADES data behaves similarly except that there is a density drop in the 75°-80° band in C.G. coordinates. This drop is also indicated in geographic coordinates. Most notable is the improved fit between 65° and 75° when referred to C.G. coordinates. The density standard deviation from the zonal mean for C.G. coordinates in the 65°-70° band is less than 60% of that for geographic latitude for both LOGACS and SPADES. In the 70°-75° band the deviations

are less than 80% of those for geographic latitude. For LOGACS in the 75°-80° band the deviation is more than 50% greater in C.G. latitude while it is unchanged for SPADES. This change in behavior between 65° and 75° is expected since these are the latitudes where the auroral oval is located. This further confirms the role of auroral heating during geomagnetically undisturbed periods in determining the density structure.

Latitudinal density variations not in conformity with density smoothly decreasing from the subsolar bulge maximum have been suspected for some time. Jacchia (1970) states that the subsolar bulge is small in the region of maximum EUV absorption but should be above the noise at heights above 150 km. From an analysis of the density from a number of low altitude satellites DeVries (1966) found a negative correlation between density and the subsolar bulge below 220 km. May (1972) found that the subsolar bulge pattern was not clear at 240 km for orbital decay derived densities obtained between Apr. and Nov. 1967. Ching (1971a, 1972a, b) analyzed 219 orbital decay derived densities obtained below 200 km from three satellites (including SPADES) between July and Nov. 1968. A poor, statistically non-significant fit was obtained with a subsolar density bulge, including that given in J71. A density bulge centered over the North Pole gave the best and only statistically significant improvement in

fitting the observed density pattern. Explorer 32 was equipped with gauges which obtained density measurements from 300 to 700 km between May and Oct. 1966. From these measurements Newton and Pelz (1969, 1973) found that the densities obtained above 55°N were 30% higher than at the equator during the day. Even on quiet days densities obtained over the auroral zone were three times equatorial densities. The ratio of density obtained between 35° and 45°N to that at the equator was the same as that given by a model of the subsolar density bulge. During the day T_∞, deduced from N_2 density profiles, between 36° and 59° was less than at the equator. Newton and Pelz inferred that auroral heating was a permanent feature of the summer hemisphere and amounted to a significant fraction of the EUV heating, even during geomagnetically quiet periods. Blamont and Luton (1972) always found higher temperatures at high latitudes than at the equator from their observations of the 6300Å OI line made from OGO-6. Their observations correspond to an altitude of about 260 km. In the analysis of some accelerometer density results from SPADES and OVI-16 (Cannonball), Marcos et al (1971) also found increased density in the auroral region with a trough near the North Pole. Philbrick and McIsaac (1972) observed a density bulge over the auroral oval and a trough between the oval and the magnetic pole. Irregular density profiles were frequently observed in the polar region. A trough was

detected at the magnetic equator on 50% of the data passes. Their observations were obtained by satellite-borne mass-spectrometers at 400 km between Dec. 1967 and Mar. 1968.

The bulk of the above-cited results of other investigators were obtained at altitudes considerably above those examined in this study. Many were obtained by methods which have a small time and space resolution relative to orbital decay derived densities. The latitudinal features found from the LOGACS and SPADES densities are not in conflict with the cited results but rather substantiate them except for the following. In contrast to the observations of Philbrick and McIsaac (1972) a density maximum is found at the C.G. equator on the average. This discrepancy is doubtless a result of season, altitude, and local time differences in the observations, the latter probably being the most important. The LOGACS and SPADES results indicate that the structure found by Newton and Pelz (1969) has its roots well down in the lower thermosphere.

LONGITUDE VARIATION

The longitudinal density variation is given in Figs. 18-20. As discussed earlier, much of the scatter of the individual data points shown in these figures is the result of uncompensated density changes associated with time variations of solar EUV and geomagnetic heating. The solar EUV flux increase, indicated by the solar 2800 MHz flux, over the rev 5-43 period of LOGACS (and the few preceding days as well) contributed particularly to the scatter of the LOGACS data points but does not alter the general sense of the longitudinal variation. The significance of the individual 30° longitude averages is not very high due to lack of sufficient data. Still, the data do indicate a clear higher density between 150° and 290°E in Figs. 18 and 19. Lower density predominates from 330° to 80°E in the same figures. Between 80° and 150°E the pattern is rather mixed though there is a tendency for higher density in this region at low latitudes (Fig. 18) and lower density in low to middle latitudes (Fig. 19). The pattern in Fig. 20 is much less clear due possibly to the influence of varying levels of geomagnetic and auroral electrojet activity (Forbes and Marcos, 1973). Lower density clearly exists from 210° to 270°E and higher density between 270° and 330°E. At the remaining longitudes there is no pronounced trend.

The existence of longitudinal density variations

was reported by Jacobs (1967) from an analysis of orbital decay densities from eleven satellites flown in 1964-5 with perigees between 165 and 215 km and inclinations ranging from 75° to 85°. Jacobs attributed the variation to an earth-fixed eccentric "density bulge" at high latitudes. In a subsequent study Jacchia and Slowey (1968) were unable to detect any such density bulges from orbital decay data at higher altitudes. In a separate study of orbital decay data from 11 low eccentricity satellites flown in 1963-4 with perigees between 160 and 210 km, inclinations of 70-85°, and perigee latitudes from 40° to 60°N, DeVries et al (1967) found a density maximum near 0°-30°E and a minimum at 150°-180°W. Using higher resolution orbital decay densities obtained from ten days of very precise tracking data on each of three satellites, DeVries et al (1972) found periodic daily density variations of 10% at 140 km. The phase of the 24 hour variation was reported to change with time. This could be due to the movement of perigee latitude toward higher latitudes. All of these results were obtained from orbital decay observations of satellites with low altitude, low eccentricity orbits.

Mass spectrometer observations of N_2 density in the southern hemisphere at 430 km were made from OGO-6 during a quiet period between Aug. 28-Sept. 4, 1969 (Hedin and Reber, 1972). The N_2 density was found to be cyclic over

a 24 hour period. The N_2 density was averaged over 30° longitude and 5° latitude and plotted for analysis. A strong, well-defined maximum was found at 70°S, 160°W and a minimum at 80°S, 0-30°W. The observations were made between 2000-2400LT. Similar effects were found in an initial examination of North Polar data. Hedin and Reber attribute this pattern to asymmetrical electron precipitation resulting in increased ionization, joule heating, enhanced N_2 densities, and an induced circulation pattern similar to that caused by a geomagnetic storm. Taeusch et al (1971b) found 12 and 24 hour periodicities in N_2 concentration during the geomagnetically disturbed period of Sept. 27-Oct. 3, 1969. Their observations were obtained from OGO-6 in the northern hemisphere near 1600LT between 400 and 500 km. An examination of their time-geomagnetic latitude plot of N_2 density (their Fig. 4) reveals a 180° change in the phase of their 24-hour variation above 45° geomagnetic latitude. This corresponds very closely to the findings from the LOGACS and SPADES densities at 150 and 160 km.

GEOMAGNETIC ACTIVITY EFFECTS

Two geomagnetic storms occurred during the periods of density observations used in this study. A moderate geomagnetic storm on July 13, 1968 occurred during the rev 21-57 period of SPADES when perigee was near the equator. Only the low latitude effects of this storm were observed. The density response to the "great" geomagnetic storm of May 25-26, 1967 was observed by LOGACS from 30°S up to 88.5°N on the dayside of the orbit and back down on the nightside as far as 30°N. Only the dayside characteristics were studied. The storm of May 25-26, 1967 was one of the most intense geomagnetic disturbances recorded over the last 40 years. In this sense the density observations of LOGACS are rather unique in that the storm may have excited thermospheric response mechanisms that are not brought into play by the more common, lesser intensity disturbances.

During the storm period (revs 45-66) the average LOGACS density at 150 km increased over the rev 5-43 period by 26%. This increase was far from uniform (Table 8). The maximum increase of 37% occurred in the 35°-40°N latitude band. A negligible 1% increase occurred between 60° and 70°N. A 37% increase also occurred in the 35°-40° band in C.G. coordinates. At 60°-65° C.G. just south of the auroral oval position a density increase of 1.4% was recorded. Between 10° and 50°N the increase averaged 35%, tending to fill the mid-latitude density minimum slightly. Significantly

higher density is still found at the equator as compared to 30°-35°N, 3.60 vs. 3.26 against a latitudinal mean and standard deviation of 3.40 and 0.21 (see Table 8). The effect of the moderate geomagnetic storm on the SPADES revs 29-37 density is quite modest by comparison (see Fig. 10). The average density on revs 33 and 37 were only increased by 4.4% and 9.3% from the average of revs 21-57, both below the level of significance. In fact, the highest density area occurs on revs 41 and 45, well after the end of the storm (see the bottom of Fig. 10).

Considerable orbital decay density data has been obtained and analyzed for geomagnetically disturbed periods. The most thorough analysis was made by Roemer (1971b). From observations of 210 storms from 6 satellites over the 250-800 km height range during 1961-6 Roemer found the density response to be 30% greater at night and to increase with latitude. The lag time of the density response was 5.5 ± 0.3 hrs., independent of geographic latitude, local time, storm intensity, and altitude. DeVries et al (1967) found shorter delay times at high latitudes and longer times at low latitudes from an analysis of 11 low eccentricity satellites with perigees between 160 and 215 km. Orbital decay density measurements from low eccentricity satellites with perigees below 140 km have indicated that the level of heating during geomagnetic disturbances is below 140 km (Ching, 1971b; DeVries et al, 1972). High-

resolution measurements from OGO-6 of the thermospheric temperature (Blamont and Luton, 1972) and composition (Taeusch et al, 1971a, b) confirm that greatly enhanced changes occur above 50° geomagnetic latitude as a result of a geomagnetic storm. A local time dependence of the storm effect is also observed. In sharp contrast to Roemer's findings, the response time of the atmosphere is almost immediate (less than one hour) in the vicinity of the auroral zone. Low latitudes are found to be relatively unaffected.

The density response observed by LOGACS to the great storm beginning at 1236 UT on May 25 is shown in Figs. 8 and 9. At high latitudes there is an immediate increase of density to a high center on rev 46 corresponding to the first peak in the 3 hour planetary range index, a_p, plotted along the bottom of Figs. 8 and 9. The high center is located well inside the auroral oval (indicated by the hatched area on Fig. 9). What follows on rev 48 is very unexpected, a deep low density center forms at high latitudes, right in the auroral oval, while a high appears near the equator. The center density in the low is 29% less than the average density of 2.70 observed on revs 5-43. The rev 48 equatorial high is 39% above the quiet-time average and lags the first a_p peak by about 4 1/2 hours. On rev 53 high density occurs at high latitudes in response to the highest geomagnetic activity peak. Lack of high latitude data on

rev 52 prevents an accurate determination of the response time lag. Simultaneously, the lowest observed density (33% below the non-storm average) occurs near 67°N or about 6° south of the expected auroral oval location. Near the equator on rev 53 the density level is slightly more than double the quiet-time average. A lag of about 3 hours occurs between the time of the initial peaking of the a_p index and the high density on rev 53. On rev 55 a high density region occurs near 50°N while the equatorial peak is considerably reduced, even though high geomagnetic activity still persists. By rev 57 all but the highest latitudes have experienced a considerable relative decline in density levels to an extent far greater than anticipated by the reduction of geomagnetic activity. The longitude on rev 57 is about 45°E where a longitudinal variation of density indicates lower density at equatorial and low to middle latitudes (Figs. 18 and 19). Generally higher density occurs at low and middle latitudes on revs 59-61. The peak observed density on the dayside occurs at 82°N on rev 62. The peak value is 104% greater than the non-storm average. Curiously, this high density level is reached a full 12 hours after the end of the geomagnetic activity peak. The longitude of rev 62 is about 298°E, the location of the longitudinal density maximum for high latitudes in Fig. 20. Except for scattered small-scale features the density generally declines following rev 62.

In general, high density centers form in response to the storm at 35° - 55° C.G. and -15° to +15° C.G. between revs 47 and 62. Throughout the entire period beginning with rev 47 a persistent density trough exists between 55° and 75° C.G. (Fig. 9). This trough forms shortly after the beginning of the storm. It moves south of its initial location in the auroral oval to its southernmost position at 61° C.G. on rev 56, coincident with the end of peak storm intensity. The trough then fills and moves northward in the same manner as the auroral oval but somewhat more rapidly. Density minima occur in the trough coincident with or immediately following the two peaks in the storm intensity. The auroral oval may coincide more closely with the density trough. Its position was determined by using the relatively crude K_p indices. Further, at the extremely high geomagnetic activity levels, which occurred during this storm, the relation of the oval position to geomagnetic activity (auroral electrojet) level is very poorly known (due to a lack of occurrences of such high levels of activity). Even so, the indicated oval position is probably in error by three or four degrees of latitude at most.

Joule heating associated with the auroral electrojet can produce local heating in the 110-180 km region (Banks, 1972). This heating may peak near 150 km (Cole, 1971). In the density trough it appears that with the intense geomagnetic storm, sufficient local heating occurs

near the 150 km level to overcome any density increase from the lifting of the atmosphere due to heating at lower levels. Dynamical effects may also play a role in the creation of the density trough. For the local time of the LOGACS dayside density observations Cole (1971) and Fedder and Banks (1972) have shown that ion motion induced by auroral electric fields is from W to E equatorward of the auroral oval and oppositely directed poleward of the oval. The ion motions accelerate the neutral atmosphere through collisions to velocities of as much as 2 km/sec (Cole, 1971). Such motions, oppositely directed, on either side of the auroral oval, could contribute to the formation and maintenance of the observed density trough. Winds derived by Feess (1968) from observed side forces on the LOGACS vehicle show exactly such a direction reversal of the wind across the auroral latitudes for revs 51-59. High density gradients are formed on either side of the trough implying strong pressure gradients existed as well. These facts are in conformity with the predictions of Cole (1971) as pointed out by DeVries (1972b).

The matter of the time delay of the atmospheric density response is more complex than described by DeVries (1972) who found time delays increasing from 0 hours above 60° to 6 hours equatorward of 30°. The high density maximum near the equator on rev 53 lagged the beginning of peak a_p by about 3 hours. The equatorial high on rev 48

lagged the first a_p peak by about 4 1/2 hours. The equatorial high on rev 59 occurred 7 1/2 hours after the a_p index began to decline from its peak value of 400 units. The large density peak at about 45° C.G. near rev 60 follows the end of the a_p peak by 9 hours and the peak density at 82°N on rev 62 was 12 hours after the end of the a_p maximum. The average density in the 15°S-15°N latitude band reached maxima on revs 48, 53 (main maximum), 59 (secondary peak), and 63. In the 15°N-45°N latitude band, average density maxima occurred on revs 47, 50, 54 (secondary peak), and 59 (main maximum). The first maximum in the 15°-45°N band on rev 47 occurs 1 1/2 hours before the equatorial band maximum but is not nearly as strong or distinct. The mid-latitude average peak on rev 50 has no apparent equatorial counterpart. Equatorial observations were not available on rev 54. Thus it is impossible to determine whether the equatorial main maximum occurred on rev 54 at the same time as the mid-latitude secondary maximum or 1 1/2 hours earlier on rev 53 where it was observed. The main mid-latitude average density maximum on rev 59 coincides with equatorial average secondary maximum. In both cases, missing data on revs 58, 60, and 61 prevents any conclusive determination of a difference in the response time in the two latitude bands.

Mayr and Volland (1973) conducted a theoretical study on the density and composition changes in the

thermosphere in response to simulated auroral heating symmetrical about the equator with maximum input at midnight at about 68° latitude. They show contours of the density response with time and latitude at 200 km. The maximum density increase occurs above 65° latitude lagging the maximum heat input by about 3 hours. At the equator the density increase is roughly one-half that at polar latitudes. The equatorial maximum lags the peak heating by about ten hours. The isolines of constant density increase shift smoothly to later times as they approach the equator from latitudes above 65° thus giving a 6-7 hour longer response time at the equator. This time-shifting of the density contours as they extend to lower latitudes does not appear in Figs. 8 or 9. The observed latitudinal density response for subauroral latitudes at 150 km appears to be nearly independent of time. This discrepancy between the LOGACS density response and that predicted by Mayr and Volland is probably due to some of the simplifications they made in deriving their model. These include auroral heating symmetric about the equator, omission of the advection terms in the equations of motion, and no provision for momentum generation induced by electric fields. The differences between 150 and 200 km may also be very important.

In summary, the amplitude of the density response near 150 km is nearly independent of latitude between 5°S and 50°N. There is almost no density response in the 10°

latitude band south of the auroral oval on the average during a great geomagnetic storm. The average amplitude of the density response inside the polar cap is the same as at low and middle latitudes. There appears to be somewhat less response in the Southern Hemisphere probably due to seasonal differences. The quiet-time minimum density found near 30°-35°N is maintained during the storm. The latitudinal density variation is more consistent in C.G. coordinates during the storm, especially poleward of 10° C.G. The general response to the storm at 150 km is not the general build-up of density at high latitudes and the gradual cascading of increased density equatorward with time decribed by Mayr and Volland (1973), but the creation of a number of individual high and low centers which are frequently located at the same latitudes and longitudes as during undisturbed conditions but with enhanced amplitudes. Determination of the delay in the density response to geomagnetic activity is complicated by the 1 1/2 hour time resolution of the density observations and the 3-hour span of the a_p geomagnetic index. It appears that the response delay to increases in a_p is of the order of 4-6 hours, nearly independent of latitude below about 55°N. The density response is immediate in and poleward of the auroral oval.

GRAVITY WAVES

Gravity wave effects in the lower thermosphere have been observed by various techniques. Newton et al (1969) observed waves in the density of amplitudes up to 50% which they interpreted as free internal gravity waves with wavelengths between 130 and 520 km traveling N to S. Their observations were obtained by density gauges on Explorer 32 in the Northern Hemisphere near the auroral zone between 286 and 510 km. Large-scale traveling ionospheric disturbances (TIDs), a manifestation of gravity waves, have been observed by ionospheric sounders (Hunsucker and Tveten, 1967), radar backscatter (Testud, 1970; Thome, 1968), and changes in the Faraday rotation (Davis and daRosa, 1969; Davis, 1971). In all cases the general direction of travel is from N to S (in the Northern Hemisphere). They are generated by auroral events or high geomagnetic activity (Chimonas and Hines, 1970; Testud, 1970; Davis, 1971) predominantly with an apparent source in the evening sector of the auroral oval. The observed phase velocity of large-scale TIDs varies from 400 to 725 m/sec (Davis and daRosa, 1969; Davis, 1971; Thome, 1968) and the period is in excess of one hour. TID's carry auroral energy toward the equator (Blumen and Hendl, 1969; Chimonas and Hines, 1970; Testud, 1970).

With high resolution density observations from LOGACS during the great magnetic storm it is only natural

to examine the data for gravity waves. Several excellent examples are seen in Figs. 1c (rev 55), 2k (rev 63), and 2m (rev 65). Other cases appear on rev 53 in Fig. 2a, rev 55 in Fig. 2c, rev 45 in Fig. 2i, rev 47 in Fig. 2k, and rev 50 in Fig. 2n. Indications of gravity waves are found on other revolutions but lack of sufficient data resolution prevents unambiguous identification. The wavelengths range from 450 to 1000 km and the amplitudes are less than 1%. Gravity waves are found from 30°N to over the North Pole (mostly 45°-60°) and down to 140 km. All the observed gravity waves occurred during the period of high geomagnetic activity.

Gravity waves appear in the SPADES data also. Reliable identification of the waves is somewhat difficult because of possible errors in the data filtering technique discussed previously. Possible gravity waves exist on revs 277, 286, 289, and 291 in Fig. 6i, l, m, and n. However only mild auroral electrojet activity occurred during this period (see Figs. 12 or 16). Clearer gravity wave displays occur on revs 358, 385, 388 and 391 in Figs. 7d, m, n, and o. These have the same general characteristics as those found by LOGACS. The amplitudes are greater, especially at higher altitudes. Marcos and Champion (1972) found that the amplitude of these waves decreased toward the equator and that the amplitude was longitude dependent, being largest at 245°-290°E. This latter manifestation may be

due to the periodicity of the auroral electrojet index, AE, shown at the bottom of Figs. 13 and 17.

An excellent theoretical study of thermospheric gravity wave modes has been made by Francis (1973). In his analysis he included the dissipative effects of viscosity and thermal conductivity as well as a realistic sound speed profile of the atmosphere. The long period gravity waves found by LOGACS and SPADES correspond very closely to the characteristics of his thermospheric "F" mode, an imperfectly ducted mode propagating along the steep temperature gradient at the base of the thermosphere. From the observed wavelengths a phase velocity of 650-700 m/sec and a period of 60-150 min. are derived from the results of Francis' analysis. The attenuation distances of these waves (reduction of amplitude by 1/e) are specified to be about 5000 km from Francis' results, in agreement with the observations.

CIRCULATION IMPLICATIONS

Theoretical treatments of thermospheric circulation have considered the effects of viscosity, ion drag, advection terms, coriolis acceleration, inertia, and pressure gradient forces. A Jacchia-type model of the subsolar density bulge and corresponding night-time density minimum is chosen for the determination of the pressure gradient terms. The resulting wind distribution patterns are

generally diverging from the high density region and converging into the low density region, the amount of cross-gradient drift being determined by the ionization model (ion drag) and viscous effects. The existence of a heat source in the eccentric auroral oval and momentum generation by auroral electrojet fields are neglected. Comparison of incoherent scatter observations of the meridional neutral wind component on geomagnetically quiet days with the winds calculated from theoretical considerations using a Jacchia-type subsolar bulge has shown that an imposed electric field is required in the summer to match the theoretical winds with the observed winds (Amayenc and Vasseur, 1972). Heating rates in the auroral oval are 50 ergs $cm^{-2}sec^{-1}$ during the day and 500-5000 ergs $cm^{-2}sec^{-1}$ at night during very active periods (Banks, 1972). Auroral Joule heating is on the order of EUV heating over the entire globe (Cole, 1971). The energy release through auroral electric fields, even during quiet periods, has been calculated to be on the order of the global EUV heating rate of 1-5 ergs $cm^{-2}sec^{-1}$ (Banks, 1972). The density response to geomagnetic activity is due to auroral heating and heat transport to lower latitudes (Volland, 1969). The auroral electric fields not only produce W to E winds through ion drag but the Joule heating should also produce an equatorward wind component due to the build-up of pressure gradients at higher altitudes over the auroral oval and polar

cap. Incoherent scatter measurements of the meridional neutral wind component in the lower thermosphere at 45°N have shown that the normal daytime poleward drift of 25-35 m/sec is nearly stopped during geomagnetically active days (Reddy and Vasseur, 1972). This effect was found to be most pronounced at 150-165 km.

The theoretical electric field driven winds in the auroral zone should cause divergence in the morning side of the auroral oval and convergence on the evening side below 200 km (Fedder and Banks, 1972). Cole (1971b) calculates that the electric fields and Joule heating creates sufficient energy in a very short time to lift the entire auroral zone thermosphere above about 100 km, thus establishing a convection pattern on either side of the auroral zone. This is apparently what is happening at 60°-70° in Figs. 8 and 9 for the LOGACS density.

The density increase in the equatorial region is less easily explained. Joule heating by the equatorial electrojet does not appear to be sufficient to cause the observed response. It has been calculated to be nearly an order of magnitude less than auroral electrojet heating (Knudsen, 1969). Low latitude heating by gravity waves does not fit the observed storm-time, latitudinal density distribution. The influence of gravity wave energy transport would be greater at higher latitudes and diminish as the equator is approached. Only a fraction (1/e) of the gravity

wave energy would be available equatorward of 20° (assuming wave generation occurs at 65°). This does not take into account the divergence of the meridians toward the equator. The effect of gravity waves would be to strongly increase density in mid-latitudes and leave equatorial density relatively unchanged. The observed results in Table 8 contradict this hypothesis. A possible mechanism might be descending motion at equatorial latitudes. A problem associated with this is the rather impulsive nature of the equatorial density response as exhibited near rev 53 in Figs. 8 and 9. If indeed descending motion occurs at the equator where does the air come from above 150 km? For the preceding 12 hours the geomagnetic storm has been heating the auroral oval. During this time density depletion has occurred in and south of the auroral oval. West to east winds are generated south of the auroral oval by the auroral electric field. Velocities of up to 2 km/sec may be generated in this manner (Cole, 1971). Accompanying all this is an increase in the ionization of the atmosphere particularly at higher latitudes, increasing the ion drag term outside the auroral region. In the auroral region enhanced ion concentration contributes to the acceleration of the neutral wind by the auroral electric field. At some altitude above 150 km this heating produces an increase in density as observed by the OGO-6 mass spectrometer (Taeusch et al, 1971b) at 450 km. This would produce an equatorward pressure

gradient and result in equatorward winds. The cessation of the normal poleward neutral wind drift below 225 km on geomagnetically active days as observed by Reddy and Vasseur (1972) is a direct indication of this effect. This polar region high pressure may drive the atmosphere at the upper levels toward lower latitudes and possibly account in part for the observed high density at the equator during the storm through descending motion there. Initially, parcels at 60°N with 1-2 km/sec eastward velocities would have sufficient absolute angular momentum to overcome the coriolis torque in moving toward the equator. Divergence accompanying equatorward motion and dissipative effects from ion drag and viscosity would tend to reduce the eastward angular momentum. It may be that the impulsive nature of the storm along with its great strength may have created a large-scale horizontal eddy motion to produce the observed effect near the equator on rev 53. A quantitative, numerical investigation, taking into account all the relevant factors, is required to answer this question. From the evidence of the thermospheric density response in Figs. 8 and 9, the dynamics associated with the auroral heating and momentum generation (all around the oval, but principally on the nightside) must be quite complex.

One further point is the latitudinal density minimum near 30°-35°N. This feature persisted throughout the entire period of LOGACS observations. It appeared undiminished

during the storm period. SPADES density observations also showed that it was present then as well. The cause of this feature is unknown. It may be due to local heating from the sun. If so, its amplitude would decrease markedly with altitude. Also it would not be present at 0600 LT. It is curious that the longitudinal variation below and above 45°N in Figs. 19 and 20 differ in phase. It may be that the difference is associated with the occurrence of the mid-latitude density minimum. The shaded high and low density regions in Figs. 10-17 are statistically significant density departures from the average density level. They tend to indicate that eddy motions occur in the 160 km circulation in response to concomitant pressure differences.

VI. CONCLUSIONS

The density data from LOGACS and SPADES have provided a somewhat unexpected picture of the density structure near 150-160 km and its response to a very intense geomagnetic storm. The results are limited in that they cover a very short span of local time and season.

The density varies with latitude with high density at the equator, low density at 30°-40°N, and the highest density over or near the poles. In geomagnetically quiet intervals density is best ordered in geographic coordinates except near the auroral zone. During a great geomagnetic storm this basic pattern is unaltered with the exception that a density trough appears just equatorward of the auroral oval. During the storm the latitudinal density distribution is better ordered in Corrected Geomagnetic coordinates. A longitudinal density variation exists which changes phase above about 45°N. The phase of the longitudinal variation appears to be the same from about 25°S to 45°N. Plots of the density distribution at a single altitude reveal high and low density centers which suggest that large scale eddy motions may result from the pressure differences between these centers.

The density response at 150 km to the great geomagnetic storm of 25-26 May 1967 is not at all like that predicted by the theoretical model of Mayr and Volland (1973) for 200 km. A general enhancement of the density level

occurs at all latitudes. The average density response at the equator equals that over the polar cap. The mean density just south of the auroral oval remains at pre-storm levels. Large short-term variations in the density occur at all latitudes. Just south of the auroral oval a density decrease to 65% of the pre-storm level occurred in a span of three hours. Short-term density increases of 100% occurred at both equatorial and polar latitudes. Gravity waves generated by the auroral oval heating accompanying the storm are observed in the density structure down to 140 km. These waves have wavelengths ranging from 450 to 1000 km. They appear to conform to the long-period "F" mode predicted by Francis (1973).

The thermospheric circulation near 150 km is not adequately described by models which do not include permanent auroral heating and momentum generation by auroral electric fields particularly during geomagnetic storms. Auroral heating cannot be adequately modeled as being symmetrical about the equator. The effects of the auroral eccentricity must be taken into account. The 150-160 km level is dynamically far more complex than has been indicated by the simple density structure derived from orbital decay observations.

BIBLIOGRAPHY

Allen, J. H., C. C. Abston, and L. D. Morris, Auroral Electrojet Magnetic Activity Indices AE (11) for 1968, Report UAG-29, World Data Center A for Solar-Terrestrial Physics, Boulder, Colo., 1973.

Amayenc, P., and G. Vasseur, Neutral Winds Deduced from Incoherent Scatter Observations and Their Theoretical Interpretation, J. Atmos. Terr. Phys., 34, 351, 1972.

Banks, P. M., Magnetospheric Processes and the Behavior of the Neutral Atmosphere, Space Res. XII, 1051, 1972.

Blamont, J. E., and J. M. Luton, Geomagnetic Effect on the Neutral Temperature of the F Region during the Magnetic Storm of September 1969, J. Geophys. Res., 77, 3534, 1972.

Blumen, W., and R. G. Hendl, On the Role of Joule Heating as a Source of Gravity-Wave Energy Above 100 km, J. Atmos. Sci., 26, 210, 1969.

Bourdeau, R. E., S. Chandra, and W. M. Neupert, Time Correlation of Extreme Ultraviolet Radiation and Thermospheric Temperature, J. Geophys. Res., 69, 4531, 1964.

Bruce, R. W., Upper Atmospheric Density Determined from a Low-G Accelerometer on Satellite 1967 50 B, TOR - 0158 (3110-01) - 16, Aerospace Corporation, El Segundo, Ca., 1968.

Challinor, R. A., The Apparent Rotation of the Upper Atmosphere, Planet. Space Sci., 16, 557, 1968.

Challinor, R. A., Neutral-Air Winds in the Ionospheric F-Region for an Asymmetric Global Pressure System, Planet. Space Sci., 17, 1097, 1969.

Challinor, R. A., Neutral-Air Winds in the Ionospheric F-Region for an Asymmetric Global Pressure System, Planet. Space Sci., 18, 1485, 1970.

Champion, K. S. W., and F. A. Marcos, Densities from OV1-15 and OV1-16, AFCRL-69-0495, also known as Air Force Surveys in Geophysics, No. 213, L. G. Hanscom Field, Ma., 1969.

Chimonas, G., and C. O. Hines, Atmospheric Gravity Waves Launched by Auroral Currents, Planet. Space Sci., 18, 565, 1970.

Ching, B. K., A Comparison of Satellite Drag Density Data With Several Model Atmospheres at Altitudes Below 200 km, TOR-0059(6110-01)-44, Aerospace Corporation, El Segundo, Ca., 1971a.

Ching, B. K., Atmospheric Density and Rotation Below 195 km from a High-Resolution Drag Analysis of the Satellite OV1-15(1968-59A), J. Geophys. Res., 76, 197, 1971b.

Ching, B. K., A Note on the Density at High Latitudes Inferred from Low-Altitude Satellite Drag Data, J. Geophys. Res., 77, 781, 1972a.

Ching, B. K., Density Variations and Atmospheric Rotation below 200 km from the Drag on the Satellite OV1-15, Space Res. XII, 841, 1972b.

Cole, K. D., Electrodynamic Heating and Movement of the Thermosphere, Planet. Space Sci., 19, 59, 1971.

Cole, K. D., Thermospheric Winds Induced by Auroral Electrojet Heating, Planet. Space Sci., 19, 1010, 1971b.

Cook, G. E., Satellite Drag Coefficients, Planet. Space Sci., 13, 929, 1965.

Davis, M. J., and A. V. daRosa, Traveling Ionospheric Disturbances Originating in the Auroral Oval during Polar Substorms, J. Geophys. Res., 74, 5721, 1969.

Davis, M. J., On Polar Substorms as the Source of Large-Scale Traveling Ionospheric Disturbances, J. Geophys. Res., 76, 4525, 1971.

DeVries, L. L., An Investigation of Atmospheric Density Between Altitudes of 180 km and 300 km, Tech. Rept. No. 190, Air Weather Service (MAC), USAF, 1966 (Also Ph.D. Dissertation, Saint Louis University, 1965).

DeVries, L. L., Analysis and Interpretation of Density Data from LOGACS, Space Res. XII, 777, 1972.

DeVries, L. L., Structure and Motion of the Thermosphere Shown by Density Data from the Low-G Accelerometer Calibration System (LOGACS), Space Res. XII, 867, 1972b.

DeVries, L. L., E. W. Friday, and L. C. Jones, Analysis of Data Deduced from Low-Altitude High Resolution Satellite Data, Space Res. VII, 1174, 1967.

DeVries, L. L., L. Schusterman, and R. W. Bruce, Atmospheric Density Variations at 140 Kilometers Deduced from Precise Satellite Radar Tracking Data, J. Geophys. Res., 77, 1905, 1972.

Dickenson, R. E., and J. E. Geisler, Vertical Motion Field in the Middle Thermosphere from Satellite Drag Densities, Mon. Wea. Rev., 96, 606, 1968.

Fedder, J. A., and P. M. Banks, Convection Electric Fields and Polar Thermospheric Winds, J. Geophys. Res., 77, 2328, 1972.

Feess, W. A., LOGACS Wind Analysis, TOR-0200(9990)-1, Aerospace Corporation, El Segundo, Ca., 1968.

Feldstein, Y. I., and G. V. Starkov, Dynamics of Auroral Belt and Polar Geomagnetic Disturbances, Planet. Space Sci., 15, 209, 1967.

Forbes, J. M., and F. A. Marcos, Thermospheric Density Variations Associated with Auroral Electrojet Activity, J. Geophys. Res., 78, 3841, 1973.

Fotou, E. G., LOGACS - An Orbital Accelerometer Calibration Experiment, TOR-0158(3110-01)-21, Aerospace Corporation, El Segundo, Ca., 1968.

Francis, S. H., Acoustic-Gravity Modes and Large-Scale Traveling Ionospheric Disturbances of a Realistic, Dissipative Atmosphere, J. Geophys. Res., 78, 2278, 1973.

Geisler, J. E., Atmospheric Winds in the Middle F-Region. J. Atmos. Terr. Phys., 28, 703, 1966.

Geisler, J. E., A Numerical Study of the Wind System in the Middle Thermosphere, J. Atmos. Terr. Phys.,29, 1469, 1967.

Hakura, Y., Tables and Maps of Geomagnetic Coordinates Corrected by the Higher Order Spherical Harmonic Terms, Rep. Ionosph. Space Res. Japan, 19, 121, 1965.

Hayes, P. B., and R. G. Roble, Direct Observations of Thermospheric Winds, J. Geophys. Res., 76, 5316, 1971.

Hedin, A. E., and C. A. Reber, Longitudinal Variations of Thermospheric Composition Indicating Magnetic Control of Polar Heat Input, J. Geophys. Res., 77, 2871, 1972.

Hultqvist, B., The Geomagnetic Field Lines in Higher Approximation, Ark. Geofy., 3, 53, 1958.

Jacchia, L. G., Recent Advances in Upper Atmospheric Structure, Space Res. X, 367, 1970.

Jacchia, L. G., Revised Static Models of the Thermosphere and Exosphere with Empirical Temperature Profiles, Special Report NO. 332, Smithsonian Institution Astrophysical Observatory, Cambridge, Ma., 1971.

Jacchia, L. G., J. Slowey, and F. Verniani, Geomagnetic Perturbations and Upper-Atmosphere Heating, J. Geophys. Res., 72, 1423, 1967.

Jacchia, L. G., and J. Slowey, Diurnal and Seasonal-Latitudinal Variations in the Upper Atmosphere, Planet. Space Sci., 16, 509, 1968.

Jacobs, R. L., Atmospheric Density Derived from the Drag of Eleven Low-Altitude Satellites, J. Geophys. Res., 72, 1571, 1967.

Knight, D. E., R. Uribe, and B. E. Woodgate, Low-Latitude Density Variations in the Earth's Neutral Atmosphere between 200 and 400 km, from August 1969 to May 1970, Planet. Space Sci., 21, 253, 1973.

Knudsen, W. C., Neutral Atmosphere Wave Generation by the Equatorial Electrojet, J. Geophys. Res., 74, 4191, 1969.

Kohl, H., and J. W. King, Atmospheric Winds Between 100 and 700 km and Their Effects on the Ionosphere, J. Atmos. Terr. Phys., 29, 1045, 1967.

Lindzen, R. S., Crude Estimate for the Zonal Velocity Associated with the Diurnal Temperature Oscillation, J. Geophys. Res., 71, 865, 1966.

Lindzen, R. S., Reconsideration of Diurnal Velocity Oscillation in the Thermosphere, J. Geophys. Res., 72, 1591, 1967.

Marcos, F. A., K. S. W. Champion, and R. A. Schweinfurth, More Accelerometer and Orbital Drag Results from the SPADES (OV1-15) and Cannon Ball I(OV1-16) Satellites, Space Res. XI, 941, 1971.

Marcos, F. A., and K. S. W. Champion, Gravity Waves Observed in High Latitude Neutral Density Profiles, Space Res. XII, 791, 1972.

Marcos, F. A., R. McInerney, J. Corbin, R. Fioretti, and N. Grossbard, Atmospheric DEnsity Results Derived from the SPADES Satellite Accelerometer Data, AFCRL-72-0608; also under Environmental Research Papers, No. 417, Air Force Cambridge Research Laboratories, L. G. Hanscom Field, Ma., 1972.

May, B. R., The Variation of Air Density at 240 and 280 km from April to November 1967, Planet. Space Sci., 20, 1077, 1972.

Mayr, H. G., and H. Volland, Magnetic Storm Characteristics of the Thermosphere, J. Geophys. Res., 78, 2251, 1973.

Morse, F. A., Purpose and Design of the U.S.A.F. Satellite OV1-15, p. 22, in Aerospace Corporation Report SPL-1104, Symposium on the Upper Atmosphere Results and Interpretation of OV1-15 Data, II; El Segundo, Ca., 1970.

Neupert, W. M., W. E. Behring, and J. C. Lindsay, The Solar Spectrum from 50Å to 400Å, Space Res. IV, 719, 1964.

Newton, G. P., and D. T. Pelz, Latitudinal Variations in the Neutral Atmospheric Density, J. Geophys. Res., 74, 4169, 1969.

Newton, G. P., D. T. Pelz, and H. Volland, Direct In Situ Measurements of Wave Propagation in the Neutral Thermosphere, J. Geophys. Res., 74, 183, 1969.

Newton, G. P., and D. T. Pelz, Neutral Thermosphere Temperatures from Density Scale Height Measurements, J. Geophys. Res., 78, 725, 1973.

Nicolet, M., Solar Radio Flux and Temperature of the Upper Atmosphere, J. Geophys. Res., 68, 6121, 1963.

Philbrick, C. R., and J. P. McIsaac, Measurements of Atmospheric Composition Near 400 km, Space Res. XII, 743, 1972.

Reddy, C. A., and G. Vasseur, Incoherent Scatter Observations of Meridional Winds in the 150-225 km Region, Space Res. XII, 951, 1972.

Rees, D., Winds and Temperatures in the Auroral Zone and Their Relations to Geomagnetic Activity, Phil. Trans. R. Soc. Lond. A., 271, 563, 1972.

Rishbeth, H., Thermospheric Winds and the F-Region: A Review. J. Atmos. Terr. Phys., 34, 1, 1972.

Roemer, M., Recent Observational Results on the Neutral Upper Atmosphere, Space Res. XI, 761, 1971a.

Roemer, M., Geomagnetic Activity Effect in the 250- to 800-km Altitude Region, Space Res. XI, 965, 1971b.

Smith, L. B., An Observation of Strong Thermospheric Winds During a Geomagnetic Storm, J. Geophys. Res., 73, 4959, 1968.

Taeusch, D. R., G. R. Carigan, and C. A. Reber, Response of the Neutral Atmosphere to Geomagnetic Disturbances, Space Res. XI, 995, 1971a.

Taeusch, D. R., G. R. Carigan, and C. A. Reber, Neutral Composition Variation above 400 Kilometers during a Magnetic Storm, J. Geophys. Res., 76, 8318, 1971b.

Testud, J., Gravity Waves Generated during Magnetic Substorms, J. Atmos. Terr. Phys., 32, 1793, 1970.

Thome, G., Long-Period Waves Generated in the Polar Ionosphere during the Onset of Magnetic Storms, J. Geophys. Res., 73, 6319, 1968.

Volland, H., A Theory of Thermospheric Dynamics-II, Geomagnetic activity effect, 27-day variation and semi-annual variation, Planet. Space Sci., 17, 1709, 1969.

Waldteufel, P., P. Bauer, and J. P. McClure, Structure of the Thermosphere as Inferred from Incoherent Scatter Measurements, Space Res. XII, 899, 1972.

Whalen, J. A., Auroral Oval Plotter and Nomograph for Determining Corrected Geomagnetic Local Time, Latitude, and Longitude for High Latitudes in the Northern Hemisphere, AFCRL-70-0422, also under Environmental Research Papers, No. 327, Air Force Cambridge Research Laboratories, L. G. Hanscom Field, Ma., 1970.

APPENDIX

Factors for Normalizing Density to a Standard Altitude of 145 km

Alt/T_∞	900°	1000°	1100°	1200°	1300°	1400°
139.1	0.67132	0.67685	0.68140	0.68502	0.68815	.69089
.3	.68108	.68650	.69094	.69448	0.69755	.70022
.5	.69093	.69623	.70057	.70403	.70702	.70962
.7	.70088	.70605	.71029	.71366	.71657	.71911
.9	.71092	.71596	.72009	.72337	.72621	.72867
140.1	.72106	.72596	.72998	.73317	.73592	.73831
.3	.73129	.73605	.73996	.74305	.74572	.74803
.5	.74162	.74623	.75002	.75301	.75560	.76773
.7	.75204	.75650	.76017	.76306	.76556	.76773
.9	.76256	.76686	.77041	.77319	.77560	.77769
141.1	.77318	.77731	.78074	.78341	.78573	.78773
.3	.78390	.78786	.79115	.79371	.79594	.79785
.5	.79471	.79850	.80165	.80409	.80624	.80806
.7	.80562	.80923	.81224	.81457	.81662	.81835
.9	.81662	.82005	.82292	.82513	.82708	.82872
142.1	.82772	.83097	.83369	.83578	.83763	.83917
.3	.83892	.84198	.84455	.84651	.84826	.84970
.5	.85022	.85309	.85550	.85733	.85897	.86032
.7	.86162	.86429	.86654	.86824	.86976	.87102
.9	.87312	.87559	.87767	.87924	.88064	.88180
143.1	.88472	.88699	.88889	.89032	.89160	.89266
.3	.89643	.89848	.90020	.90148	.90265	.90360
.5	.90824	.91007	.91159	.91273	.91378	.91463
.7	.92015	.92175	.92308	.92408	.92500	.92574
.9	.93216	.93352	.93466	.93551	.93630	.93694
144.1	.94427	.94539	.94634	.94704	.94769	.94821
.3	.95648	.95736	.95811	.95865	.95916	.95957
.5	.96879	.96943	.96996	.97035	.97072	.97102
.7	.98120	.98159	.98191	.98215	.98237	.98256
.9	.99371	.99384	.99395	.99403	.99411	.99417

Factors for Normalizing Density to a
Standard Altitude of 145 km.

Alt/T_∞	900°	1000°	1100°	1200°	1300°	1400°
145.1	1.00633	1.00620	1.00609	1.00600	1.00593	1.00586
.3	1.01905	1.01866	1.01831	1.01806	1.01783	1.01764
.5	1.03188	1.03121	1.03063	1.03021	1.02982	1.02951
.7	1.04481	1.04385	1.04305	1.04245	1.04190	1.04146
.9	1.05785	1.05660	1.05556	1.05478	1.05407	1.05350
146.1	1.07100	1.06945	1.06816	1.06721	1.06633	1.06563
.3	1.08426	1.08240	1.08086	1.07973	1.07867	1.07783
.5	1.09762	1.09545	1.09365	1.09234	1.09110	1.09013
.7	1.111109	1.10860	1.10653	1.10504	1.10361	1.10251
.9	1.12467	1.12185	1.11952	1.11783	1.11622	1.11498
147.1	1.13836	1.13520	1.13260	1.13071	1.12892	1.12753
.3	1.15216	1.14865	1.14577	1.14368	1.14171	1.14017
.5	1.16608	1.16220	1.15904	1.15675	1.15459	1.15289
.7	1.18011	1.17586	1.17242	1.16991	1.16756	1.16571
.9	1.19425	1.18962	1.18589	1.18317	1.18062	1.17861
148.1	1.20849	1.20349	1.19946	1.19652	1.19376	1.19160
.3	1.22283	1.21746	1.21312	1.20997	1.20699	1.20468
.5	1.23730	1.23153	1.22689	1.22351	1.22032	1.2.785
.7	1.25188	1.24570	1.24075	1.23714	1.23373	1.23110
.9	1.26658	1.25999	1.25471	1.25086	1.24724	1.24445
149.1	1.28139	1.27438	1.26878	1.26468	1.26085	1.25788
.3	1.29632	1.28888	1.28295	1.27859	1.27454	1.27140
.5	1.31136	1.30348	1.29722	1.29260	1.28833	1.28500
.7	1.32651	1.31820	1.31158	1.30670	1.30221	1.29870
.9	1.34178	1.33302	1.32605	1.32090	1.31618	1.31248
150.1	1.35717	1.34795	1.34062	1.33519	1.33024	1.32635
.3	1.37268	1.36298	1.35529	1.34958	1.34439	1.34030

Factors for Normalizing Density to a
Standard Altitude of 150 km.

Alt/T_∞	1000°	1100°	1200°	1300°	1400°
144.9	.74143	.74546	.74851	.75128	.75351
145.1	.75065	.75456	.75752	.76022	.76237
.3	.75994	.76373	.76660	.76921	.77130
.5	.76930	.77297	.77575	.77828	.78030
.7	.77874	.78228	.78497	.78741	.78935
.9	.78825	.79166	.79425	.79661	.79848
146.1	.79783	.80111	.80361	.80587	.80767
.3	.80749	.81064	.81303	.81520	.81692
.5	.81722	.82023	.82252	.82459	.82624
.7	.82703	.82990	.83209	.83405	.83562
.9	.83691	.83964	.84172	.84359	.84507
147.1	.84687	.84945	.85142	.85318	.85459
.3	.85691	.85933	.86119	.86285	.86417
.5	.86702	.86929	.87103	.87258	.87381
.7	.87720	.87932	.88094	.88238	.88352
.9	.88747	.88942	.89092	.89225	.89330
148.1	.89781	.89960	.90097	.90218	.90315
.3	.90823	.90985	.91109	.91218	.91306
.5	.91873	.92017	.92129	.92226	.92304
.7	.92931	.93057	.93155	.93240	.93308
.9	.93997	.94105	.94188	.94261	.94319
149.1	.95071	.95160	.95229	.95289	.95337
.3	.96152	.96222	.96277	.96324	.96362
.5	.97242	.97292	.97332	.97366	.97393
.7	.98339	.98370	.98394	.98414	.98431
.9	.99445	.99455	.99463	.99470	.99476
150.1	1.00558	1.00548	1.00540	1.00533	1.00527
.3	1.01680	1.01649	1.01624	1.01602	1.01585
.5	1.02810	1.02757	1.02715	1.02679	1.02650
.7	1.03948	1.03873	1.03813	1.03763	1.03722
.9	1.05094	1.04996	1.04919	1.04854	1.04801

Factors for Normalizing Density to a Standard Altitude of 150 km.

Alt/T_∞	1000°	1100°	1200°	1300°	1400°
151.1	1.06248	1.06128	1.06032	1.05952	1.05886
.3	1.07410	1.07267	1.07153	1.07057	1.06979
.5	1.08581	1.08414	1.08281	1.08169	1.08079
.7	1.09760	1.09569	1.09417	1.09288	1.09185
.9	1.10947	1.10732	1.10560	1.10415	1.10298
152.1	1.12143	1.11903	1.11711	1.11548	1.11418
.3	1.13347	1.13081	1.12869	1.12689	1.12545
.5	1.14559	1.14268	1.14034	1.13837	1.13679
.7	1.15780	1.15462	1.15207	1.14992	1.14821
.9	1.17009	1.16664	1.16388	1.16155	1.15969
153.1	1.18247	1.17875	1.17577	1.17325	1.17124
.3	1.19493	1.19093	1.18773	1.18501	1.18286
.5	1.20749	1.20319	1.19976	1.19686	1.19456
.7	1.22012	1.21554	1.21187	1.20877	1.20632
.9	1.23285	1.22796	1.22407	1.22076	1.21815
154.1	1.24567	1.24047	1.23633	1.23283	1.23006
.3	1.25857	1.25305	1.24868	1.24497	1.24204
.5	1.27156	1.26572	1.26109	1.25718	1.25408
.7	1.28464	1.27848	1.27359	1.26947	1.26620
.9	1.29781	1.29131	1.28617	1.28183	1.27839
155.1	1.31107	1.30423	1.29882	1.29427	1.29066
.3	1.32441	1.31722	1.31156	1.30678	1.30299
.5	1.33785	1.33030	1.32436	1.31937	1.31540
.7	1.35138	1.34347	1.33725	1.33203	1.32788

Factors for Normalizing Density to a
Standard Altitude of 160 km.

Alt/T_∞	900°	1000°	1100°	1200°	1300°	1400°	1500°
160.1	1.00484	1.00470	1.00459	1.00451	1.00444	1.00438	1.00434
.3	1.01456	1.01412	1.01380	1.01355	1.01334	1.01317	1.01304
.5	1.02434	1.02360	1.02307	1.02264	1.02229	1.02201	1.02178
.7	1.03418	1.03314	1.03239	1.03178	1.03130	1.03090	1.03058
.9	1.04409	1.04274	1.04176	1.04097	1.04035	1.03983	1.03941
161.1	1.05407	1.05241	1.05118	1.05021	1.04945	1.04880	1.04830
.3	1.06412	1.06213	1.06066	1.05950	1.05860	1.05783	1.05723
.5	1.07423	1.07191	1.07021	1.06886	1.06780	1.06691	1.06621
.7	1.08440	1.08176	1.07981	1.07827	1.07705	1.07603	1.07523
.9	1.09465	1.09167	1.08946	1.08773	1.08634	1.08521	1.08430
162.1	1.10495	1.10164	1.09917	1.09724	1.09569	1.09443	1.09342
.3	1.11533	1.11168	1.10894	1.10680	1.10509	1.10370	1.10258
.5	1.12578	1.12177	1.11877	1.11642	1.11454	1.11302	1.11179
.7	1.13629	1.13192	1.12865	1.12609	1.12405	1.12238	1.12105
.9	1.14687	1.14214	1.13859	1.13581	1.13360	1.13180	1.13035
163.1	1.15752	1.15242	1.14859	1.14559	1.14321	1.14126	1.13970
.3	1.16825	1.16277	1.15864	1.15542	1.15287	1.15077	1.14910
.5	1.17904	1.17318	1.16875	1.16531	1.16258	1.16033	1.15855
.7	1.18991	1.18364	1.17893	1.17525	1.17235	1.16994	1.16804
.9	1.20085	1.19417	1.18916	1.18525	1.18216	1.17960	1.17758
164.1	1.21186	1.20476	1.19946	1.19530	1.19203	1.18931	1.18717
.3	1.22294	1.21542	1.20981	1.20541	1.20195	1.19907	1.19681
.5	1.23409	1.22614	1.22024	1.21557	1.21193	1.20888	1.20649
.7	1.24531	1.23692	1.23074	1.22579	1.22195	1.21874	1.21623
.9	1.25660	1.24777	1.23128	1.23606	1.23203	1.27865	1.22601

Factors for Normalizing Density to a Standard Altitude of 160 km.

Alt/T_∞	900°	1000°	1100°	1200°	1300°	1400°	1500°
154.3	.75027	.75613	.76072	.76427	.76716	.76953	.77159
.5	.75823	.76393	.76841	.77189	.77468	.77699	.77900
.7	.76624	.77178	.77615	.77954	.78225	.78450	.78645
.9	.77430	.77969	.78394	.78724	.78987	.79205	.79395
155.1	.78242	.78765	.79178	.79498	.79753	.79965	.80149
.3	.79059	.79566	.79967	.80277	.80524	.80729	.80907
.5	.79883	.80373	.80761	.81061	.81300	.81498	.81670
.7	.80712	.81185	.81560	.81849	.82081	.82271	.82437
.9	.81547	.82003	.82365	.82642	.82867	.83049	.83208
156.1	.82388	.82826	.83174	.83441	.83657	.83831	.83984
.3	.83234	.83655	.83989	.84244	.84451	.84618	.84764
.5	.84087	.84489	.84808	.85052	.85250	.85409	.85548
.7	.84945	.85329	.85633	.85865	.86054	.86205	.86337
.9	.85809	.86174	.86463	.86682	.86863	.87005	.87130
157.1	.86679	.87025	.87298	.97505	.87676	,87810	.87927
.3	.87556	.87882	.88138	.88333	.88494	.88619	.88729
.5	.88439	.88744	.88983	.89166	.89317	.89433	.89536
.7	.89328	.89611	.89834	.90004	.90144	.90252	.90347
.9	.90223	.90484	.90690	.90847	.90976	.91075	.91163
158.1	.91124	.91363	.91551	.91695	.91812	.91903	.91983
.3	.92031	.92248	.92418	.92547	.92653	.92736	.92807
.5	.92945	.93138	.93209	.93404	.93499	.93573	.93636
.7	.93865	.94034	.94168	.94267	.94350	.94415	.94470
.9	.94791	.94936	.95051	.95135	.95206	.95261	.95309
159.1	.95723	.95844	.95938	.96008	.96067	.96112	.96152
.3	.96662	.96757	.96831	.96886	.96933	.96967	.96999
.5	.97608	.97676	.97730	.97769	.97803	.97828	.97850
.7	.98560	.98601	.98634	.98658	.98678	.98694	.98707
.9	.99518	.99532	.99544	.99552	.99558	.99564	.99568

Factors for Normalizing Density to a Standard Altitude of 160 km.

Alt/T_∞	900°	1000°	1100°	1200°	1300°	1400°
165.1	1.26796	1.25869	1.25187	1.24639	1.24216	1.23861
.3	1.27940	1.26968	1.26252	1.25677	1.25233	1.24862
.5	1.29091	1.28073	1.27324	1.26721	1.26256	1.25868
.7	1.30250	1.29185	1.28401	1.27770	1.27285	1.26879
.9	1.31416	1.20204	1.29485	1.28825	1.28319	1.27895
166.1	1.32590	1.31430	1.30574	1.29887	1.29358	1.28916
.3	1.33771	1.32562	1.31670	1.30953	1.30402	1.29942
.5	1.34959	1.33701	1.32772	1.32026	1.31452	1.30972
.7	1.36155	1.34847	1.33881	1.33105	1.32506	1.32008
.9	1.37359	1.36000	1.34996	1.34188	1.33566	1.33050
167.1	1.38571	1.37160	1.36116	1.35278	1.34632	1.34097
.3	1.39790	1.38326	1.37243	1.36274	1.35704	1.35150
.5	1.41017	1.39499	1.38375	1.37475	1.36780	1.36207
.7	1.42251	1.40679	1.39514	1.38582	1.37862	1.37269
.9	1.43493	1.41866	1.40659	1.29695	1.38950	1.38337
168.1	1.44743	1.43061	1.41811	1.40814	1.40044	1.39409
.3	1.46001	1.44263	1.42970	1.41939	1.41143	1.40487
.5	1.47267	1.45470	1.44135	1.43069	1.42247	1.41570
.7	1.48541	1.46685	1.45307	1.44205	1.43357	1.42659
.9	1.49823	1.47907	1.46484	1.45347	1.44472	1.43753
169.1	1.51113	1.49136	1.47668	1.46495	1.45593	1.44853
.3	1.52411	1.50372	1.48858	1.47649	1.46720	1.45957
.5	1.53717	1.51616	1.50055	1.48810	1.47853	1.47066
.7	1.55031	1.52867	1.51258	1.49977	1.48990	1.48181
.9	1.56353	1.54125	1.52468	1.51150	1.50133	1.49301
170.1	1.57684	1.55490	1.53685	1.52329	1.51282	1.50427
.3	1.59023	1.56663	1.54908	1.53514	1.52436	1.51558
.5	1.60372	1.57943	1.56138	1.54705	1.53596	1.52695
.7	1.61730	1.59231	1.57376	1.55896	1.54761	1.53838

Factors for Normalizing Density to a Standard Altitude of 180 km.

Alt/T_∞	900°	1000°	1100°	1200°	1300°	1400°
169.3		0.66002	0.66846	0.67520	0.68053	0.68500
.5		0.66548	0.67383	0.68050	0.68578	0.69021
.7		0.67097	0.67924	0.68584	0.69106	0.69544
.9		0.67650	0.68467	0.69120	0.69136	0.70070
170.1		0.68205	0.69014	0.69659	0.70169	0.70598
.3		0.68764	0.69563	0.70201	0.70705	0.71129
.5		0.69326	0.70115	0.70746	0.71243	0.71662
.7		0.69891	0.70671	0.71293	0.71784	0.72198
.9		0.70460	0.71229	0.71843	0.72328	0.72736
171.1		0.71032	0.71790	0.72396	0.72874	0.73277
.3		0.71607	0.72355	0.72952	0.73423	0.73820
.5		0.72185	0.72922	0.73510	0.73974	0.74366
.7		0.72767	0.73493	0.74072	0.74529	0.74914
.9		0.73352	0.74066	0.74636	0.75086	0.75465
172.1		0.73940	0.74643	0.75203	0.75646	0.76019
.3		0.74532	0.75223	0.75773	0.76208	0.76575
.5		0.75127	0.75806	0.76346	0.76773	0.77133
.7		0.75526	0.76391	0.76922	0.77341	0.77695
.9		0.76328	0.76980	0.77501	0.77912	0.78258
173.1		0.76933	0.77513	0.78082	0.78485	0.78825
.3		0.77542	0.78168	0.78667	0.79061	0.79394
.5		0.78154	0.78766	0.79254	0.79640	0.79965
.7		0.78770	0.79368	0.79845	0.80221	0.80539
.9		0.79389	0.79972	0.80438	0.80805	0.81116
174.1		0.80011	0.80580	0.81034	0.81392	0.81696
.3		0.80637	0.81191	0.81633	0.81982	0.82278
.5		0.81267	0.81805	0.82236	0.82575	0.82862
.7		0.81900	0.82423	0.82841	0.83170	0.83450
.9		0.82536	0.83043	0.83449	0.83768	0.84040

Factors for Normalizing Density to a Standard Altitude of 180 km.

Alt/T_∞	900°	1000°	1100°	1200°	1300°	1400°
175.1		0.83176	0.83667	0.84060	0.84369	0.84632
.3		0.83819	0.84295	0.84674	0.84973	0.85228
.5		0.84466	0.84925	0.85291	0.85580	0.85826
.7		0.85117	0.85559	0.85912	0.86190	0.86426
.9		0.85771	0.86196	0.86535	0.86802	0.87029
176.1		0.86429	0.86836	0.87161	0.87417	0.87635
.3		0.87090	0.87480	0.87791	0.88036	0.88244
.5		0.87755	0.88127	0.88423	0.88657	0.88856
.7		0.88424	0.88777	0.89059	0.89281	0.89470
.9		0.89086	0.89431	0.89697	0.89908	0.90086
177.1		0.89772	0.90088	0.90339	0.90537	0.90706
.3		0.90452	0.90749	0.90984	0.91170	0.91328
.5		0.91135	0.91413	0.91632	0.91806	0.91953
.7		0.91823	0.92080	0.92284	0.92444	0.92581
.9		0.92514	0.92750	0.92938	0.93086	0.93211
178.1		0.93208	0.93424	0.93595	0.93730	0.93845
.3		0.93907	0.94102	0.94256	0.94377	0.94481
.5		0.94609	0.94783	0.94920	0.95028	0.95119
.7		0.95316	0.95467	0.95587	0.95681	0.95761
.9		0.96026	0.96155	0.96257	0.96337	0.96405
179.1		0.96740	0.96846	0.96930	0.96997	0.97053
.3		0.97457	0.97541	0.97607	0.97659	0.97703
.5		0.98179	0.98239	0.98287	0.98324	0.98356
.7		0.98905	0.98941	0.98970	0.98992	0.99011
.9		0.99634	0.99646	0.99656	0.96337	0.96405
180.1		1.00367	1.00355	0.00345	1.00338	1.00331
.3		1.01105	1.01068	1.01038	1.01015	1.00995
.5		1.01846	1.01784	1.01734	1.01695	1.01663
.7		1.02591	1.02503	1.02434	1.02378	1.02332
.9		1.03341	1.03227	1.03136	1.03064	1.03005

Factors for Normalizing Density to a Standard Altitude of 180 km.

Alt/T_∞	900°	1000°	1100°	1200°	1300°	1400°
181.1		1.04094	1.03954	1.03842	1.03754	1.03681
.3		1.04851	1.04684	1.04552	1.04446	1.04359
.5		1.05613	1.05418	1.05264	1.05142	1.05041
.7		1.06378	1.06156	1.05980	1.05840	1.05725
.9		1.07148	1.06898	1.06700	1.06542	1.06412
182.1		1.07921	1.07643	1.07422	1.07247	1.07102
.3		1.08699	1.08342	1.08148	1.07955	1.07795
.5		1.09481	1.09144	1.08878	1.08666	1.08491
.7		1.10267	1.09901	1.09611	1.09380	1.09190
.9		1.11057	1.10661	1.10347	1.10098	1.09892
183.1		1.11852	1.11425	1.11086	1.10819	1.10597
.3		1.12650	1.12192	1.11829	1.11542	1.11304
.5		1.13453	1.12963	1.12576	1.12269	1.12015
.7		1.14260	1.13739	1.13325	1.12999	1.12728
.9		1.15071	1.14518	1.14079	1.13732	1.13445
184.1		1.15887	1.15300	1.14835	1.14469	1.14164
.3		1.16707	1.16087	1.15596	1.15208	1.14887
.5		1.17531	1.16877	1.16359	1.15951	1.15612
.7		1.18360	1.17672	1.17127	1.16697	1.16341
.9		1.19192	1.18470	1.17897	1.17446	1.17072
185.1		1.20030	1.19272	1.18672	1.18199	1.17807
.3		1.20872	1.20078	1.19450	1.18955	1.18545
.5		1.21718	1.20888	1.20231	1.19714	1.19285
.7		1.22568	1.21702	1.21016	1.20477	1.20029
.9		1.23423	1.22520	1.21805	1.21242	1.20776
186.1		1.24283	1.23341	1.22597	1.22011	1.21526
.3		1.25147	1.24167	1.23393	1.22784	1.22279
.5		1.26015	1.24997	1.24192	1.23560	1.23035
.7		1.26888	1.25830	1.24995	1.24339	1.23794
.9		1.27766	1.26668	1.25802	1.25121	1.24556

Factors for Normalizing Density to a Standard Altitude of 180 km.

Alt/T_∞	900°	1000°	1100°	1200°	1300°	1400°
187.1		1.28648	1.27510	1.26612	1.25907	1.25321
.3		1.29534	1.28355	1.27426	1.26696	1.26090
.5		1.30426	1.29205	1.28244	1.27488	1.26861
.7		1.31321	1.30059	1.29065	1.28284	1.27636
.9		1.32222	1.30917	1.29890	1.29083	1.28414
188.1		1.33127	1.31779	1.30719	1.29885	1.29194
.3		1.34036	1.32646	1.31551	1.20691	1.29978
.5		1.34951	1.33516	1.32387	1.31501	1.30765
.7		1.35870	1.34391	1.33227	1.32313	1.31556
.9		1.36793	1.35269	1.34070	1.33129	1.32349
189.1		1.37722	1.36152	1.34918	1.33949	1.33146
.3		1.38655	1.37039	1.35769	1.34772	1.33945
.5		1.39592	1.37931	1.36623	1.35598	1.34748
.7		1.40535	1.38826	1.37482	1.36428	1.35555
.9		1.41482	1.39726	1.38344	1.37261	1.36364
190.1		1.42434	1.40630	1.39210	1.38098	1.37176
.3		1.43391	1.41539	1.30080	1.38938	1.37992
.5		1.44353	1.42451	1.40954	1.39782	1.38811
.7		1.45320	1.43368	1.41832	1.40629	1.39633

Factors for Normalizing Density to a Standard Altitude of 200 km.

Alt/T_∞	1000°	1100°	1200°	1300°	1400°
187.9	0.67468	0.68537	0.69412	0.70128	0.70731
188.1	0.67930	0.68989	0.69855	0.70564	0.71161
.3	0.68394	0.69442	0.70299	0.71002	0.71593
.5	0.68860	0.69898	0.70746	0.71442	0.72026
.7	0.69329	0.70356	0.71195	0.71883	0.72462
.9	0.69800	0.70816	0.71646	0.72327	0.72899
189.1	0.70274	0.71278	0.72098	0.72772	0.73338
.3	0.70750	0.71743	0.72553	0.73219	0.73778
.5	0.71229	0.72209	0.73010	0.73668	0.74220
.7	0.71710	0.72678	0.73469	0.74119	0.74664
.9	0.72193	0.73149	0.73929	0.7472	0.75110
190.1	0.72679	0.73622	0.74392	0.75026	0.75558
.3	0.73167	0.74098	0.74857	0.75483	0.76007
.5	0.73658	0.74576	0.75324	0.75941	0.76458
.7	0.74151	0.75056	0.75793	0.76401	0.76911
.9	0.74647	0.75538	0.76265	0.76863	0.77365
191.1	0.75145	0.76023	0.76738	0.77327	0.77822
.3	0.75646	0.76509	0.77213	0.77793	0.78280
.5	0.76149	0.76998	0.77690	0.78261	0.78740
.7	0.76654	0.77490	0.78170	0.78731	0.79201
.9	0.77162	0.77983	0.78652	0.79203	0.79665
192.1	0.77673	0.78479	0.79135	0.79677	0.80130
.3	0.78187	0.78977	0.79621	0.80152	0.80597
.5	0.78703	0.79478	0.80109	0.80630	0.81066
.7	0.79221	0.79981	0.80599	0.81110	0.81537
.9	0.79742	0.80486	0.81091	0.81591	0.82009
193.1	0.80266	0.80993	0.81586	0.82075	0.82483
.3	0.80792	0.81503	0.82082	0.82560	0.82959
.5	0.81321	0.82016	0.82581	0.83048	0.83438
.7	0.81853	0.82530	0.83082	0.83537	0.83917
.9	0.82387	0.83047	0.83585	0.84028	0.84399

Factors for Normalizing Density to a Standard Altitude of 200 km.

Alt/T_∞	1000°	1100°	1200°	1300°	1400°
194.1	0.82924	0.83567	0.84090	0.84522	0.84882
.3	0.83463	0.84089	0.84597	0.85017	0.85368
.5	0.84005	0.84613	0.85107	0.85515	0.85855
.7	0.84550	0.85140	0.85618	0.86014	0.86344
.9	0.85098	0.85668	0.86132	0.86515	0.86835
195.1	0.85648	0.86200	0.86648	0.87019	0.87328
.3	0.86201	0.86734	0.87166	0.87524	0.87822
.5	0.86757	0.87270	0.87687	0.88032	0.88319
.7	0.87315	0.97809	0.88210	0.88541	0.88817
.9	0.87876	0.88350	0.88735	0.89052	0.89318
196.1	0.88440	0.88894	0.89262	0.89566	0.89820
.3	0.89007	0.89440	0.89791	0.90082	0.90324
.5	0.89576	0.89989	0.90323	0.90599	0.90830
.7	0.90148	0.90540	0.90857	0.91119	0.91338
.9	0.90723	0.91093	0.91393	0.91641	0.91848
197.1	0.91301	0.91649	0.91932	0.92165	0.92360
.3	0.91881	0.92208	0.92472	0.92691	0.92874
.5	0.92465	0.92769	0.93016	0.93219	0.93389
.7	0.93051	0.93332	0.93561	0.93749	0.93907
.9	0.93640	0.93899	0.94109	0.94282	0.94426
198.1	0.94232	0.94467	0.94659	0.94816	0.94948
.3	0.94827	0.95039	0.95211	0.95353	0.95471
.5	0.95424	0.95613	0.95766	0.95892	0.95997
.7	0.96025	0.96189	0.96323	0.96432	0.96524
.9	0.96628	0.96768	0.96882	0.96975	0.97053
199.1	0.97235	0.97350	0.97444	0.97521	0.97585
.3	0.97844	0.97934	0.98008	0.98068	0.98118
.5	0.98457	0.98521	0.98574	0.98617	0.98653
.7	0.99072	0.99111	0.99143	0.99169	0.99191
.9	0.99690	0.99703	0.99714	0.99722	0.99730

Factors for Normalizing Density to a Standard Altitude of 200 km.

Alt/T_∞	1000°	1100°	1200°	1300°	1400°
200.1	1.00311	1.00298	1.00287	1.00278	1.00271
.3	1.00935	1.00895	1.00863	1.00836	1.00814
.5	1.01562	1.01496	1.01441	1.01397	1.01360
.7	1.02192	1.02192	1.02022	1.01959	1.01907
.9	1.02826	1.02704	1.02605	1.03524	1.02457
201.1	1.03462	1.03312	1.03190	1.03091	1.03008
.3	1.04101	1.03923	1.02778	1.03660	1.03562
.5	1.04743	1.04537	1.04368	1.04231	1.04117
.7	1.05388	1.05153	1.04961	1.04804	1.04675
.9	1.06037	1.05772	1.05556	1.05380	1.05235
202.1	1.06688	1.06394	1.06154	1.05958	1.05796
.3	1.07343	1.07019	1.06754	1.06539	1.06360
.5	1.08001	1.07646	1.07357	1.07121	1.06926
.7	1.08662	1.08276	1.07962	1.07706	1.07494
.9	1.09326	1.08909	1.08570	1.08293	1.08064
203.1	1.09993	1.09545	1.09180	1.08882	1.08636
.3	1.10663	1.10183	1.09793	1.09474	1.09210
.5	1.11337	1.10825	1.10408	1.10068	1.09787
.7	1.12014	1.11469	1.11026	1.10664	1.10365
.9	1.12694	1.12116	1.11646	1.11263	1.10945
204.1	1.13377	1.12766	1.12269	1.11864	1.11528
.3	1.14063	1.13419	1.12894	1.12467	1.12112
.5	1.14753	1.14074	1.13523	1.13072	1.12699
.7	1.15446	1.4733	1.14153	1.13680	1.13288
.9	1.16142	1.15394	1.14786	1.14290	1.13879
205.1	1.16342	1.16059	1.15422	1.14902	1.14472
.3	1.17544	1.16726	1.16061	1.15517	1.15067
.5	1.18250	1.17396	1.16702	1.16134	1.15664
.7	1.18960	1.18069	1.17345	1.16754	1.16264
.9	1.19672	1.18745	1.17991	1.17375	1.16865

Factors for Normalizing Density to a Standard Altitude of 200 km.

Alt/T_∞	1000°	1100°	1200°	1300°	1400°
206.1	1.10388	1.19424	1.18640	1.17999	1.17469
.3	1.21108	1.20106	1.19292	1.18626	1.18075
.5	1.21831	1.20791	1.19946	1.19255	1.18683
.7	1.22557	1.21479	1.20603	1.19886	1.19294
.9	1.23286	1.22170	1.21262	1.20520	1.19906
207.1	1.24019	1.22864	1.21924	1.21156	1.20521
.3	1.24756	1.23561	1.22589	1.21794	1.21138
.5	1.25495	1.24260	1.23257	1.22435	1.21757
.7	1.26238	1.24963	1.23927	1.23079	1.22379
.9	1.26985	1.25669	1.24600	1.23724	1.23002
208.1	1.27736	1.26378	1.25275	1.24373	1.23628
.3	1.28489	1.27090	1.25953	1.25023	1.24256
.5	1.29247	1.27805	1.26634	1.25676	1.24886
.7	1.30007	1.28524	1.2718	1.26332	1.25519
.9	1.30772	1.29245	1.28005	1.26990	1.26153
209.1	1.31540	1.29969	1.28694	1.27650	1.26790
.3	1.32311	1.30697	1.29386	1.28313	1.27430
.5	1.33086	1.31428	1.30080	1.28979	1.28071
.7	1.33865	1.32161	1.30778	1.29647	1.28715
.9	1.34647	1.32898	1.41378	1.30317	1.29361
210.1	1.35433	1.33638	1.32181	1.30990	1.30009
.3	1.36222	1.34382	1.32887	1.31665	1.30660
.5	1.37016	1.35128	1.33596	1.32343	1.31312
.7	1.37812	1.35878	1.34307	1.33024	1.31968
.9	1.38613	1.36631	1.35021	1.33707	1.32625
211.1	1.39417	1.37387	1.35738	1.34392	1.33285
.3	1.40224	1.38147	1.36458	1.35080	1.33947
.5	1.41036	1.38909	1.37181	1.35771	1.34611
.7	1.41851	1.39675	1.37906	1.36464	1.35277
.9	1.42670	1.40444	1.38635	1.37160	1.35946
212.1	1.43493	1.41217	1.39366	1.37858	1.36617